POWDER DISSOLUTION AS A TOOL TO ESTIMATE PARTICLE SIZE AND SHAPE PARAMETERS OF CRYSTALLINE SOLIDS

by

Mandar V. Dali

A dissertation submitted in partial fulfillment of the requirements

for the degree of

Doctor of Philosophy

(Pharmacy)

at the

UNIVERSITY OF WISCONSIN - MADISON

1997

A dissertation entitled

Powder Dissolution as a Tool to Estimate Particle Size and Shape Parameters of Crystalline Solids

submitted to the Graduate School of the
University of Wisconsin-Madison
in partial fulfillment of the requirements for the
degree of Doctor of Philosophy

by

Mandar V. Dali

Date of Final Oral Examination: June 6, 1997

Month & Year Degree to be awarded: **December** **May** **August** 1997

* *

Approval Signatures of Dissertation Readers:

Signature, Dean of Graduate School

ACKNOWLEDGMENTS

The best of my vocabulary fails me to express the deep sense of gratitude and respect to my major professor, Jens T. Carstensen, Ph.D. whose valuable input and constant encouragement has made this dissertation a reality. The past four years of research have been a rewarding experience. My sincere thanks are extended to Dr. Ronald Burnette for many an intellectually stimulating discussion. The author would like to take this opportunity to thank all the pharmaceutics faculty from whose courses the author has gained a fair degree of understanding in the fundamentals of pharmaceutics.

Many thanks to Dr. Joseph Robinson and my colleagues in his laboratory for permitting the use of their instruments. The author would like to thank Mr. Christopher Kailhofer for help with the photomicrographs, Dr. Madhu Pudipeddi for all his help on and off the field, Mr. Srinivas Bollepalli for assistance with programming in Matlab, and all my other friends at the school of pharmacy who have made these past four years memorable. Financial support provided by Schering Plough corp., NJ and Hoechst-Marion-Roussel, MO is highly appreciated. My thanks are extended to Ms. Gayatri Desai, Mr. Shyam Vangala, and Ms. Su-Jyen Wu for all their help.

Last but not the least, I thank Ms. Manisha Desai, Ph.D. who never failed to lend her support in good and bad times.

POWDER DISSOLUTION AS A TOOL TO ESTIMATE PARTICLE SIZE AND SHAPE PARAMETERS OF CRYSTALLINE SOLIDS

Mandar V. Dali

Under the supervision of Professor Jens T. Carstensen

At the University of Wisconsin-Madison

A parallelepiped geometry has been considered to mimic *real* particles, instead of a spherical approximation. A model that describes the dissolution of a single non-isometric particle has been developed which takes into account the change in the so-called volume shape factor, α_v and the surface-volume shape factor, Γ. This model has been extended to multiparticulate systems with the intention of obtaining such parameters like the intrinsic dissolution rate constant, the average volume shape factor for a distribution of particles, and the size distribution parameters from *powder dissolution data*.

Single crystal dissolution studies were carried out on potassium dichromate crystals. It was observed that both, α_v and Γ are fairly invariant during the early stages of dissolution of the single crystal. The upward curvature in the cube root law plot for dissolution of such a particle could be explained by accounting for its inherent non-isometry.

Four compounds, viz., oxalic acid dihydrate, salicylic acid, phthalimde and acetaminophen were considered for powder dissolution studies. The dissolution rate constant K, of these compounds under USP dissolution apparatus conditions were obtained from the fraction undissolved and particle size analysis data.

These values were compared with those obtained from the critical times in the cube root law plot and the smallest dimension in the distribution. They were in good agreement. The powder samples could be characterized by an average α_{v0} that was estimated from the amount undissolved, K, and particle size analysis data.

A method has been proposed for the estimation of particle size distribution parameters from *powder dissolution* data and this has been demonstrated for sieve fractions of oxalic acid dihydrate.

In all of the above isotropic dissolution has been assumed. An attempt has been made to address the issue of anisotropy in non-isometric solids in another model. Six parameters that account for the polydispersity and anisotropy have been defined in this model. By way of computer simulations, dissolution profiles of log-normally distributed particles have been generated.

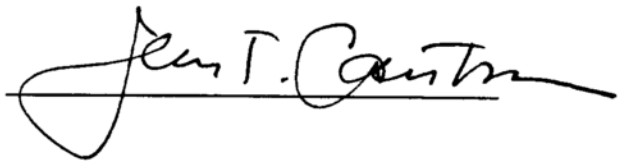

Prof. Jens T. Carstensen

LIST OF FIGURES

LIST OF TABLES

TABLE OF CONTENTS

CHAPTER I. INTRODUCTION

The thesis to follow will, to some extent, be written in a historical fashion. The conventional approaches to particle size characterization and dissolution will be presented early in this thesis, and they will serve here, to define more precisely the problems that exist in this research area, and show a sequence of events leading to the final steps, that is shape factors, and particle size distribution parameters as they influence dissolution. In this chapter, the importance of particle size and shape characeterization is emphasized, and an attempt has been made to provide the reader with an overall perspective of the present work.

I.1 General overview

Historically, dissolution testing became of importance in the late fifties when it was realized that, in many cases, the rate with which a drug substance dissolved from the dosage form was of importance in the rate and extent to which it was absorbed by the body [Nelson, 1959, Levy, 1961].

In the following two decades there was a raft of reports and theories dealing with dissolution [Higuchi and Hiestand, 1963, Brooke, 1974, Pothisiri and Carstensen, 1973], and the first official dissolution test appeared in the USP

(United States Pharmacopoeia) in 1970 (method I) followed by a second (method II) in the issue of 1975.

In today's climate virtually all solid dosage form products are routinely subjected to dissolution testing, and the most common cause for product recall is failure of a product to meet dissolution specifications [Cabana and O'Neil, 1980].

The question that intrigues the formulator is, if a product is carefully developed, and the pre-NDA (new drug application) product is found to meet dissolution standards, why will it often fail when produced routinely? In other cases, overcoming dissolution-related problems by manipulation of properties of excipients and drug substance is a difficult task. At the chemical development stage, the solvent of crystallization can affect the crystal habit and disssolution behavior of solids [Fini, et al., 1995].

For a given drug substance the single most important parameter affecting the dissolution is the surface area, or to be more exact, the particle size distribution. The FDA (Food and Drug Administration), the USP and pharmaceutical companies are aware of this, and for this reason specifications are always required (e.g. by the FDA) for particle size distribution determination of the drug substance.

But, with present methods, these particle size determinations are inadequate in relating to the actual dissolution of the product, and more to the point, the exact correlation between a particle size distribution and the ensuing dissolution of the particular batch of drug substance cannot be established with present methods. Hence it would be worthwhile to find a means of obtaining and presenting particle size distributions that are more realistic than the ones used at present by such techniques as the electrical zone sensing methods.

To this end, it serves well to briefly describe the shortcomings of presently used methods. Electrical capacitance, sedimentation, and laser based methods of particle size distributions give distributions of volumes of particles and then convert these volumes to equivalent spherical diameters. This serves well in an administratively descriptive sense, but it fails to recognize that *real* particles are not spherical. To establish the important parameters of drug substances, both technologically and as regards dissolution, it is necessary to take into account the fact that particles have distinctive shapes [Chakrabarti, et al., 1978, Hostomsky, et al., 1986, Nyvlt and Zacek, 1992]. Barnett and Nystrom have cautioned the blind-folded use of the Coulter counter technique for particle size analysis of highly irregular shaped particles, as this may lead to erroneous results [Barnett and Nystrom, 1982].

By converting volumes into a linear dimension (e.g. by using the diameter of the sphere with the same volume as that of the particle), the fact that particles can dissolve with different rates in different directions (anisotropy) is not taken into account. The impression is given that the particle will just have dissolved when this linear dimension becomes zero. On the contrary, in reality, it is only one of the dimensions (usually the smallest dimension) which will disappear at a given time, and it is when this happens that the particle will have dissolved completely, regardless of what the other dimensions are. Fig. I.1-1 exemplifies this argument. If the dissolution rate was such that the linear dimension, a, disappeared at a constant rate K, say 0.1 mm/sec, then the real shape would disappear after 10/0.1 = 100 sec, because the smallest dimension is 10 mm, whereas the equivalent spherical diameter is 30 mm and, with the knowledge of K, one might expect the particle to disappear after 300 sec.

Usually, when research is carried out, there is an ancillary theme which, originally, was not intended, but results as a natural consequence of the work being done. In this case this ancillary theme is the determination of volumetric shape factor. This is an important quantity because such properties as powder flow rates and cohesion, bulk density [Rupp, 1977, Ridgway and Rupp, 1969], porosity [Pitkin and Carstensen, 1990], syringeability, depend on both particle

size and *particle shape*. The latter has, heretofore, not been determinable by other than two-dimensional approximations (mostly from microscopy) and one of the goals of this thesis is to provide a method for determining three-dimensional volumetric shape factors for fine particles. Podczeck and Newton have described a three-dimensional shape factor for spheronized pellets that combines surface roughness and eccentricity (of an ellipsoid) [Podczeck and Newton, 1995]. It was possible to evaluate such a shape factor because the dimensions of the pellets were of the order of a few millimeters.

I.2. Historical background

All dissolution work is carried out by presenting the solid to a stirred liquid, and measuring the concentration of drug, C, in solution as a function of time, t.

By studying the dissolution of constant surface cylindrical molds of benzoic acid and lead chloride, Noyes and Whitney proposed an equation that could describe the dissolution of such substances [Noyes and Whitney, 1897]. An approximation of this is that the dissolution rate of a drug from a particle or a surface, dm/dt, (where m is mass not dissolved), is proportional to the surface area, a, of the particle, and its solubility, S:

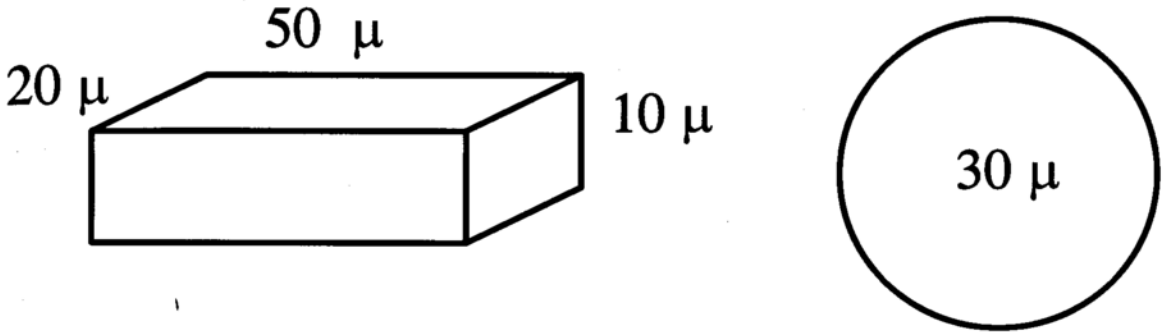

Fig.I.1-1 An actual prismatic particle and its volume equivalent sphere counterpart.

$$\frac{dm}{dt} = -k\,a\,S \qquad \text{(I.2-1)}$$

k is the so-called intrinsic dissolution rate constant. It should be pointed out, at this point, that lower case letters will be used in the following for the volume, v, surface area, a, and mass, m of a *single particle*, whereas capital letters will be used for the total volume, V, the total surface area, A and the total mass, M, of a *polydisperse powder sample*.

Eq. I.2-1 holds in situations where sink conditions apply, i.e. when the concentration, C, is less than 15% of the solubility of the compound. Early work in dissolution attempted to measure k and interpret it, but k is not really a constant, it is a function of the existing hydrodynamics of the dissolution fluid. In the pharmaceutical literature, reports on preformulation studies of new drug candidates advocate the use of the so-called Wood's apparatus for determination of the intrinsic dissolution rate constant under constant surface area conditions [El-Arini and Leuenberger, 1996]. Typically a powder under investigation is compressed under high pressure in a die and this is suspended in the dissolution apparatus so that a constant surface of the powder compact is exposed to the dissolution medium at all times [Carstensen, 1977]. This is futile as far as particulate dissolution is concerned, because the hydrodynamics associated with

this apparatus are different from the hydrodynamics encountered in a USP dissolution apparatus, more so in the case of dissolution of a powder or a solid dosage form [Underwood and Cadwallader, 1976]. It does serve a purpose, for instance, if experiments are carried out at different rotational speeds, for then it is possible to estimate the diffusion coefficient of the drug substance in the dissolution medium.

The important goal of dissolution experiments is to determine the dissolution profile of particles. In the early thirties, Hixson and Crowell developed a theory which took into account the change in surface area of a monodisperse population of spherical particles [Hixson and Crowell, 1931]. This led to the well known cube root law:

$$1-\left(\frac{M}{M_0}\right)^{1/3}=\kappa t \qquad \text{(I.2-2)}$$

where M is the mass undissolved, M_0 is the initial mass, and where the cube root dissolution rate constant, κ, was given by:

$$\kappa=\frac{2kSN^{1/3}}{\rho d_0} \qquad \text{(I.2-3)}$$

ρ is the density, S is the saturation solubility and d_o is the diameter of the monodisperse ensemble of N spherical particles prior to the onset of dissolution. The awareness for polydispersity in a powder sample triggered several interesting approaches to this problem, but all that work was limited to spherical particles. A detailed literature review on this topic will be presented in Chapter III. One of the goals of this thesis is to suggest an approach that enables one to estimate the intrinsic dissolution rate constant of a substance from powder dissolution, using a non-spherical geometry for the single particle.

I.3. Importance of particle size and shape

Processing of pharmaceutical solids, its success and failures, is often ascribed to two parameters: particle size and shape. Particle flow studies have been carried out on wet-processed granulations and the effect of particle size on such properties as flow and repose angles has been investigated [Carstensen and Chan, 1977]. In effect the size and the shape (and the material itself) affects the cohesional forces between particles, which in turn affect the repose angle, and this influences the flow rate. It is known that particle size and shape can affect segregation of powder mixtures, and this has been demonstrated in terms of the so-called Johanson indices [Johanson, 1996]. There are means of measuring

cohesion (Jenike cells) [Carstensen, et al., 1993] but it, in itself, is not sufficient to predict blending behavior of powders. The Barr decision [Carstensen, et al., 1996] is an example of how blending and content uniformity, in recent years have gained immense attention especially for low drug content formulations.

The fact that flow is a function of particle "size" is important, and most studies have used sieve fractions as "samples" and their "mean diameter" as the parameter against which to plot flow rates [Carstensen and Laughlin, 1979]. The "mean diameter" implies the midpoint of the apertures of the two confining screens; one through which the particles pass and the other one which they are retained.

When a concept is used frequently, its basic problems are often ignored. In the present day situation, many NDA's and ANDA's contain information on particle size distribution, however the term "particle size" is still not devoid of ambiguity. At best it can be interpreted as the equivalent spherical diameter.

This tacitly leaves the reader with the impression that only the distribution of a fictitious number is what characterizes the behavior of the drug in the dosage form, or the technological performance of the drug or its dosage form.

There is a need to define "diameter" and "shape", and attempts to do this have been made in the past [Chow et. al, 1989, Lu et. al, 1993]. However, the

only real experimental work in the field is almost 30 years old [Ridgway and Rupp, 1969].

I.4. Particle size

The first question that arises is what is the "size" of a non-spherical particle? The best approximate geometric description of a crystalline substance is by way of a parallelepiped, as shown in Fig. I.4-1. This is the simplest conceivable geometry that can potentially mimic *real* crystal shapes such as needles, platelets, prisms, which are so often encountered in pharmaceutically important solids.

To describe the "size" of such a particle several possibilities present themselves, viz. the longest dimension, i.e., the diagonal AG, length (AD = ℓ), breadth (AB = b) and height, which sometimes is referred to as the thickness (BF = h) in the decreasing order of magnitude. In most situations where microscopy is used, either ℓ or b will be useful, as long as they are used consistently. As far as particle size is concerned, there are certain subtleties with the technique of microscopy which are worth mentioning at this point. The experimentalist has to deal with a very small sample size, which is assumed to be representative of the entire population of a powder. By virtue of a two dimensional image of a particle

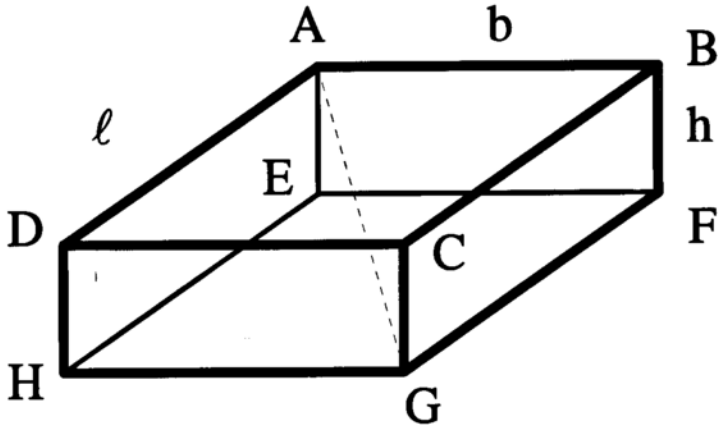

Fig.I.4-2 A parallelepiped: model for real crystals with defined shapes like needles, platelets and prisms.

only two (ℓ and b) of the three principal dimensions can be obtained by microscopy. Also, one does not necessarily know if the crystal lies on side HEFG or on side GCBF. Hence the possibility of the inability to distinguish between b and h, on the part of the experimenter cannot be denied. It is crucial to adopt a suitable sampling procedure to minimize bias in the process of getting a representative sample from the population [Allen, 1968]. The technique encompasses an implicit assumption that the particles orient themselves in the most stable position, so that ℓ and b can be measured without much difficulty.

Though microscopy is a time demanding technique, it has advantages over many other methods in the awareness it inspires of the *particle shape*. A measurement that yields two dimensions of the particle makes more physical sense and also furnishes more information about the particle, than merely knowing the spherical equivalent diameter.

Having made length and breadth measurements on a representative sample, the next step is to present those data in the form of averages. To this end the arithmetic mean size is defined as:

$$x_{avg} = \frac{\sum N_i x_i}{\sum N_i} \qquad \text{(I.4-1)}$$

where N_i is the number of particles with size x_i. This is a logical choice (instead of surface-mean or weight-mean averages), because the number distribution is most pertinent in crystallization [Carstensen and Rodriguez-Hornedo, 1985] and dissolution work [Carstensen and Patel, 1975].

I.5. Particle Size Distributions

Once the specific dimension of the particle to be measured, is identified, the next problem that presents itself is the one of distributions. Much (if not all) of *the work reported in literature assumes a log-normal distribution of the particles* [Carstensen and Patel, 1975, Brooke, 1973].

It should be noted that the mathematical description of a polydisperse powder sample by way of a normal or a log-normal distribution is just an approximation. It must be mentioned that the emphasis on such an approximation is rather statistical, than being scientific. One of the purposes of the work to be described, is to attempt to *make conclusions of particle distributions independent of what the distribution is*. Since a reason for determin-ing particle size distributions is to ascertain, from a quality control specification point of view, that the drug substance dissolves as rapidly or slowly as it should, the approach will be *to use powder dissolution for the actual particle size distribution determination.*

Keeping in mind the general picture of a *real* particle as shown in Fig.I.4-1, it is of interest to investigate which dimension of the particle, for which the distribution parameters are obtained, is "recognized" in such a scenario.

It should be pointed out that if a particle size, a, is approximated by a number distribution function f(a) which is normalized then, of course,

$$\int_{a_{min}}^{a_{max}} f(a)da = 1 \qquad \text{(I.5-1)}$$

It is noted that this simply states that when all the particles are added up they add up to the number of particles in the sample, and that it matters not what the type of function f(a) is. It follows, from statistical principles [Bennett, 1961] that the mean size is the first moment of the function, μ_1, i.e.

$$a_{avg} = \mu_1 = \int_{a_{min}}^{a_{max}} [f(a)][a]da \qquad \text{(I.5-2)}$$

hence it should be possible to obtain a "mean size" without resorting to assumptions of which type of function, f(a), is at play. Furthermore, the second moment, μ_2, is:

$$\mu_2 = \int_{a_{min}}^{a_{max}} [f(a)][a^2]da \qquad \text{(I.5-3)}$$

and from Eq. I.5-2 and I.5-3 it is possible to obtain the standard deviation of the distribution. *It is noted then that one of the purposes of this work is to devise a method for obtaining the mean and the standard deviation of a particle size distribution, regardless of what the distribution function is.*

It is a frequently encountered observation that particulate solids obtained by unit operations like crystallization and milling exhibit skewed size distributions [Carstensen and Patel, 1975]. As mentioned, it is commonplace to assume a log-normal distribution and report a geometric mean, in terms of a spherical equivalent diameter[Carstensen, 1972, Brooke, 1973]. The above proposals would circumvent these assumptions.

I.6. Particle Shape (Non-isometry)

Quantitative descriptions of particle shapes have been proposed many decades back [Heywood, 1937] but the one of importance and relevance to this work is the volume shape factor, α_v, given by:

$$\alpha_v = \frac{v}{a^3} \qquad \text{(I.6-1)}$$

where v is the volume of the particle, and a is any dimension, which could be either the length, breadth or height of a particle. The value of the volumetric shape factor depends on the choice of dimension. Self-consistency would prevail if one identifies the "correct" dimension by microscopy.

Similarly a surface shape factor, α_s, is given by

$$\alpha_s = \frac{\mathcal{A}}{a^2} \qquad \text{(I.6-2)}$$

where $\mathcal{A}$ is the surface area of the particle. These quantities, which were defined by Dallavale, are indicative of the degree of non-isometry associated with a particle [Dallavalle, 1948]. The meaning of this term will be clear to the reader, shortly.

Although these quantities could be measured for an individual particle, their estimation for a polydisperse sample (e.g. a sieve fraction) would be more useful.

When one considers the ratio of surface area to volume the following surface-volume shape factor results:

$$\Gamma = \frac{a}{v^{2/3}} \qquad \text{(I.6-3)}$$

It thus follows that,

$$\Gamma = \frac{\alpha_s}{\alpha_v{}^{2/3}} \qquad \text{(I.6-4)}$$

The Hixson-Crowell cube root law for monodisperse spherical particles can be derived from Eq. I.1-1 by substituting for the area term in Eq. I.6-1.

$$\frac{dm}{dt} = -k\Gamma v^{2/3} S = -k\Gamma \left(\frac{m}{\rho}\right)^{2/3} S \qquad \text{(I.6-5)}$$

On integration of Eq. I.6-5 the cube root equation for a single particle ensues, but it does not lend itself to dissolution of polydisperse systems.

A particle for which Γ (and α_v for that matter) are constant and not a function of the magnitude of its dimensions, is called an *isometric* particle. Cubes, spheres, right circular cylinders (those where the height equals the diameter) are examples of isometric geometries. For such particles, Eq. I.6-5 and the resulting cube root equation holds, but in the case of real particles, for which Γ is not a constant, the non-isometry needs to be addressed. It has been shown that for cylindrical discs [Lai and Carstensen, 1978] and single crystals [Dali and Carstensen, 1996], Γ and hence α_v change with dissolution time. Since these served as models for real particles, it is of interest to decipher the implications of non-isometry on dissolution.

I.7. Isotropy versus Anisotropy

If all the surfaces of a particle dissolve at the same rate in a particular solvent, the dissolution is considered isotropic. Attempts to model the dissolution of polydisperse spheres [Brooke, 1974, Carstensen and Patel, 1975] and of single non-isometric particles [Dali and Carstensen, 1996, Pedersen and Brown, 1976] have resorted to the assumption of isotropic dissolution.

Burt and Mitchell demonstrated crystal *anisotropy* in nickel sulfate α-hexahydrate [Burt and Mitchell, 1979]. Their studies furnished evidence for a higher dissolution rate for the (112) face in comparison with the (111) face. Such preference for dissolution of one particular face has been attributed to differences in the surface free energies of the faces. More importantly, such anisotropic behavior has been encountered with hexamethylmelamine, an anti-tumor drug [Rodley, et al., 1993]. Crystal defects are suggested to play a role in the dissolution anisotropy of aspirin but there is no direct experimental evidence to this effect.

Kitamori and Iga suggested an approach to modeling anisotropy in non-isometric particles by assuming that the dissolution rates of the three different faces of a parallelepiped-like particle are proportional to their respective dimensions [Kitamori and Iga, 1978]. With this being the only theoretical report dealing with anisotropy in multiparticulate systems, experimental support for dissolution anisotropy in polydisperse systems has been a difficult target to achieve because of the complexity of the problem.

CHAPTER II. STATEMENT OF THE PROBLEM

With a formal introduction provided in chapter I, serving as the basis for the contents of this thesis, the following goals can be recognized:

1. To propose a model geometry for non-spherical particles which exhibit defined shapes like needles, platelets and prisms.
2. To develop a method by which the isotropic intrinsic dissolution rate constant can be determined for a powder under *relevant hydrodynamic conditions*, e.g. that of the USP paddle apparatus at a stirrer speed of 50 rpm.
3. To develop a method for determining the volumetric shape factor of crystalline solids confined to sieve fractions.
4. To develop a method for determining particle size distribution parameters from dissolution data.
5. To propose a model that takes into account polydispersity, non-isometry, and anisotropy.

These challenges will be tackled in a systematic manner by first considering a model for a single non-isometric particle assuming isotropic dissolution. The inferences drawn at that stage will contribute to the extension of the model to

multiparticulate systems. In the process, as and when the situation calls for then, the assumptions and limitations of the approach will be stated. The purpose of single crystal dissolution kinetics is to study the dissolution behavior of a non-isometric particle and compare the experimental data with the predictions of a model that takes into account such non-isometry in *real* particulate systems. The implications of terms associated with the shape of the particle (that were alluded to in chapter I) will hopefully become clear at this point, and that shall serve as the basis for the extension of the model to multiparticulate non-isometric systems. To make the problem tractable, isotropic dissolution will be assumed until this stage. The next step would be to develop a methodology to obtain the intrinsic dissolution rate constant and the volumetric shape factor of well-defined crystalline solids. Finally, an attempt will be made to address the issue of anisotropy with regards to powder dissolution and actual particle size distributions.

CHAPTER III. LITERATURE SURVEY

III.1 Fundamental theories of dissolution:

The present day approach to powder dissolution is based on the following laws governing dissolution.

Fick's first law of diffusion [Fick, 1885]

The rate at which a certain quantity of solute, dM, diffuses through a cross sectional plane of area, A, per incremental time dt, when the concentration of the species changes by an amount, dc, through a distance, dx, perpendicular to the plane is given by

$$\frac{dM}{dt} = -DA\frac{dc}{dx} \qquad \text{(III.1-1)}$$

where D is called the diffusion coefficient of the solute. This law is stated for diffusion of the dissolved solute in one direction only. Furthermore it is assumed that D is concentration independent. The distribution of the dissolved solute takes place by such a diffusion process and it can be facilitated by agitation of the liquid. Under conditions of minimal stirring, the forces of diffusion are enabled to

establish equilibrium and thereby reach a uniform state of distribution quite rapidly.

Noyes-Whitney equation [Noyes and Whitney, 1897]

The law governing dissolution of solids in their own solutions was proposed by Noyes and Whitney in 1897. If S is the saturation solubility, C is concentration at any time t, k is the intrinsic dissolution rate constant, and A is the surface area of the dissolving solid then the rate at which this solid would dissolve is given by the Noyes-Whitney equation.

$$\frac{dM}{dt} = kA(S - C) \qquad \text{(III.1-2)}$$

They used cylindrical molds of benzoic acid and lead chloride in their study. The amounts taken were such that the change in the surface area of these cylinders was very small and hence the surface area exposed to the solvent could be considered constant. This law advocates that the rate of dissolution is directly proportional to the difference in the concentration of the saturated solution and the instantaneous concentration.

Nernst believed in his theoretical generalization about the existence of a thin film of saturated solution around the dissolving solid [Nernst, 1904]. He postulated that such a film was formed almost instantaneously around the solid. This hypothesis came in for strong criticism, both from experimental and theoretical standpoints. There was no direct evidence for the presence of such a film and also such rapid rates of attainment of equilibrium were thought of as being far-fetched. The Noyes-Whitney equation has been tested for its validity by other researchers [Carstensen and Musa, 1972, Lu, et al., 1993] and does not rely on any assumptions regarding the diffusion layer. It stands to reason that this equation is used as a vantage point for the derivation of Hixson-Crowell cube root law.

Hixson-Crowell Cube Root Law [Hixson and Crowell, 1931].

As opposed to the Noyes-Whitney equation, the Hixson-Crowell cube root law accounts for the changing surface area of the dissolving solid. As mentioned in chapter I, the following is the mathematical statement of the law.

$$1-\left(\frac{M}{M_0}\right)^{1/3} = K t$$

where M_0 is the initial amount, M is the amount undissolved at any time t and κ is called the cube root dissolution rate constant. κ comprises several other constants such as density (ρ), saturation solubility (S), intrinsic dissolution rate constant (k) of the dissolving solid, total number of spherical particles with initial diameter d_0. A plot of $1-(M/M_0)^{1/3}$ versus time is referred to as the cube root law plot. Thus one would expect a linear relationship between $1-(M/M_0)^{1/3}$ and time. The law is based on following assumptions:

(a) The dissolving particles are spheres, cubes or possess an isometric geometry.

(b) All particles are of the same size, i.e. they are monodisperse.

(c) The dissolution rate is the same throughout the surface of the particle, i.e. dissolution is isotropic.

(d) The solubility is independent of the particle size.

(e) The particles dissolve under sink conditions ($C << S$).

This is the most widely accepted law governing multiparticulate dissolution. Invariably, when one deals with crystalline solids, particles with non-spherical shapes and varying sizes are encountered. Thus one has to deal with practical situations that are beyond the scope of some of the assumptions of this law. The situation where non-sink dissolution conditions can prevail has been considered by Carstensen and Pothisiri and other authors [Pothisiri and

Carstensen, 1973, Yonezawa, et al., 1994]. However, in the present work, dissolution will be considered strictly under sink conditions. As mentioned earlier, the first two assumptions are very unlikely to hold with real particulates. Monodispersity is a rare occurrence in nature. The extremely narrow size distributions exhibited by ragweed pollens is one of such rare incidences [Ramadan and Tawashi, 1990]. Crystalline solids that exhibit extreme shapes like needles and prisms are characterized by high degree of non-isometry in that the ratio of surface area to their volume would be considerably higher than that for equivalent spheres [Rodley, et al., 1993, Chow, et al., 1995]. Such non-isometry is interrelated to the observed anisotropy. For example, in acicular crystal habits, there is a preferentially higher growth rate along one of the principal axes. Since crystallization and dissolution are often visualized as opposite phenomena, one would expect a correspondingly higher dissolution rate along that axis. Finally, the variation of solubility with particle size is given by the Ostwald-Freundlich equation. However, in order to see significant differences in solubility, the particles have to be in the sub-micron range [Martin, et al., 1983]. Hence for all practical purposes, assumption (d) can be considered to be a fairly reasonable one. This thesis is intended to address issues related to the first three assumptions of Hixson-Crowell cube root law. The following section deals

with three prime aspects influencing dissolution kinetics. They are polydispersity, non-isometry, and anisotropy.

III.2. Important considerations in multiparticulate dissolution kinetics:

This section deals with some of the approaches reported in the literature, which were intended to take into account the departures from the assumptions of the cube root law. In most of the theoretical work reported along these lines, the dissolving particles are assumed to be spherical. This is especially true in the case of polydispersity. Pedersen and Brown have developed equations for the isotropic dissolution of *single* particles belonging to six crystal systems [Pedersen and Brown, 1976]. However, in order to apply those equations to real powders they had to introduce an equivalent spherical diameter for each particle. The only attempt to model anisotropy in polydisperse systems is by Kitamori and Iga [Kitamori and Iga, 1978]. However, the theoretical approach put forth by these authors was flawed by the paradox in their assumptions. In short, a challenge as it stands, modeling polydispersity, non-isometry, and anisotropy all in one, still poses itself as an unresolved research problem.

Polydispersity

Hintz and Johnson have shown that differences in particle size distribution of a blend of poorly-soluble drug with its excipients can lead to differences in blood plasma levels [Hintz and Johnson, 1989]. It is known that particulate solids prepared by procedures like crystallization, precipitation, and milling exhibit skewed size distributions [Carstensen and Patel, 1975]. Thus it is quite common to ascribe a functional relationship to the distribution. A good approximation for most commonly encountered particle size distributions is a *log-normal* distribution function [Carstensen and Musa, 1972, Brooke, 1973, Irani and Callis, 1963]. The mathematical form of this function and its utility in powder dissolution is discussed in detail in this section. It must be mentioned that this discussion on polydispersity pertains to spheres. This part is intended to give the reader an overview of the manner in which polydispersity has been treated so far.

Higuchi et. al used the following simplified expression for the distribution function [Higuchi, et al., 1963].

$$g(r_0) = \frac{A}{(r_0)^2} \qquad \text{(III.2-1)}$$

where r_0 denotes the initial radii of the particles in the given distribution and A is a constant. Carstensen and Musa embellished this by considering a more appropriate function for the particle size distribution [Carstensen and Musa, 1972]. They used the following equation for the probability frequency of a particle of diameter a_0, which was based on the number of particles in the system.

$$f(a_0) = \frac{1}{(\ln \sigma')\sqrt{2\pi}} . \exp\left[\frac{-(\ln \mu' - \ln a_0)^2}{2(\ln \sigma')^2}\right] \qquad \text{(III.2-2)}$$

where σ' is the geometric standard deviation and μ' is the geometric mean of the distribution. Simply stated, a *log-normal* distribution of particles is one in which the logarithm of diameters of the particles are normally distributed. In a realistic situation, there will be a maximum diameter, a_0^{max} and a minimum diameter, a_0^{min} for a given distribution of particles. These two truncations were assumed to be at $\pm 3 \ln\sigma$ units from the geometric mean, respectively. The diameters decrease as a function of dissolution time. It can be shown from the Noyes-Whitney equation that

$$a = a_0 - \left(\frac{2kS}{\rho}\right)t = a_0 - \tau \qquad \text{(III.2-3)}$$

The theoretical basis [Dali and Carstensen, 1996] for Eq. III.2-3, and its experimental validation for single crystals [Schoonen, et al., 1979] and polydisperse powders [Edmundson and Lees, 1965], has been well documented. As dissolution begins, there will be a phase in which the particles simply decrease in size but the total number remains the same. As the particles dissolve, there will a definite instant in time when the smallest particle completely disappears. From this point onwards, the number of particles in the system begin to decrease continuously. The time when this happens is referred to as the *critical time*. Such a transition is manifested in the form of a "break" in the cube root law plot [Carstensen and Patel, 1975, Swarbrick and Ma, 1981]. Carstensen and Musa were the first investigators to suggest a mathematical approach for dissolution before and after the *critical time* [Carstensen and Musa, 1972]. As long as the total number of particles in the dissolution medium remains unchanged, the amount undissolved can be calculated from the *initial* number distribution of the particles by numerical integration. At this stage it becomes pertinent to discuss this approach in depth because there have been instances in the literature where the integrand and the limits of integration are inconsistent with each other, or

where the limits of integration do not reflect actuality [Brooke, 1973, Carstensen and Musa, 1972].

For the sake of argument consider an ensemble of N polydisperse spherical particles whose diameters a_0 are log-normally distributed with a geometric mean μ' and geometric standard deviation σ'. Let a_0^{min} and a_0^{max} be the minimum and maximum diameters in the distribution respectively. Each particle dissolves according to Eq. III.2-3 and the *initial* frequency distribution function of these N particles is given by Eq. III.2-2. If ρ is the true density of the particles then the amount undissolved at any time t before the critical time is given by the following expression.

$$M = N\rho\left(\frac{\pi}{6}\right) \int_{\ln(a_0^{min})}^{\ln(a_0^{min})} \left[(a_0 - \tau)^3 f(a_0) d\ln a_0\right] \qquad \text{(III.2-4)}$$

It must be emphasized that this is the only correct approach to calculate the amount undissolved before the critical time. As long as the total number of particles in the system remains unchanged, the product $f(a_0)d\ln a_0$ would remain the same for a certain interval $d\ln a_0$. As the particles dissolve, the number distribution indeed shifts to a lower geometric mean, but the shape of the

distribution remains the same [Pedersen and Brown, 1975]. Hence until the critical time one can use Eq. III.2-4 and the limits of integration need not be changed.

Not all distributions are log-normal. Sieve fractions of log-normally distributed powders have been shown to follow a normal distribution [Carstensen and Patel, 1975, Steiner, et al., 1974]. In such a case a normal distribution function for $f(a_0)$ is in order. Whatever the distribution function is, the approach of using the initial size distribution until the critical time still holds.

Yet another approach to model polydispersity is population balance modeling [LeBlanc and Fogler, 1987]. It also requires assuming a certain distribution function for the particles. The approach calls for a mass balance for the rate of dissolution of the particles into and out of an infinitesimally small increment of the diameter. This kind of treatment is popular among the engineers who have studied other particle shrinkage processes like combustion, grinding, and sublimation.

Non-isometry

Isometrics are those shapes for which the ratio of their area to $(\text{volume})^{2/3}$ is independent of the dimensions. Thus a sphere, a cube and a right circular cylinder are examples of isometric shapes. The surface-volume shape factor is given by this ratio.

$$\Gamma = \frac{A}{V^{2/3}} \qquad \text{(III.2-5)}$$

As a sphere dissolves, at any given time, the distances between the center and every point on the surface of the sphere are the same. Hence for any isometric, Γ does not change with dissolution time. For a non-isometric particle, like a non-right circular cylinder or a parallelepiped, Γ depends on the dimensions of the particle. Hence, one would expect Γ for such a particle to change as a function of dissolution time. The influence of shape factors on dissolution kinetics of drugs has been studied for tablets and sustained release tablets [Cleave, 1965, Cobby, et al., 1974a, Cobby, et al., 1974b], but very little attention has been given to dissolution of single drug particles [Lai and Carstensen, 1978].

Pedersen and Brown developed equations to describe the isotropic dissolution of single particles belonging to six crystal systems [Pedersen and

Brown, 1976a]. Their approach involves calculating the diameter of hypothetical spherical particles whose dissolution approximates non-spherical particles. Based on the specified dimensions of the non-spherical particle, a univariate distribution for particle size was obtained. The applicability of their theory was tested on a -60/+85 mesh fraction of tolbutamide [Pedersen and Brown, 1976b]. However, the method called for assuming a single particle model and a corresponding intrinsic dissolution rate constant. Though the experimental set-up and theoretical considerations in their work were impeccable, this was not a direct method of determining the intrinsic dissolution rate constant of the drug substance.

To elucidate the effect of particle shape on dissolution kinetics, Kitamori and Iga suggested a three-dimensional approach to the problem [Kitamori and Iga, 1978]. They developed an equation for dissolution of powders whose particles are rectangular parallelepipeds and are log-normally distributed. Their model was an improvisation of Brooke's model for spherical particles [Brooke, 1974]. The shape effect in cubes, needles, and plates was examined on the basis of this theory. Exactly calculated dissolution profiles indicated differences in the dissolution behavior by virtue of differences in particle shape. These authors did not furnish any experimental evidence to corroborate their theory. This is another instance where one has to work from a vantage point at which the intrinsic

dissolution rate constant has to be known in order to calculate the dissolution profiles.

Lai and Carstensen proposed a cylindrical geometry to mimic real particles like needles and platelets [Lai and Carstensen, 1978]. They presented a methodology by way of which one can calculate the change in shape factor (Γ) of a dissolving cylinder as a function of dissolution time. In their study they used compressed discs of oxalic acid as models for non-isometric single particles. Dissolution studies on these indicated an upward curvature in the cube root law plot. Such a deviation in the cube root dissolution behavior was speculated to be due to the non-isometry of the dissolving cylinder. It was shown that the shape factor does not vary much from its initial value until about 50% of the total dissolution time and after that point it increases quite rapidly.

Lu, Frisella, and Johnson used the same concept to show that a cylindrical geometry was a better model than spheres to describe the dissolution of hydrocortisone powder [Lu, et al., 1993]. In an attempt to explore the contribution of hydrodynamics in multiparticulate dissolution, they included in their model a time-dependent diffusion layer with thickness h. However the computer simulations failed to show any improvement in the agreement between

experimental data and predictions of the model as a result of the consideration of the time-dependent diffusion layer.

Anisotropy

The phenomenon by which different faces of a crystal can dissolve at different rates is called dissolution anisotropy. Burt and Mitchell demonstrated dissolution anisotropy in nickel sulfate α-hexahydrate crystals [Burt and Mitchell, 1979]. A careful study showed that the (112) face of the crystal dissolved at a faster rate than the (111) face under mixed surface-transport controlled conditions. This behavior was speculated to be due to the differences in the surface free energies of the two faces because of differences in the arrangement and packing densities of the atoms on the surface. If different faces of the same crystal dissolved at different rates then it would be possible that modification of the crystal habit of such a compound would lead to differences in bulk dissolution rates [Burt and Mitchell, 1980, Carstensen, 1973].

Dissolution anisotropy can also be a result of crystal defects [Frank, 1949]. They are broadly classified into point defects and line defects; thermodynamically speaking, the former being stable and the latter being unstable. Point defects are those where there is a vacant site in the crystal lattice or there is the presence of a

foreign atom occupying interstitial or substitutional positions in the crystal lattice. Line defects, or dislocations as they are termed, are characterized by a discontinuity in a whole lattice array. It is believed that crystals with higher dislocation density would be metastable with respect to the one with a lower dislocation density and hence lead to a higher dissolution rate for the former. Whether or not such anisotropy is observed depends upon whether the dissolution is surface-controlled or transport-controlled. Anisotropy due to crystal defects is suggested to play a role in the dissolution of aspirin, but there is no direct experimental evidence of this effect [Mitchell, et al., 1971]. Burt and Mitchell studied the effect of mean dislocation density (dd) in potassium perchlorate crystals and found that the observed dissolution rate constant for crystals with a higher dd was greater than the ones having a lower dd [Burt and Mitchell, 1981].

Chow and Grant have presented a semi-empirical relationship between the intrinsic dissolution rate constant and certain physical and thermo-chemical properties of acetaminophen crystals doped with p-acetoxyacetanilide as an impurity [Chow and Grant, 1989]. These authors adopted a simplistic approach to model crystal anisotropy. The length to width ratio of the acicular crystals was used as a measure of crystal anisotropy. The entropy of fusion was the suggested means of quantitating crystal defects. Though their treatise may be a subject of

debate, to the best of my knowledge, this was the first attempt to correlate the intrinsic dissolution rate constant with such factors as crystal anisotropy, habit-related hydrodynamic conditions during dissolution, and crystal defects. In more recent years, Rodley et.al have shown evidence for anisotropy in crystals of hexamethylmelamine, an anti-tumor drug [Rodley, et al., 1993]. Through single crystal experiments it was observed that the ends of the crystal dissolve at a faster rate than the edges. Recently, studies conducted on single crystals of acetaminophen have shown differences in the etching abilities of certain non-aqueous solvents on the (001) and the (010) crystal faces [Vasil'Chenko, et al., 1996]. It was suggested that the arrangement of hydrogen bonds in the crystal structure plays an important role in the observed anisotropy.

Almost all of the work reported on anisotropic dissolution has been with single crystals except for the work by Kitamori and Iga, which is a theoretical presentation with no experimental support [Kitamori and Iga, 1978]. Anisotropy in multiparticulate dissolution kinetics still continues to be an area unexplored.

CHAPTER IV. THEORETICAL CONSIDERATIONS

This chapter is intended to provide the reader with an overall view of the theoretical considerations of this thesis. With a non-isometric geometry in mind, it is important to consider the single particle dissolution kinetics from a theoretical and experimental standpoint. The primary purpose of studying single crystal dissolution kinetics is to present the case of a non-spherical particle, with a shape that is representative of commonly observed crystal habits. One aspiration of this writing is to construct the link between single particle dissolution kinetics and multiparticulate dissolution kinetics for *real* crystalline solids. In the process, several terms will have to be defined, and they will be dealt with in detail. The motivation for considering a non-isometric geometry as a model for a single particle will become apparent, as this chapter makes its transition to the multiparticulate regime, at the point where volumetric shape factors are encountered.

The assumptions made in the model are stated, wherever pertinent. The model for dissolution of a single non-isometric particle is discussed first followed by the one for dissolution of an ensemble of parallelepipeds, assuming isotropic

dissolution. Finally, an approach to consider anisotropy in multiparticulate dissolution kinetics is suggested.

IV.1 Model for the isotropic dissolution of a single non-isometric particle [Dali and Carstensen, 1996]

The *model geometry* is a parallelepiped (as shown in Fig. I.4-1, reproduced here for convenience) and the *target crystal habits* are platelets, needles, and prisms.

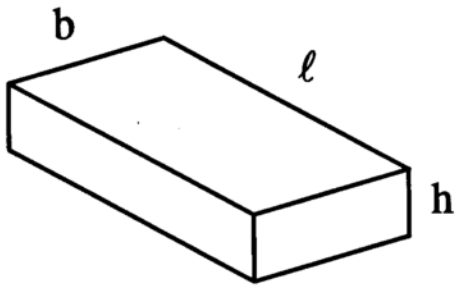

ℓ = length of the particle at any time t

b = breadth of the particle at any time t

h = height of the particle at any time t

The surface area and volume are given by,

$$\text{Area, } a = 2(\ell\, b + bh + \ell\, h) \qquad \text{(IV.1-1)}$$

$$\text{Volume, } v = \ell\, bh \qquad \text{(IV.1-2)}$$

If ℓ_0, b_0, and h_0, are the initial length, breadth, and height of the particle respectively, then we can define the following shape ratios:

$$m = \frac{\ell_0}{b_0} \qquad \text{(IV.1-3)}$$

$$\text{and} \quad n = \frac{h_0}{b_0} \qquad \text{(IV.1-4)}$$

Initial surface-volume shape factor is $\Gamma_0 = \frac{a_0}{v_0^{2/3}} = \frac{2(\ell_0 b_0 + b_0 h_0 + \ell_0 h_0)}{(\ell_0 b_0 h_0)^{2/3}}$

If the geometry of the particle is based on the breadth of the particle (the dimension conventionally considered to be "seen" by sieve analysis) then the initial area and initial volume of the particle can be written in the following form:

$$a_0 = \alpha_{s0} (b_0)^2 \qquad \text{(IV.1-5)}$$

$$\text{and} \quad v_0 = \alpha_{v0} (b_0)^3 \qquad \text{(IV.1-6)}$$

where α_{s0} and α_{v0} are the initial surface and volume shape factors for the parallelepiped particle [Dallavalle,]. From Eqs. (IV.1-1) to (IV.1-4) it can be shown that

$$\alpha_{s0} = 2(m+n+mn) \qquad \text{(IV.1-7)}$$

and

$$\alpha_{v0} = mn \qquad \text{(IV.1-8)}$$

The three shape factors are related by the following equation:

$$\Gamma_0 = \frac{\alpha_{s0}}{(\alpha_{v0})^{2/3}} \qquad \text{(IV.1-9)}$$

It is quite obvious that as the particle dissolves in a medium, its dimensions decrease, and hence the shape factors would undergo a change from their initial values. The question then is, how do these shape factors change with dissolution time, and how significant is this change?

The following assumptions are made. All faces of the particle, like the one shown in Fig.I.4-1, dissolve at the same rate of k distance units per unit time(isotropy). It is assumed that the particle retains its shape for most of its

dissolution lifetime. When the smallest dimension (height of the crystal) goes to zero the particle is dissolved. It is assumed that dissolution proceeds under sink conditions.

The immediate goal is to arrive at an expression for the fraction undissolved for a single non-isometric particle. The Noyes-Whitney equation is an appropriate starting point.

$$\frac{dm}{dt} = -k\alpha(S-C) \qquad \text{(IV.1-10)}$$

Under sink conditions, $C << S$, thus Eq.IV.1-10 becomes

$$\frac{dm}{dt} = -k\alpha S \qquad \text{(IV.1-11)}$$

Expressing mass in terms of volume and density

$$m = \rho v$$

Hence,

$$\frac{dm}{dt} = \rho \frac{dv}{dt} \qquad \text{(IV.1-12)}$$

Substituting Eqs. (IV.1-1) and (IV.1-12) in Eq. (IV.1-11) gives

$$\rho\frac{dv}{dt}=-2kS(\ell b+b h+\ell h)) \qquad \text{(IV.1-13)}$$

Since v is a composite function of ℓ, b, and h, the rate of change of volume with respect to time can be written as,

$$\frac{dv}{dt}=\left(\frac{dv}{d\ell}\right)\left(\frac{d\ell}{dt}\right)+\left(\frac{dv}{db}\right)\left(\frac{db}{dt}\right)+\left(\frac{dv}{dh}\right)\left(\frac{dh}{dt}\right) \qquad \text{(IV.1-14)}$$

Treating these as partial derivatives the following equation is obtained:

$$\frac{dv}{dt}=bh\left(\frac{d\ell}{dt}\right)+\ell h\left(\frac{db}{dt}\right)+\ell b\left(\frac{dh}{dt}\right) \qquad \text{(IV.1-15)}$$

Combining Eqs. (IV.1-13) and (IV.1-15), now yields:

$$bh\left(\frac{d\ell}{dt}\right)+\ell h\left(\frac{db}{dt}\right)+\ell b\left(\frac{dh}{dt}\right)=-\frac{2kS}{\rho}(\ell b+b h+\ell h) \qquad \text{(IV.1-16)}$$

$$\frac{1}{\ell}\left(\frac{d\ell}{dt}\right)+\frac{1}{b}\left(\frac{db}{dt}\right)+\frac{1}{h}\left(\frac{dh}{dt}\right)=-\frac{2kS}{\rho}\left(\frac{1}{\ell}+\frac{1}{b}+\frac{1}{h}\right) \qquad \text{(IV.1-17)}$$

$$\frac{1}{\ell}\left(\frac{d\ell}{dt}\right)+\frac{1}{b}\left(\frac{db}{dt}\right)+\frac{1}{h}\left(\frac{dh}{dt}\right)=-\frac{K}{\ell}-\frac{K}{b}-\frac{K}{h} \qquad \text{(IV.1-18)}$$

where $K = \frac{2kS}{\rho}$

Hence it follows that,

$$\frac{d\ell}{dt}=\frac{db}{dt}=\frac{dh}{dt}=-K \qquad \text{(IV.1-19)}$$

Eq. (IV.1-19) implies isotropic dissolution and complies with the model proposed by Kitamori and Iga [Kitamori and Iga, 1978]. If ℓ_0, b_0, and h_0 are the initial length, breadth and height of the particle, then Eq. (IV.1-19) integrates to give the following expressions:

$$\ell = \ell_0 - Kt \qquad \text{(IV.1-20)}$$

$$b = b_0 - Kt \qquad \text{(IV.1-21)}$$

$$h = h_0 - Kt \qquad \text{(IV.1-22)}$$

At this point a quantity u called the reduced time is introduced. This quantity indicates the extent of dissolution of the smallest dimension of the parallelepiped. The motivation for defining such a term will be evident shortly.

$$u = 1 - \frac{h}{h_0} \qquad \text{(IV.1-23)}$$

A similar approach was adopted by Lai and Carstensen while studying the dissolution of compact discs of oxalic acid dihydrate [Lai and Carstensen, 1978]. They modeled the situation for a cylindrical geometry and used the diameter of the cylinder as the basis for defining the reduced time. This parameter u, is indicative of the extent of dissolution of a single particle based on its smallest dimension. The particle would disappear from the dissolution medium, when the smallest dimension, h goes to zero. It is clear that u has to be a dimensionless, real, positive number whose domain is [0,1]. Thus the entire dissolution event for a single crystal can be scaled down to this domain. If one is able to obtain an estimate of u from dissolution data, then it would be possible to get information

about the change in Γ and α_v for a single non-isometric crystal. It will be shown that there is a one-to-one correspondence between u and t.

Combining Eq.(IV.1-22) and Eq.(IV.1-23),

$$u = \frac{Kt}{h_0} \qquad \text{(IV.1-24)}$$

Substituting Eq.(IV.1-24) in Eqs.(IV.1-20), (IV.1-21), and (IV.1-22) the following equations ensue:

$$\ell = \ell_0 - uh_0 \qquad \text{(IV.1-25)}$$

$$b = b_0 - uh_0 \qquad \text{(IV.1-26)}$$

$$h = h_0 - uh_0 \qquad \text{(IV.1-27)}$$

These equations imply that if we can obtain u from dissolution data then we can get information about all the shape factors as a function of dissolution time. Single crystal dissolution studies play an important role in this respect.

Substituting for K in Eq. (IV.1-24) the following relationship between u and t is obtained:

$$u = \left(\frac{2kS}{\rho h_0}\right) t \qquad \text{(IV.1-28)}$$

Thus a linear relationship exists between u and t. The slope of the plot of u versus t gives an estimate of the intrinsic dissolution rate constant, if all other quantities are determined experimentally.

The reduced time u can be obtained indirectly from the fraction undissolved in the following manner.

$$F = \frac{m}{m_0} = \frac{\ell bh}{\ell_0 b_0 h_0} = \frac{(\ell_0 - uh_0)(b_0 - uh_0)(h_0 - uh_0)}{\ell_0 b_0 h_0}$$

$$F = [1-u]\left[1-\left(\frac{h_0}{b_0}\right)u\right]\left[1-\left(\frac{h_0}{\ell_0}\right)u\right] \qquad \text{(IV.1-29)}$$

This is a third degree polynomial in u. F can be obtained experimentally and Eq. (IV.1-29) can be solved for u. The criterion for selecting the "correct" root of the possible three is that it should be a real number between 0 and 1.

Logically, the next step would be to obtain Γ and α_v from u.

$$\Gamma = \frac{2(\ell b + bh + \ell h)}{(\ell bh)^{2/3}} \qquad \text{(IV.1-30)}$$

By substituting for ℓ, b, and h, Γ and α_v can be written in terms of ℓ_0, b_0, h_0, and u.

$$\Gamma = 2\left\{\frac{\left[\left(\frac{\ell_0}{h_0}-u\right)\left(\frac{b_0}{h_0}-u\right)\right]^{1/3}}{(1-u)} + \frac{\left[(1-u)\left(\frac{b_0}{h_0}-u\right)\right]^{1/3}}{\left(\frac{\ell_0}{h_0}-u\right)} + \frac{\left[(1-u)\left(\frac{\ell_0}{h_0}-u\right)\right]^{1/3}}{\left(\frac{b_0}{h_0}-u\right)}\right\}$$

..... (IV.1-31)

$$\alpha_v = \frac{\ell h}{b^2} = \frac{\left(\frac{\ell_0}{h_0}-u\right)(1-u)}{\left(\frac{b_0}{h_0}-u\right)^2} \qquad \text{(IV.1-32)}$$

Since there exists a linear relationship between u and t Eqs. (IV.1-31) and (IV.1-32) also reveal the time dependencies of Γ and α_v. These expressions can be used for non-isometric particles that can be approximated to a parallelepiped.

The Hixson-Crowell cube root law can be derived from the Noyes-Whitney equation by taking into account the changing surface area of a dissolving particle. By substituting for the surface area term in the modified form of Noyes-Whitney equation under sink conditions, the dissolution rate of a single non-isometric particle is given by:

$$\frac{dm}{dt} = -k\Gamma v^{2/3} S = -k\Gamma \left(\frac{m}{\rho}\right)^{2/3} S$$

For isometrics like spheres, right circular cylinders, and cubes Γ is constant ($[6^{2/3}\pi^{1/3}]$, $[3x2^{1/3}\pi^{1/3}]$, and [6]) respectively, independent of their dimensions. For a parallelepiped, Γ is given by Eq.(IV.1-31). For a spherical particle, or a mondisperse population of spherical particles, integration of the above equation results in the cube root law. But for a single non-isometric particle, it would be desirable to obtain the time dependency of Γ in a more simplified mathematical form, than Eq. (IV.1-31).

At this juncture, it is important to note that to know more about the change in Γ and α_v, single crystal dissolution experiments take precedence over any further analysis in this direction. The goal at this point would be to obtain a functional relationship between Γ and dissolution time and to account for that in

the derivation of the cube root law for non-isometric particles. Concomittantly, inferences about how the volumetric shape factor changes with respect to dissolution time can be drawn as well. It is of interest, to compare the predictions of the model with actual experimental data for single crystals. The choice of single crystals used in this study will be dictated by their geometry. The results and discussion, pertaining to single crystal dissolution can be found in chapter VI.

IV.2. Model for the isotropic dissolution of a polydisperse ensemble of parallelepipeds

As mentioned in chapter II, there are three reasons to consider the extension of the model for a single non-isometric particle to multiparticulate systems. (i) To obtain the intrinsic dissolution rate constant of a substance from powder dissolution under *realistic* hydrodynamic conditions. (ii) From a shape perspective, to characterize a sieve fraction of the substance with an *average* volumetric shape factor. (iii) To obtain particle size distribution parameters for a crystalline powder, independent of its distribution, from powder dissolution.

The following assumptions are made in this model: All the particles dissolve at a same overall rate of K distance units per unit time. The distribution parameters of

a sample drawn from a powder population will be assumed to be representative of the whole sample. Typically, a powder will be segregated into several sieve fractions. The particles in each sieve fractions will be characterized by an average volumetric shape factor. It is not unreasonable to expect a certain distribution of α_{v0} within a sieve fraction. So the validity of the assumption about assigning a particular average value α_{v0} for a sieve fraction, depends upon how "narrow" this distribution is. As discussed in chapter III, dissolution until the critical time (time when the smallest particle dissolves completely) will be considered. It will be assumed that average α_{v0} does not change significantly until the critical time. The following methodology is based on the second dimension of the particle (breadth) because it has been observed that the mesh size of a sieve in particle size determination by sieve analysis, usually corresponds to the breadth of the particle. Experimentally, it may not be feasible to measure the height of the crystal. Finally, sink conditions will be maintained during dissolution.

Let $f(b_0)$ be the initial distribution of breadths of an ensemble of N particles, b_0^{min} and b_0^{max} be the minimum and maximum breadths in that distribution, α_{v0} be the initial average volume shape factor of any particle and let

ρ be the true density of the powder. The mass of any particle with breadth b_0 at time t is given by,

$$m = \rho\alpha_{v0}(b_0 - Kt)^3 \qquad \text{(IV.2-1)}$$

As discussed in chapter III.2, mass undissolved until the critical time is given by the following integral:

$$M = \int_{b_0^{min}}^{b_0^{max}} \left[N\rho\alpha_{v0}(b_0 - Kt)^3 f(b_0) db_0 \right] \qquad \text{(IV.2-2)}$$

If α_{v0} is constant until the critical time then Eq.(IV.2-2) would be a third degree polynomial in t. Further discussion about α_{v0} will be carried out in chapter VI. Expanding the cubed term in Eq. (IV.2-2), the following equation ensues:

$$M = \int_{b_0^{min}}^{b_0^{max}} \left[N \rho \alpha_{v0} (b_0)^3 f(b_0) db_0 \right] -$$

$$N\rho\alpha_{v0} \left\{ \int_{b_0^{min}}^{b_0^{max}} \left[3(b_0)^2 K f(b_0) db_0 \right] t - \int_{b_0^{min}}^{b_0^{max}} \left[3 b_0 K^2 f(b_0) db_0 \right] t^2 + \int_{b_0^{min}}^{b_0^{max}} \left[K^3 f(b_0) db_0 \right] t^3 \right\}$$

..... (IV.2-3)

The first term in Eq.(IV.2-3) is the initial mass of the powder, M_0. Thus the fractional amount undissolved can be expressed as,

$$\frac{M}{M_0} = 1 - \left\{ \frac{\int_{b_0^{min}}^{b_0^{max}} \left[3(b_0)^2 f(b_0) db_0 \right] Kt - \int_{b_0^{min}}^{b_0^{max}} \left[3 b_0 f(b_0) db_0 \right] K^2 t^2 - \int_{b_0^{min}}^{b_0^{max}} \left[f(b_0) db_0 \right] K^3 t^3}{\int_{b_0^{min}}^{b_0^{max}} \left[(b_0)^3 f(b_0) db_0 \right]} \right\}$$

..... (IV.2-4)

In order to calculate K and α_{v0}, information from two different experiments viz., *dissolution* (fraction dissolved as a function of time) and *particle size analysis* (distribution of the two measurable dimensions of single particles) is required. The observables M/M_0, b_0^{min}, b_0^{max}, and $f(b_0)$ can thus be obtained

experimentally. The integrals in Eqs.(IV.2-3) and (IV.2-4) can be evaluated by numerical methods once the function $f(b_0)$ is known. A multiple regression analysis on the actual dissolution data can be done to obtain the coefficients of the third degree polynomial in t, as dictated by Eqs.(IV.2-3) and (IV.2-4). The stage is now set for the calculation K. The *intrinsic dissolution rate constant*, k, is related to K through the following expression.

$$K = \frac{2kS}{\rho}$$

There is more to the integrals in Eq.(IV.2-4) than what meets the eye.

For convenience, the integrals are denoted as follows.

$$I_0 = \int_{b_0^{min}}^{b_0^{max}} [f(b_0)db_0] \qquad \text{(IV.2-5)}$$

$$I_1 = \int_{b_0^{min}}^{b_0^{max}} [b_0 f(b_0)db_0] \qquad \text{(IV.2-6)}$$

$$I_2 = \int_{b_0^{min}}^{b_0^{max}} [(b_0)^2 f(b_0)db_0] \qquad \text{(IV.2-7)}$$

$$I_3 = \int_{b_0^{min}}^{b_0^{max}} \left[(b_0)^3 f(b_0) db_0 \right] \qquad \text{(IV.2-8)}$$

If the number frequency distribution function $f(b_0)$ is normalized to the total number of particles in the distribution, then the value of the integral I_0 should be unity. The quantity ($I_3.N.\rho.\ \alpha_{v_0}$) gives the initial weight of the powder. I_1 is the *mean* of the distribution and the variance is given ($I_2 - I_1^2$). Working backwards, if the intrinsic dissolution rate constant for a substance under a certain set of conditions is known, then there is a means of obtaining the distribution parameters. Most powders can be approximated to a normal or a log-normal distribution. Hence the integrals in Eqs.(IV.2-5) through (IV.2-8) can be evaluated by routine numerical integration. At this point, a note on distributions is in order. It is not imperative to approximate the observed size distribution to a Gaussian or a log-normal distribution function. The integrals I_0 through I_1 may also be evaluated simply from frequency histograms by the trapezoidal rule.

Another attractive feature of this model is that one can obtain an estimate of the average initial volume shape factor of a crystalline sample. From Eq.(IV.2-3) it is obvious that, if we can estimate the total number of particles in a sample which is to undergo dissolution, then α_{v_0} for that sample can be

estimated. For such a parameter to make any physical sense, it would be desirable to have particles with a narrow distribution for the length to breadth ratio. α_{v0} estimated from dissolution data can be compared with the one that can be obtained from particle size analysis. The details of this approach are discussed in chapter VI.

So far, the average α_{v0} for the dissolving particles has been considered to be constant until the critical time. The single crystal dissolution experiments will hopefully provide some information about the change in shape factors as a function of dissolution time. If α_{v0} changes with dissolution time then the following questions ensue:

(1) What is the nature of this change?

(2) Is the assumption about α_{v0} before the critical time a valid one?

These issues are addressed in chapter VI.

IV.3. Model for the anisotropic dissolution of a polydisperse ensemble of parallelepipeds

To date there has been only one citation in the literature that has addressed the issue of anisotropy in polydisperse systems [Kitamori and Iga, 1978]. These authors assigned three different rate constants to the three parallel faces, these

constants being proportional to the corresponding lengths of those faces. The model described in this section intends to address polydispersity and anisotropy by assigning certain parameters, and to arrive at relationships between these parameters and mass undissolved.

This model does not require any assumption regarding the volumetric shape factor. However, there are other simplications that need to be invoked, in order to render the problem amenable. Also an attempt has been made to model anisotropy in polydisperse systems.

For a polydisperse sample of prismatic particles, one can visualize a corresponding distribution of the lengths, breadths, and heights of the individual particles. As mentioned earlier, most particle size distributions can be approximated to a normal or log-normal distribution. Powders obtained by processes like crystallization can be approximated to log-normal distribution. In order to characterize the distribution of such powders it is sufficient to know the geometric mean and the geometric standard deviation of their respective dimensions. Distributions of real particles are truncated, as there exists a minimum and a maximum dimension. It is safe to truncate at ±3 geometric standard deviations, which accounts for 99.74% of an "ideal" distribution. In this model, anisotropy is modeled by assigning different rate constants to the

individual pair of faces of the parallelepiped. The following nomenclature is used:

$$\ln(\mu_\ell') = \mu_\ell\,,\ \ln(\mu_b') = \mu_b\,,\ \ln(\mu_h') = \mu_h$$

$$\ln(\sigma_\ell') = \sigma_\ell\,,\ \ln(\sigma_b') = \sigma_b\,,\ \ln(\sigma_h') = \sigma_h$$

A list of all the parameters with their meanings is given in Table IV.3-1.

The following assumptions have been invoked in the model:

1. The individual dimensions of the particles are log-normally distributed.
2. The particles dissolve under sink conditions.
3. There are differences in the rates of dissolution of different faces of the particle but those rates are same for different particles.
4. The distribution is truncated at ±3 geometric standard deviations, i.e.,

$$l_0^{max} = \exp[\mu_l + 3\sigma_l] \qquad \text{(IV.3-1)}$$

$$l_0^{min} = \exp[\mu_l - 3\sigma_l] \qquad \text{(IV.3-2)}$$

$$b_0^{max} = \exp[\mu_b + 3\sigma_b] \qquad \text{(IV.3-3)}$$

$$b_0^{min} = \exp[\mu_b - 3\sigma_b] \qquad \text{(IV.3-4)}$$

$$h_0^{max} = \exp[\mu_h + 3\sigma_h] \qquad \text{(IV.3-5)}$$

$$h_0^{min} = \exp[\mu_h - 3\sigma_h] \qquad \text{(IV.3-6)}$$

Table IV.3-1 Variables that describe the polydispersity and anisotropy of the multiparticulate system.

Dimension	Maximum (microns)	Minimum (microns)	Geometric mean (microns)	Geometric standard deviation	Dissolution rate constant μ/unit time
Length	ℓ_0^{max}	ℓ_0^{min}	μ_ℓ	σ_ℓ	K_ℓ
Breadth	b_0^{max}	b_0^{min}	μ_b	σ_b	K_b
Height	h_0^{max}	h_0^{min}	μ_h	σ_h	K_h

5. Since it is not feasible to measure the smallest dimension of fine particles the following simplifying assumption needs to be made. The particles are considered to be tetragonal in that the height is set equal to the breadth. Thus it follows that $\mu_b = \mu_h$, and $\sigma_b = \sigma_h$. This simplifies to a two-dimensional problem.

As a result of this the number of parameters reduce to the following:

Dimension	Maximum (microns)	Minimum (microns)	Geometric mean (microns)	Geometric standard deviation	Dissolution rate constant μ/unit time
Length	ℓ_0^{max}	ℓ_0^{min}	μ_ℓ'	σ_ℓ	K_ℓ
Breadth	b_0^{max}	b_0^{min}	μ_b'	σ_b	K_b

6. If the following relationships are defined,

$$P = \frac{\mu_\ell'}{\mu_b'} \qquad \text{(IV.3-7)}$$

$$Q = \frac{\sigma_\ell}{\sigma_b} \qquad \text{(IV.3-8)}$$

$$R = \frac{K_\ell}{K_b} \qquad \text{(IV.3-9)}$$

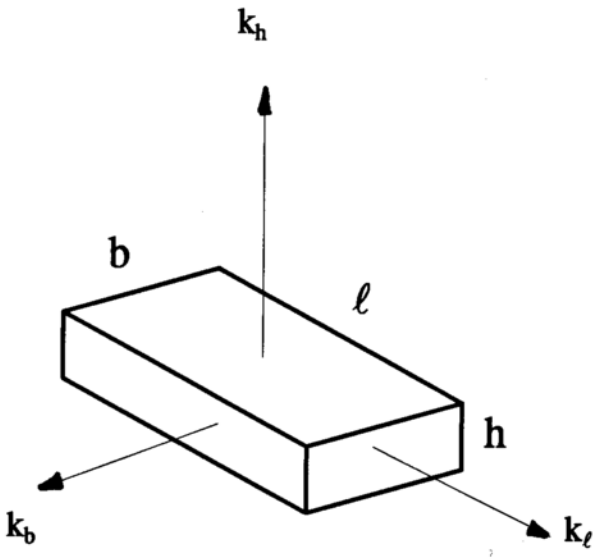

Fig. IV.3 Dissolution anisotropy showing differences in the dissolution rates of various faces of a crystal.

then there would be a total of six parameters, viz., μ_b', P, σ_b , Q, K_b, and R.

The probability density functions for the two characteristic dimensions of the particles are:

$$f(\ell_0)=\frac{1}{\sigma_\ell\sqrt{2\pi}}\exp\left[-\frac{(\mu_\ell-\ln(\ell_0))^2}{2\sigma_\ell{}^2}\right] \qquad \text{(IV.3-10)}$$

$$f(b_0)=\frac{1}{\sigma_b\sqrt{2\pi}}\exp\left[-\frac{(\mu_b-\ln(b_0))^2}{2\sigma_b{}^2}\right] \qquad \text{(IV.3-11)}$$

Considering anisotropy the following relationships can be written:

$$l = l_0-\left(\frac{2k_1S}{\rho}\right)t \;=\; l_0-K_1t \;=\; l_0-\tau_1 \qquad \text{(IV.3-12)}$$

$$b = b_0-\left(\frac{2k_bS}{\rho}\right)t \;=\; b_0-K_bt \;=\; b_0-\tau_b \qquad \text{(IV.3-13)}$$

Based on these single particle equations the amount undissolved at any time t before the critical time can be calculated as follows:

$$M = N\rho\left\{\int_{\ln(\ell_0^{min})}^{\ln(\ell_0^{max})}(\ell_0 - \tau_\ell)f(\ell_0)d\ln(\ell_0)\int_{\ln(b_0^{min})}^{\ln(b_0^{max})}(b_0 - \tau_b)f(b_0)d\ln(b_0)\int_{\ln(b_0^{min})}^{\ln(b_0^{max})}(b_0 - \tau_b)f(b_0)d(\ln b_0)\right\}$$

..... (IV.3-14)

The total initial amount of the solid is given by the following equation:

$$M_0 = N\rho\left\{\int_{\ln(\ell_0^{min})}^{\ln(\ell_0^{max})}\ell_0 f(\ell_0)d\ln(\ell_0)\int_{\ln(b_0^{min})}^{\ln(b_0^{max})}b_0 f(b_0)d\ln(b_0)\int_{\ln(b_0^{min})}^{\ln(b_0^{max})}b_0 f(b_0)d\ln(b_0)\right\}$$

..... (IV.3-15)

By assigning realistic values to the parameters μ_b' , P, σ_b , and Q the upper and lower limits of the integrals in Eqs. (IV.3-14) and (IV.3-15) can be varied within a certain range. In this manner the effect of particle size distribution on dissolution of powders can be quantitated. The model implicitly accounts for non-isometry and no assumption regarding the change in shape factor needs to be made in this case. Assigning different values to K_b and R is intended to account for substances with differences in their intrinsic dissolution rates, saturation

solubilities, and true densities. Thus by proper design of parameters by way of computer simulations dissolution curves can be obtained using Eq. (IV.3-14). Assuming that the Hixson-Crowell cube root law holds during the dissolution before the critical time, the following equation can be envisaged.

$$1-\left(\frac{M}{M_0}\right)^{1/3} = \kappa t \qquad \text{(IV.3-16)}$$

where κ is the slope of the cube root law plot and is a composite of the distribution parameters, anisotropy parameters, density, solubility, and shape factor. The goal of this model is to deconvolute the dependencies between the six parameters (μ_b' , P, σ_b , Q, K_b, and R) and κ .

CHAPTER V. EXPERIMENTAL

Since the emphasis is on size and shape of particulate solids as regards dissolution, a major part of the experimental work bears heavily on crystallization, dissolution studies, and particle size analysis of particulate solids. Single crystal studies were carried out on potassium dichromate because of its propensity to form fairly large crystals. Powder dissolution studies were conducted on four compounds, oxalic acid dihydrate, salicylic acid, phthalimide, and acetaminophen.

V.1 Materials

Potassium dichromate (99%) and concentrated hydrochloric acid GR were obtained from EM Science, Gibbstown, NJ. Oxalic acid dihydrate (97%), salicylic acid (99%), phthalimide (98%), acetaminophen (98%), concentrated sulfuric acid (95-98%), and Tween 80 were obtained from Aldrich Chemical Co., Milwaukee, WI. Deionized water was obtained by using a Barnstead PCS cartridge ion exchange water filtration system (The Barnstead Co., Boston, MA).

0.1N Sulfuric acid was used as the dissolution medium for single crystals of potassium dichromate. It was prepared by diluting 2.8 mL conc. H_2SO_4 to 1

liter with deionized water. 0.1N HCl was prepared by diluting 8.3 mL conc. HCl to 1 liter with deionized water, which served as the dissolution medium for oxalic acid dihydrate. To minimize wetting problems encountered with salicylic acid, phthalimide, and acetaminophen, a 0.0005% w/v Tween 80 solution in 0.1N HCl was employed as the dissolution medium [Weintraub and Gibaldi, 1969, Cobby, 1974]. This concentration of Tween 80 is well below its critical micelle concentration [Choulis and Loh, 1971].

Samples from solubility studies were filtered through a Rainin (Woburn, MA) Nylon-66 0.2 micron membrane filter housed in a disposable 13 mm Swinnex filter holder fitted to a syringe. Teflon-coated stoppers (20 mm 4416/50 gray butyl), aluminum caps, and Type-1 flint glass 10 mL vials used for holding solubility samples were obtained from West.

V.2. Instrumentation

An Image-1/AT image analyzer (Fryer Co. Inc., Huntley, IL) was used for particle size analysis. For measurement of dimensions of single crystals, the following set up was used. A Javelin Ultrachip™ CCD camera bearing a 55 mm f/2.8 Nikon lens captures an image of the crystal, and feeds digital information to a Trinitron SONY® color video monitor through an interface, a Gateway 2000

P4D-66 PC (North Sioux City, SD). The position of the camera can be adjusted on a vertical COPYMATE II bench stand (obtained from Fryer Co.) to increase magnification. Data acquisition and image processing was achieved by using a software, IMAGE-1, version 4.0 (Universal Imaging Corporation, West Chester, PA). For particle size analysis of sieve fractions (in the microns range) the Nikon lens was replaced by a Nikon microscope with a 4X magnification on the objective. A special adapter was used to attach the CCD camera to the microscope.

Dissolution studies were carried out in a USP paddle apparatus, Distek model 2000 (Distek Inc., New Brunswick, NJ). The water bath of the dissolution assembly was maintained at a temperature of 25°C using a Model VWR 1120 thermostat (Polyscience, Niles, IL).

The dissolution samples of potassium dichromate were analyzed using a Perkin Elmer 559A UV/VIS spectrophotometer. The samples from the powder dissolution of the other compounds were analyzed using a Varian DMS 500 UV/VIS spectrophotometer, both in a quartz cell of path length 1 cm.

The melting points of the crystallized compounds were determined using a Thomas Hoover capillary melting point apparatus (Arthur H. Thomas Company, Philadelphia, PA).

V.3. Crystallization

Single crystals of potassium dichromate:

Potassium dichromate was used as supplied, to grow single crystals. A saturated solution was made at 25°C. This solution was placed in a large porcelain dish, and was allowed to evaporate at this temperature. Fine prismatic crystals (length 1-3 mm) resulted within 24 hours. Some of these crystals were further grown individually, by suspending them with a thread, in jacketed glass jars, containing a supersaturated solution (degree of supersaturation 1.05) of potassium dichromate at 40°C [Mullin, 1972]. As the crystals grew in size, the supersaturated solution was maintained at 40°C by circulating water at that temperature from a thermostated water bath. Typically, it took about 24 hours for the small crystals to grow to a length of about 9 mm. Finally these single crystals were dried under vacuum.

Crystallization of the four model compounds:

350 g oxalic acid dihydrate was dissolved in 800 mL deionized water that was pre-heated to 60°C. The solution was filtered and cooled slowly, with stirring, to room temperature (25°C). The solution was allowed to stand at this temperature, overnight. The crystals were filtered under suction and dried under vacuum. To

avoid vitrification, the crystallized sample was stored in desiccators over saturated sodium chloride solution with excess sodium chloride [Carstensen and Patel, 1975].

For salicylic acid 16.5 g was dissolved in 700 mL deionized water that was preheated to 90°C. 8 g of Phthalimide was dissolved in 1 L deionized water pre-heated to 90°C while 20 g of acetaminophen was dissolved in 300 mL deionized water, pre-heated to 70°C. The rest of the procedure is the same as that followed for oxalic acid dihydrate. However, the dried crystals of these three compounds were stored in a desiccator over drierite.

The melting points of all the four crystallized compounds were recorded using a capillary melting point apparatus and they were tallied with the reported values [Budavari, 1996].

V.4 Size separation by sieving:

The crystalline powders were subjected to sieve analysis using U.S. Standard sieves with the following mesh sizes: 30(600μ), 40(425μ), 50(300μ), 60(250μ), 80(177μ), 100(150μ), and 200(75μ). The numbers in the parenthesis are the actual sieve openings in microns. The set of sieves were mounted on a sieve shaker (CSC Scientific Co.) and it was operated for a period of 30 minutes. At

all times, fines were neglected. Table V.4-1 gives the sieve fractions considered for the four compounds after sieving. In a sieve fraction, the negative sign indicates the sieve through which the material passes, and the positive sign signifies the sieve on which the material is retained. Acetaminophen was used as crystallized without subjecting it to sieve analysis.

V.5 Particle size analysis

For single crystals of potassium dichromate, a series of measurements along several faces of the crystal were made to determine their length, breadth and height. The height of the crystal was measured by resting the crystal on one of the smaller faces. An average length, breadth, and height from a series of measurements on one crystal was reported. For these measurements, the image acquisition system was calibrated with the use of a scale in two dimensions.

The lengths and breadths of the particles of the four compounds; oxalic acid dihydrate, salicylic acid, phthalimide, and acetaminophen were measured by microscopy coupled with image analysis as described in section V.2. The magnification on the objective lens was 4X. Calibration of the microscope was done by a 1mm stage micrometer. The crystals were dispersed, as evenly as possible, on a microscope slide for particle size measurement. A representative

sample from any sieve fraction was obtained by the "coning and quartering" procedure [Allen, 1968]. Particle size analysis of 300 particles was assumed to be representative of the population from that particular sieve fraction. Lengths and breadths of such particles were classified into class intervals determined by the Sturges rule and a frequency distribution was obtained [Carstensen, 1996]. In order to get an estimate of the number of particles in a given weight of any sample, about 300 to 400 particles were counted by microscopy, using the "object count" mode of the image analysis software (which performs semi-automated counting). From the weight of these counted particles, the total number of particles N, in any given sample, for a particular sieve fraction could be estimated.

The methodology of obtaining the probability distribution function (number basis) from the frequency is explained in chapter VI.

V.6 Dissolution studies

All dissolution studies were conducted in a USP paddle apparatus at 50 rpm and 25°C. The following dissolution media were used for the five compounds:

1. Single crystals of potassium dichromate - 0.1N H_2SO_4
2. Oxalic acid dihydrate - 0.1N HCl

3. Salicylic acid - 0.1N HCl containing 0.0005% w/v Tween 80

4. Phthalimide - 0.1N HCl containing 0.0005% w/v Tween 80

5. Acetaminophen - 0.1N HCl containing 0.0005% w/v Tween 80

Single crystal dissolution studies:

On an average, the total dissolution time for single crystals of potassium dichromate was about 20 minutes. Depending upon the dimensions of these crystals, their weight ranged between 150 mg to about 300 mg. 5 ml samples were withdrawn at regular intervals over this time period without replacement of the dissolution medium. The decrease in volume on subsequent sampling was taken into account while computing the concentrations. These concentrations were such that sink conditions prevailed throughout the experiment. The volume of dissolution medium used was such that no further dilutions were required for analysis of samples. The samples were analyzed by spectrophotometry at 457 nm. To ascertain the linear decrease of the dimensions of the crystals with dissolution time, the following was done. A single crystal of potassium dichromate, undergoing dissolution, was removed from the medium at equal intervals. The length, breadth, and height were measured, then the crystal was dropped back into the medium, and dissolution was resumed. This was repeated

Table V.4-1 Sieve fractions for the crystallized samples of model compounds.

Compound	Sieve Fractions
Oxalic acid dihydrate	-30/+40, -40/+50, -50/+60, -60/+80
Salicylic acid	-40/+60, -60/+100, -100/+200
Phthalimide	-40/+60, -60/+100

for subsequent time intervals until a point where the smallest dimension did not lend itself to any further measurement.

Powder dissolution studies:

In case of oxalic acid dihydrate, about 3 g of the material was taken for dissolution in 800 mL of the medium. 4 mL samples were withdrawn at regular intervals and they were analyzed without any further dilution at 255 nm. The dissolution was followed until all of the powder had dissolved. For salicylic acid, the initial weight of the powder was about 0.150 g in 600 mL of dissolution medium. Samples of 250 μL were withdrawn with the help of a glass syringe bearing a needle tip. The tip of this syringe was plugged with very little non-adsorbent cotton, to prevent fine particles from being sampled out. The sample volumes were replenished each time with fresh dissolution medium. The samples were diluted 13 times, with the dissolution medium and were analyzed by spectrophotometry at 296 nm.

In case of phthalimide, about 0.035 g of solid was taken for dissolution in 600 mL of the dissolution medium. Using a pipettor, samples of 3.5 mL were withdrawn at regular intervals and these were analyzed spectrophotometrically, at

299 nm. Here again, the pipette tips were plugged with non-adsorbent cotton, for reasons mentioned earlier.

Lastly, for studies on acetaminophen, about 0.5 g of the recrystallized powder (unsieved) was subjected to dissolution in 800 mL of the medium. 0.25 mL samples were withdrawn from the dissolution medium by a syringe (as described earlier) and the sample volume was replaced with the dissolution fluid. These samples were diluted 30 times with the medium before analyzing them at 243 nm.

Salicylic acid, phthalimide, and acetaminophen experienced wetting problems when their dissolution was carried out in 0.1 N HCl. To decrease the interfacial tension at the solid-liquid interface, Tween 80 at very low concentrations (below its cmc) was used in the dissolution medium. Also to ensure pre-wetting the following was done [Ullah and Cadwallader, 1970]. The powder sample was weighed out in a syringe whose tip had been cut off to expose the circular rim. The powder was prewetted in this syringe by stirring gently with a melting point capillary tube and then injected into the dissolution medium by moving the piston of the syringe. Problems associated with the initial wetting could be minimized by a fair degree by employing such a modification.

V.7. Solubility determinations:

For all the compounds an excess of solid was suspended in 10 mL of the respective dissolution medium in stoppered vials. These vials were fitted with teflon-coated rubber stoppers that were sealed with aluminum caps. These vials were then mounted on a motor-driven rotating shaft assembly placed in a large water bath. The temperature of this water bath was maintained at 25°C. Samples were withdrawn after 48 hours and were filtered through 0.2 micron Nylon-66 filters. The solutions were analyzed by spectrophotometry, after proper dilution. Standard curves of all the five compounds at their respective λ_{max} were generated for concentration determination. Table V.7-1 gives the dilutions for all the five compounds and the respective wavelength at which the diluted samples were analyzed.

V.8 Density determinations

Densities of oxalic acid dihydrate and phthalimide were determined by pycnometry at 25°C using the saturated solutions of the respective compounds as the liquid vehicle. A specific gravity bottle was used for this purpose. Deionised water and the saturated solution required in this determination were equilibrated at 25°C before the measurement. These measurements were done in triplicate.

Reported values for the densities of potassium dichromate, salicylic acid, and acetaminophen were used [Budavari, 1996].

V.9 Computer programs

The solutions of the third degree polynomials in reduced time (u) were obtained using two different mathematical programs: MATHEMATICA (version 2.2 for Macintosh, Wolfram Research Inc., Champaign, IL) and Student MATLAB (The Mathworks Inc., Prentice-Hall, Engelwood Cliffs, NJ,). Programs were written in these two softwares utilizing the numerical integration routines to calculate the integrals originating from the frequency distribution functions. A program was written in MATLAB for simulating the anisotropic dissolution profiles of well defined crystalline solids. For linear, non-linear, and multiple regression analysis of the data two statistical curve fitting packages were used, ORIGIN (version 3.5, Microcal Software Inc., Northampton, MA), and SCIENTIST (Micromath Scientific Software, Salt Lake City, UT).

Table V.7-1 Solvents, dilution factors, and wavelength of absorbance measurements for the five compounds used in their solubility determinations.

Compound	Dilution	λ_{max} for analysis	Solvent
Potassium dichromate	1000 X	457 nm	0.1 N H_2SO_4
Oxalic acid dihydrate	100 X	255 nm	0.1 N HCl
Salicylic acid	100 X	296 nm	0.1 N HCl with 0.0005% Tween 80
Phthalimide	25 X	299 nm	0.1 N HCl with 0.0005% Tween 80
Acetaminophen	100 X	243 nm	0.1 N HCl with 0.0005% Tween 80

CHAPTER VI. RESULTS AND DISCUSSION

VI.1. Results from density and solubility measurements and concentration calibration.

The true densities of oxalic acid dihydrate and phthalimide were determined by pycnometry in their respective saturated solutions.

Oxalic acid dihydrate : 1.63±0.01 g/mL

Phthalimide : 1.22±0.01 g/mL

For all other compounds reported values were used [Budavari, 1996].

Potassium dichromate : 2.68 g/mL

Salicylic acid : 1.44 g/mL

Acetaminophen : 1.29 g/mL

Results from experiments on solubility studies are summarized in Table VI.1-1.

Table VI.1-1 Saturation solubilities of all the compounds in their respective dissolution media.

Compound	Solvent	Saturation Solubility in g/mL
Potassium dichromate	0.1N H_2SO_4	0.139 ± 0.001
Oxalic acid dihydrate	0.1N HCl	0.1443 ± 0.0007
Salicylic acid	0.1N HCl with 0.0005% Tween 80	$1.705 \times 10^{-3} \pm 0.005 \times 10^{-3}$
Phthalimide	0.1N HCl with 0.0005% Tween 80	$0.357 \times 10^{-3} \pm 0.003 \times 10^{-3}$
Acetaminophen	0.1N HCl with 0.0005% Tween 80	0.0155 ± 0.0002

All the compounds absorbed light in the UV range of the electromagnetic spectrum, except for potassium dichromate, which absorbed light in the visible range. The λ_{max} for each compound in the respective solvent was determined by running a UV scan. They are listed below:

Potassium dichromate : 457 nm

Oxalic acid dihydrate : 255 nm

Salicylic acid : 296 nm

Phthalimide : 299 nm

Acetaminophen : 243 nm

The Beer's law plots for these compounds are given on pp 84-88. These standard curves were used to estimate the concentration of dissolution samples.

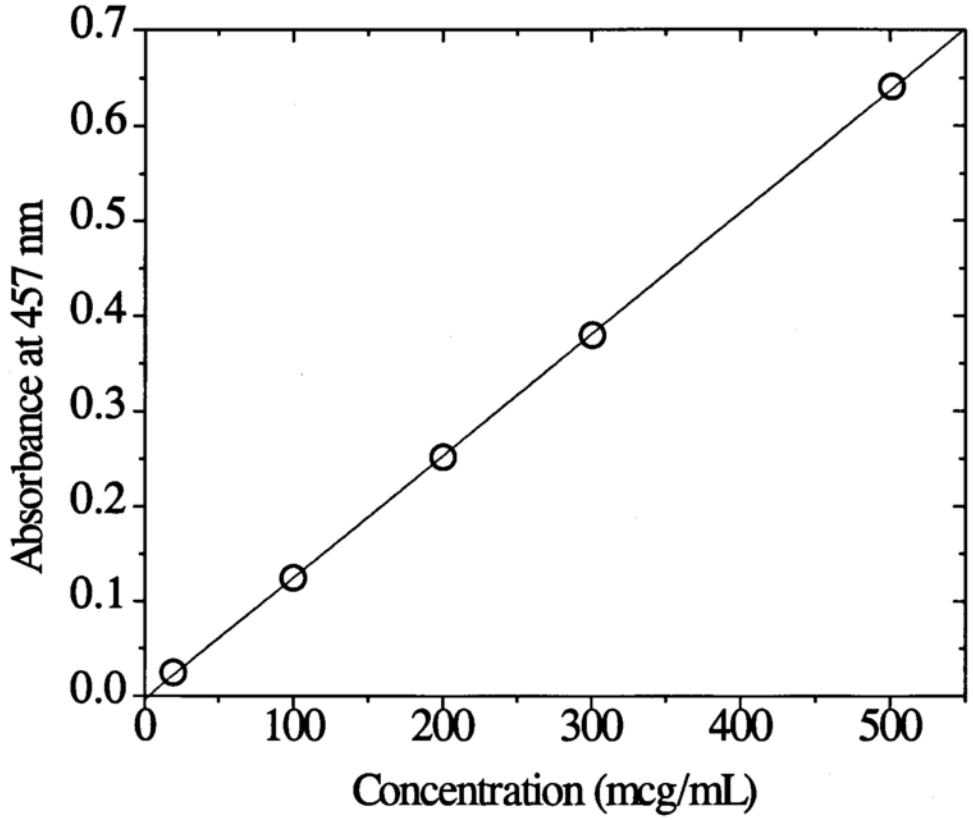

Fig. VI.1-1 Standard curve for potassium dichromate in 0.1N H_2SO_4. The regression is $y = -0.003 + 0.00128x$, $R^2 = 0.9999$.

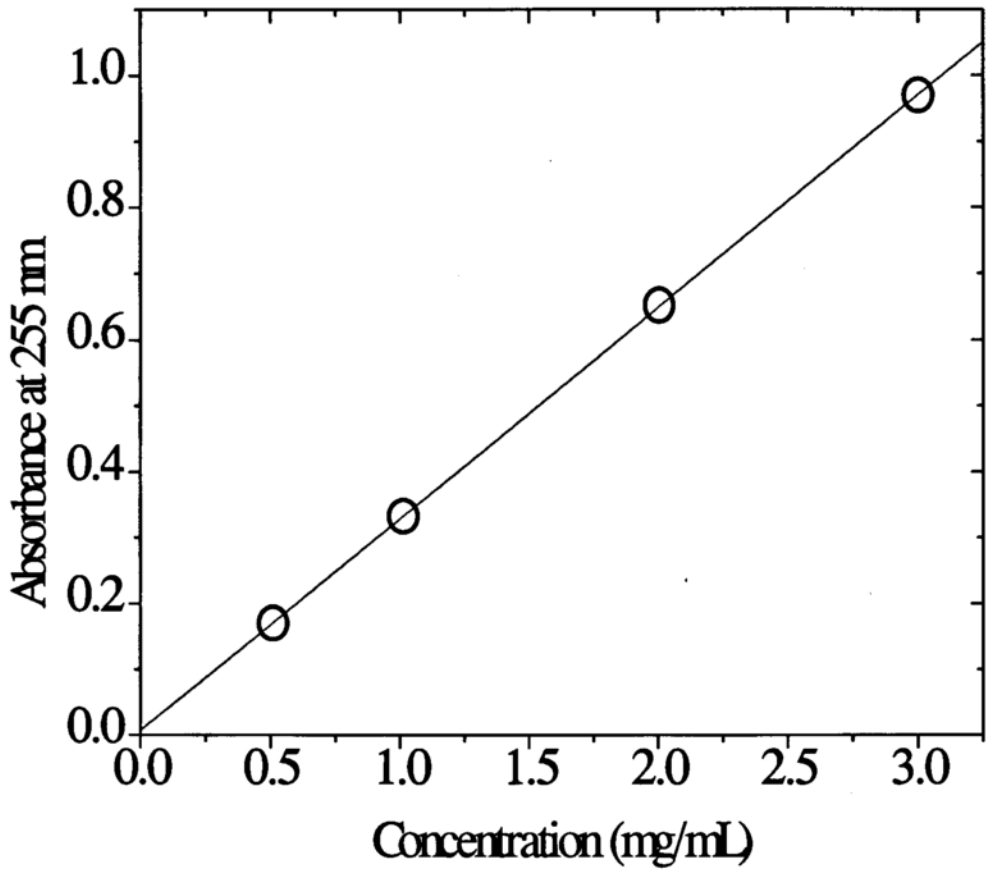

Fig. VI.1-2 Standard curve for oxalic acid dihydrate in 0.1N HCl. The regression is $y=-0.007+0.32106x$, $R^2=1.000$

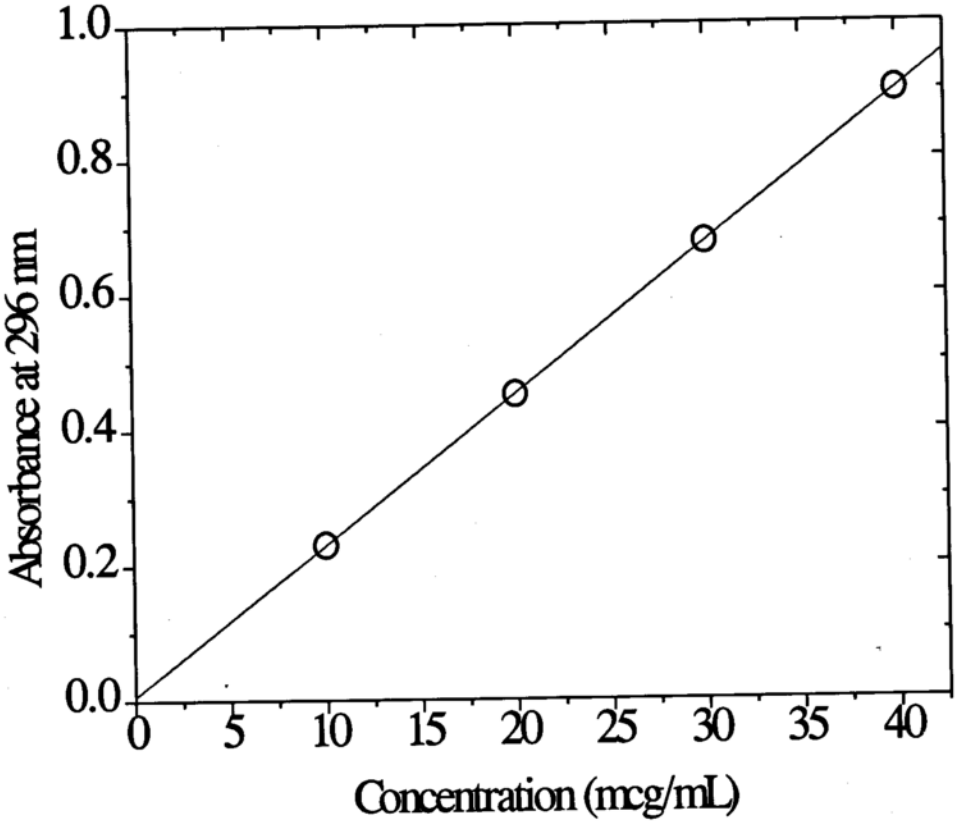

Fig. VI.1-3 Standard curve for salicylic acid in 0.1N HCl containing 0.0005% Tween 80. The regression is $y = 0.007 + 0.02231x$, $R^2 = 1.000$.

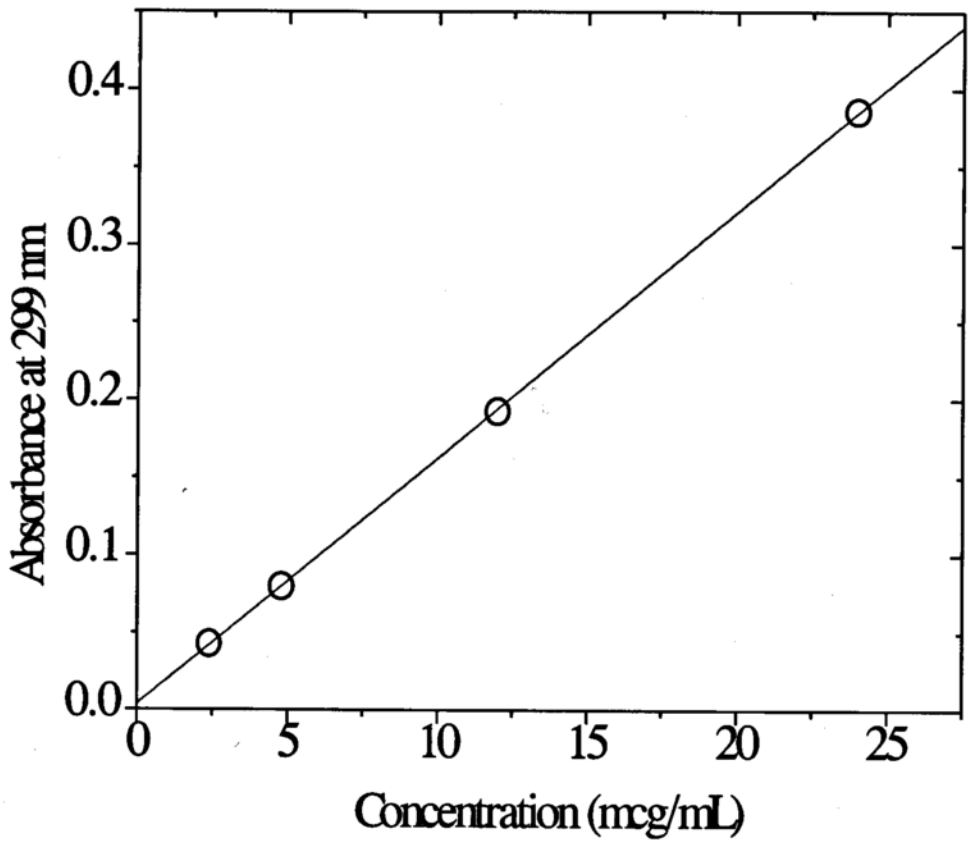

Fig. VI.1-4 Standard curve for phthalimide in 0.1N HCl containing 0.0005% Tween 80. The regression is $y = 0.004 + 0.01589x$, $R^2 = 0.9999$.

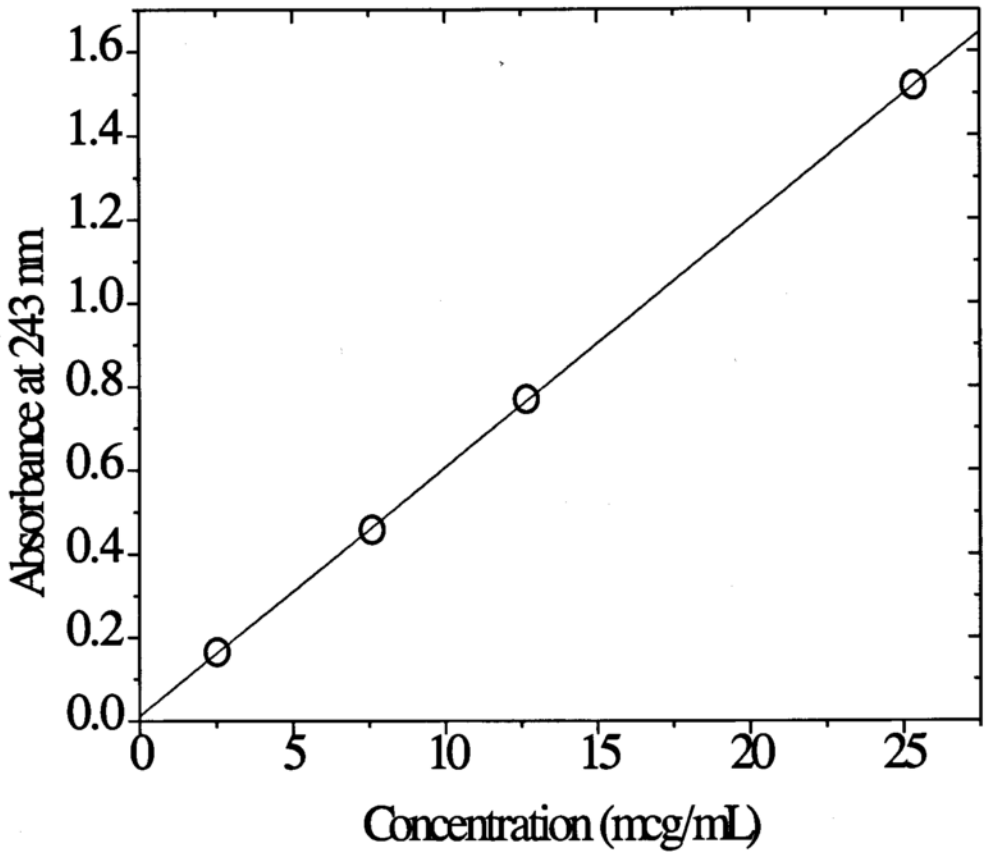

Fig. VI.1-5 Standard curve for acetaminophen in 0.1N HCl containing 0.0005% Tween 80. The regression is $y = 0.013 + 0.0594x$, $R^2 = 0.9999$.

VI.2 Single crystal dissolution kinetics

VI.2.1 *Change in surface-volume shape factor with dissolution time*

There are three important issues which will be discussed in this section of the chapter. They are change in the surface-volume shape factor, Γ; change in the volume shape factor, α_v, of a non-isometric particle with dissolution time; and the effect of this change on the predictions of the Hixson-Crowell cube root law. Dissolution studies were conducted on five crystals of potassium dichromate differing in their respective dimensions. The relevant plots from the data for one representative crystal will be presented here. The results for the other four crystals will be given in a tabulated form.

Figs. VI.2-2 and VI.2-3 show the amount and fraction undissolved for a single crystal with the following dimensions: ℓ_0=1.120 cm, b_0=0.518 cm, and h_0=0.299 cm. For identity purposes, this crystal will be referred to as crystal A. With the knowledge of the initial dimensions of the crystal and the fraction undissolved at each time point, the reduced time u can be calculated using Eq. IV.1-29. u emerges as one of the solutions of a third degree polynomial, which is a positive real number between zero and unity. There was no ambiguity in the selection of the "correct" root of Eq.IV.1-29, because in all the cases, two of the three roots were either imaginary or greater than unity.

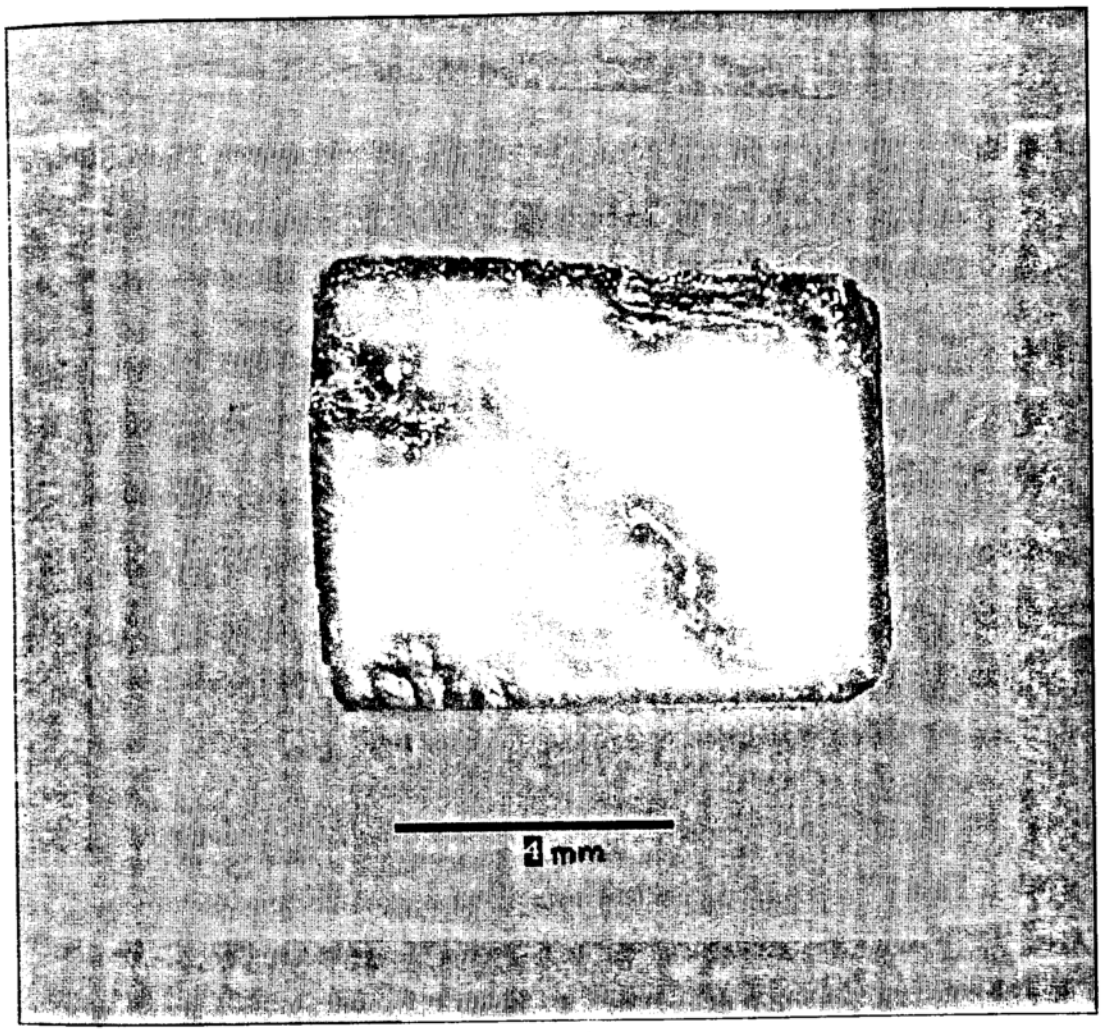

Fig. VI.2-1 A single crystal of potassium dichromate

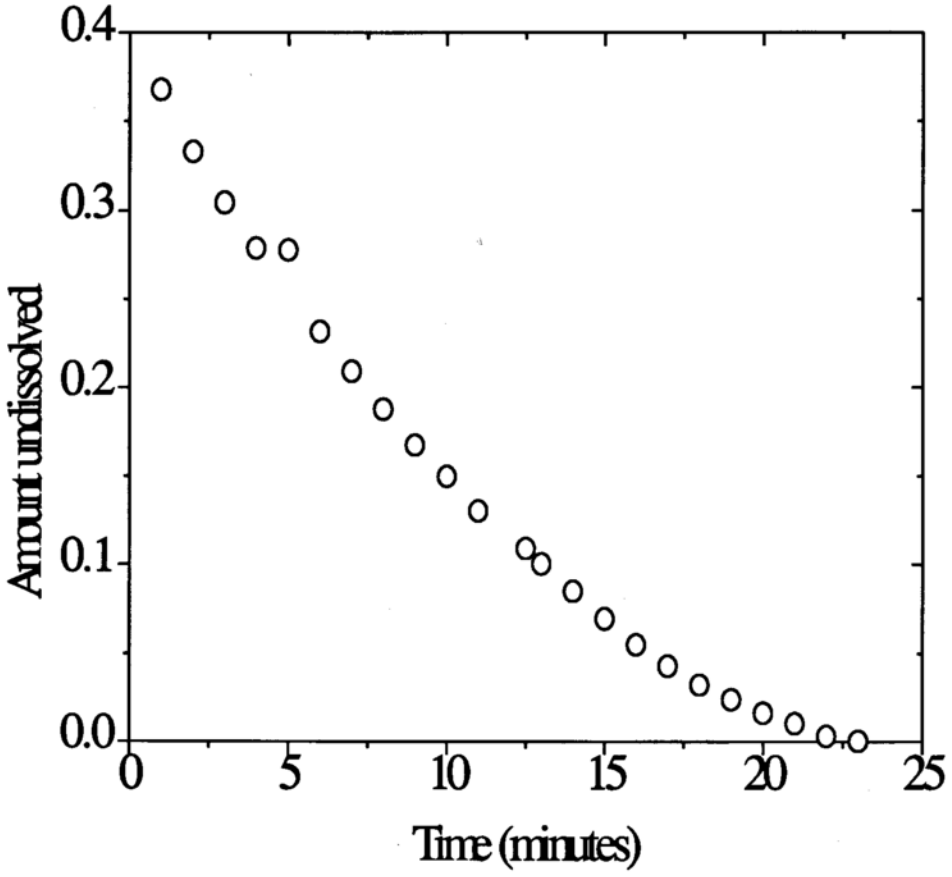

Fig. VI.2-2 Amount undissolved for crystal A with dissolution carried out in 0.1N H_2SO_4 at 25°C and 50 rpm speed.

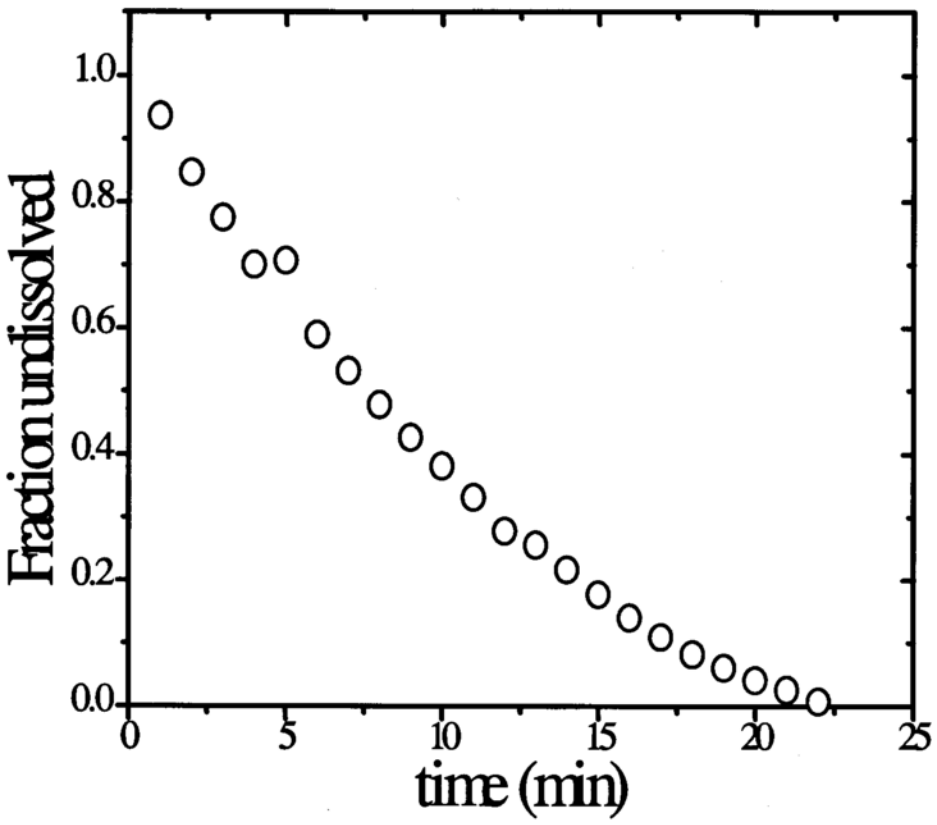

Fig. VI.2-3 Fraction undissolved for crystal A, with dissolution carried out in 0.1N H_2SO_4 at 25°C and 50 rpm speed.

The actual roots of the third degree polynomial in u for crystal A are shown in Table VI.2-1. Γ and α_v, as a function of dissolution time can be calculated from Eqs. IV.1-31 and IV.1-32 respectively. These values are given in table VI.2-2 for the same crystal. As defined in Eq.IV.1-23, u is a measure of the extent of dissolution of the smallest dimension of the crystal, i.e. height. It appears that both Γ and α_v do not change significantly in the early stages of dissolution, but after about 60% of the height of the crystal has dissolved, Γ increases rapidly and α_v decreases correspondingly. The nature of the change in these two parameters will be dealt with in depth at a later point in this section.

For crystal A, the linear relationship between u and t, as suggested by Eq. IV.1-28, is quite evident from Fig. VI.2-4.

$$u = \left(\frac{2kS}{\rho h_0}\right) t \quad = \quad c_3 t$$

With the knowledge of saturation solubility of $K_2Cr_2O_7$ in 0.1N H_2SO_4 (0.139 g/mL), density (2.68 g/mL), and h_0 for crystal A (0.299 cm), the intrinsic dissolution rate constant k, for $K_2Cr_2O_7$ under these hydrodynamic conditions can be calculated from the slope of u versus t plot. The value of k was found to be 2.14×10^{-3} cm/s.

Table VI.2-1 The three roots of the polynomial in u calculated from the fraction undissolved for crystal A.

time	Fraction	Reduced time u		
(min)	undissolved F	Root 1	Root 2	Root 3
1	0.93712	0.0347	3.2171+1.168*i*	3.2171-1.168*i*
2	0.84757	0.0866	3.1911+1.0960*i*	3.1911-1.0960*i*
3	0.77535	0.1308	3.1690+1.0322 *i*	3.1690-1.0322 *i*
4	0.71024	0.1728	3.1480+0.9692 *i*	3.1480-0.9692 *i*
5	0.70762	0.1745	3.1472+0.9665 *i*	3.1472-0.9665 *i*
6	0.58978	0.2565	3.1061+0.8338 *i*	3.1061-0.8338 *i*
7	0.53239	0.2998	3.0845+0.7571 *i*	3.0845-0.7571 *i*
8	0.47860	0.3429	3.0630+0.6745 *i*	3.0630-0.6745 *i*
9	0.42676	0.3680	3.0504+0.6221 *i*	3.0504-0.6221 *i*
10	0.38168	0.4276	3.0206+0.4794 *i*	3.0206-0.4794 *i*
11	0.33208	0.4754	2.9967+0.3279 *i*	2.9967-0.3279 *i*
12.5	0.27802	0.5320	3.1492	2.7876
13	0.25589	0.5567	3.2602	2.6519
14	0.21664	0.6034	3.3831	2.4824
15	0.17763	0.6539	3.4720	2.3429
16	0.14041	0.7072	3.5415	2.2201
17	0.10961	0.7560	3.5919	2.1209
18	0.08206	0.8046	3.6328	2.0314
19	0.06077	0.8463	3.6624	1.9602
20	0.04113	0.8890	3.6883	1.8916
21	0.02612	0.9254	3.7072	1.8362
22	0.00824	0.9745	3.7290	1.7653

Table VI.2-2 Change in the surface-volume shape factor, volume shape factor, and area shape factor of crystal A undergoing dissolution in 0.1N H_2SO_4 at 25°C and 50 rpm.

Time (min)	Γ	α_v	α_s
1	6.913	1.24	6.18
2	6.972	1.23	6.23
3	7.028	1.23	6.28
4	7.086	1.22	6.32
5	7.089	1.22	6.33
6	7.221	1.19	6.42
7	7.303	1.18	6.47
8	7.395	1.16	6.53
9	7.454	1.15	6.56
10	7.614	1.12	6.64
11	7.766	1.09	6.71
12.5	7.985	1.05	6.79
13	8.096	1.02	6.82
14	8.343	0.98	6.89
15	8.678	0.92	6.97
16	9.106	0.85	7.05
17	9.737	0.77	7.14
18	10.587	0.67	7.22
19	11.694	0.57	7.29
20	13.569	0.45	7.35
21	16.585	0.32	7.41
22	30.776	0.12	7.47

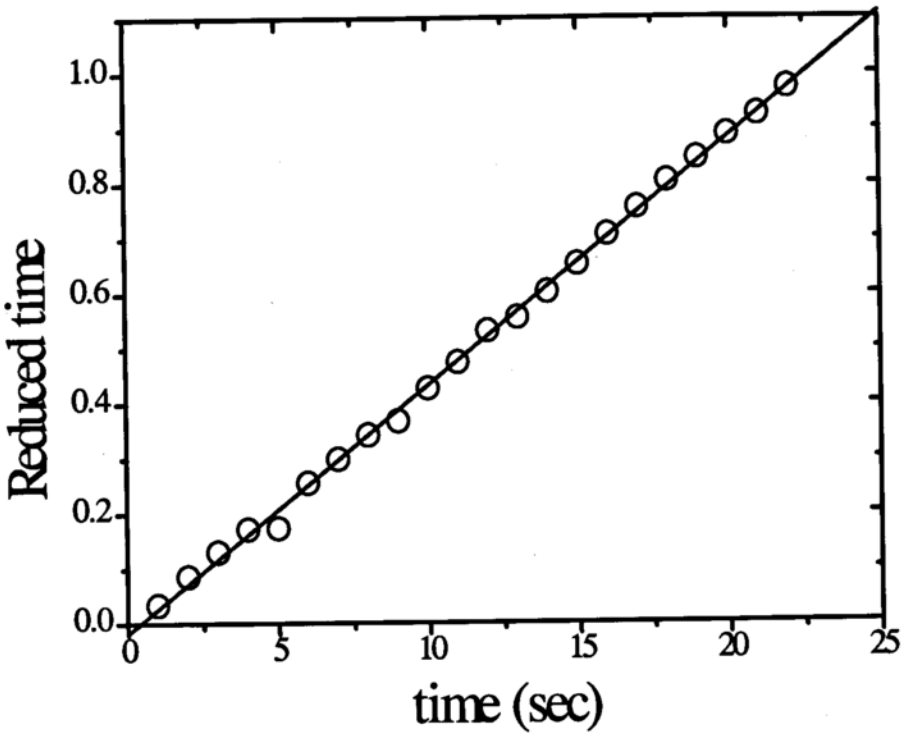

Fig. VI.2-4 u versus t for dissolution of crystal A in 0.1N H_2SO_4 at 25°C and 50 rpm. Linear regression on these data yields $u = -0.018+(7.508x10^{-4})\ t$ with $R^2 = 0.998$.

Similar studies were carried out on other single crystals of $K_2Cr_2O_7$, and in all cases, the u versus t plots were linear. This observation is in concordance with the fact that the dimensions of the crystal decrease linearly with time. The results obtained from these studies are summarized in Table VI.2-3. The mean value of k for $K_2Cr_2O_7$ with 95% confidence limits was $2.74 \pm 0.62 \times 10^{-3}$ cm/s.

As discussed in chapter IV, the Noyes-Whitney equation for a single non-isometric particle can be written in the following form:

$$\frac{dm}{dt} = -k\Gamma v^{2/3} S = -k\Gamma \left(\frac{m}{\rho}\right)^{2/3} S$$

From table VI.2-2 it is seen that Γ changes with dissolution time. A plot of Γ versus u is shown Fig. VI.2-5. Lai and Carstensen observed a similar behavior with cylindrical discs of oxalic acid dihydrate [Lai and Carstensen, 1978]. It should be noted that in the initial stages of dissolution, Γ does not change significantly, but after a point where the height of the crystal has decreased to 40% of its initial value, Γ increases rapidly. As a matter of fact, the value of Γ approaches infinity as u approaches 1. At the beginning of dissolution, i.e. at $u=0$, Γ has a finite value corresponding to the initial shape factor of the crystal. With these features about Fig. VI.2-5 in mind, the following equation was proposed to describe the observed data for the change in Γ.

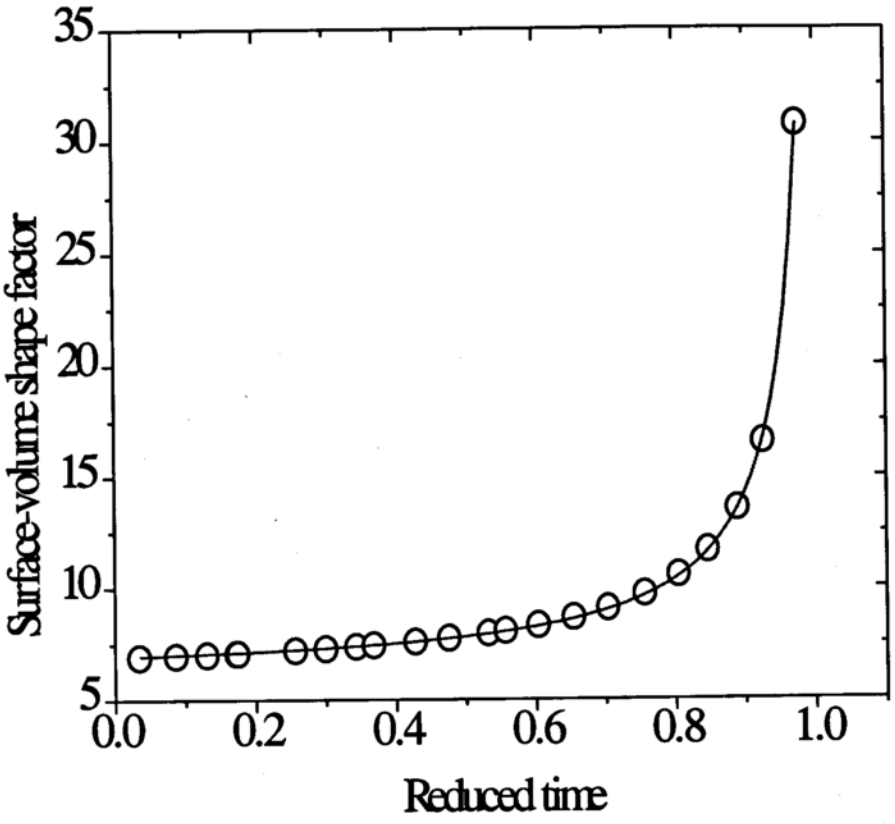

Fig. VI.2-5 Change in surface-volume shape factor of crystal A as a function of reduced time. The open circles represent experimental data points and the curve is a least square fit to the data.

Table VI.2-3 The smallest dimension, shape ratios, and calculated intrinsic dissolution rate constants for the five single crystals of $K_2Cr_2O_7$.

Crystal	h_0 cm	m	n	$c_3 \times 10^4$	$k \times 10^3$ cm/s
A	0.299	2.16	0.58	7.47	2.14
B	0.400	1.41	0.62	9.76	3.74
C	0.372	1.99	0.84	7.31	2.61
D	0.173	1.33	0.32	13.61	2.25
E	0.304	1.78	0.59	10.22	2.97

$$\Gamma = c_1 + \frac{c_2}{(u^* - u)} \qquad \text{VI.2-1}$$

c_1, c_2, are constants and u^* is almost equal to 1. These can be obtained from nonlinear regression analysis of the data. For an isometric particle such as a sphere or a cube, one would expect c_2 to be equal to zero, so that the surface-volume shape factor would be independent of u. At $u=0$, $\Gamma = \Gamma_0 = (c_1+c_2)$ as u^* is equal to unity. Γ_0 can also be calculated from ℓ_0, b_0, and h_0. These two values can be compared to check for consistency. As u approaches 1, Γ tends to infinity. This is well demonstrated by Eq. VI.2-1.

Non-linear regression analysis of the data shown in Fig.VI.2-5 by the method of least squares resulted in the following outcome for the constants in Eq.VI.2-1:

$c_1 = 6.021$, $c_2 = 0.930$, $u^* = 1.012$,

The nature of change of Γ with reduced time was similar for all the five crystals, but the values of the constants c_1, and c_2 differed to a certain degree. u^* was almost equal to 1 in all cases. These results have been complied in table VI.2-4. For crystal A, Γ_0 obtained from the initial dimensions (6.88) and that

calculated from the fit (6.94) are in good agreement. The change in Γ as a result of dissolution for all the five crystals is shown in Fig. VI.2-6.

In the process of describing the shape factor data mathematically, other functions such as polynomials, logarithmic, and exponential functions in u were tried but they did not give good fits. The goodness of fit of all the functions were determined on the basis of a statistical parameter called the *Model Selection Criterion* (MSC). It is given by the following expression:

$$MSC = \ln\left[\frac{\sum_{i=1}^{n}\left(Y_{obs_i} - \overline{Y}_{obs}\right)^2 w_i}{\sum_{i=1}^{n}\left(Y_{obs_i} - \overline{Y}_{cal_i}\right)^2 w_i}\right] - \frac{2p}{n} \qquad \text{VI.2-2}$$

where w_i are the weights applied to each point in a set of data, n is the number of points, and p is the number of parameters in the model equation. Y represents the dependent variable and "obs" and "cal" indicate the observed and calculated value for that variable respectively. This parameter is particularly useful in comparing two different models with different number of parameters. Larger the value of MSC, greater is the "information content" of the model, and better is the fit. It was found that this value was largest for Eq. VI.2-1 as compared to the other functions used.

Table VI.2-4 Initial dimensions of the five crystals of potassium dichromate, constants for the surface volume shape factor, and comparison between Γ_0 obtained from the initial dimensions of the crystals and that obtained from the fit.

Crystal	ℓ_0 cm	b_0 cm	h_0 cm	c_1	c_2	u^*	Γ_0 from fit	Γ_0 actual
A	1.120	0.518	0.299	6.021	0.930	1.012	6.94	6.88
B	0.902	0.642	0.400	5.753	0.578	1.008	6.33	6.34
C	0.876	0.441	0.373	6.072	0.394	1.008	6.46	6.39
D	0.712	0.535	0.173	5.915	1.549	1.016	7.44	7.31
E	0.912	0.511	0.304	5.909	0.756	1.009	6.65	6.61

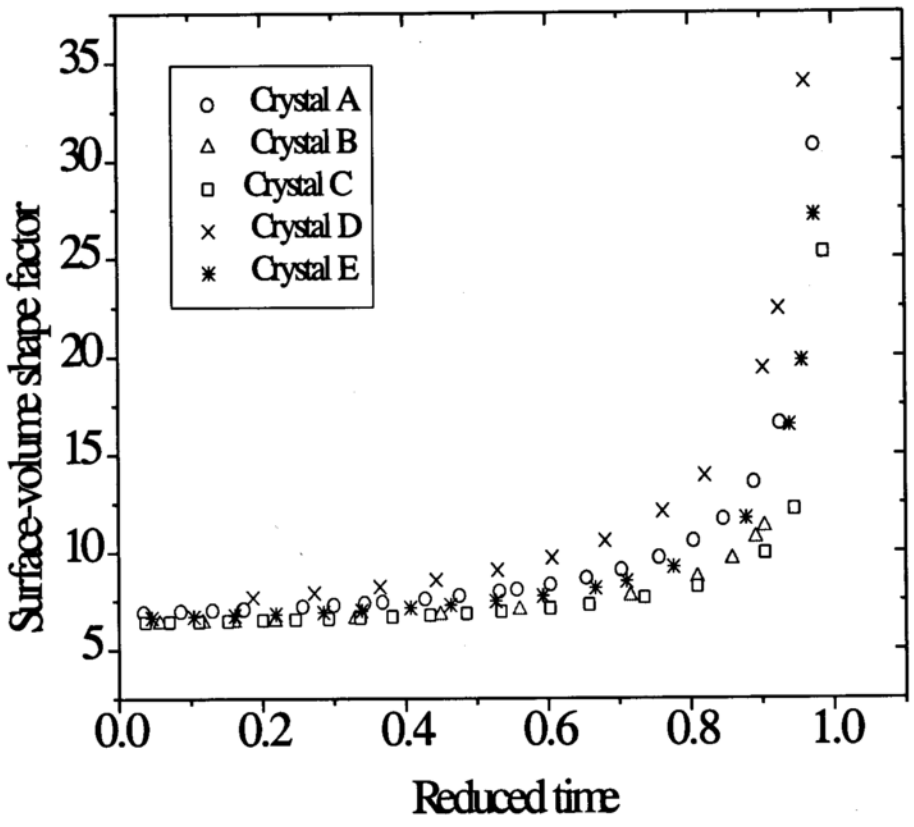

Fig. VI.2-6 Change in Γ as a function of reduced time for five crystals of potassium dichromate.

VI.2.2 *Derivation of the modified cube root equation for dissolution*

As stated earlier,

$$u = \left(\frac{2kS}{\rho h_0}\right) t \quad = \quad c_3 t$$

Hence Eq. VI.2-1 can be written as

$$\Gamma = c_1 + \frac{c_2}{\left(u^* - c_3 t\right.} \qquad \text{VI.2-3}$$

Using this expression for Γ, the Hixson-Crowell cube root law for a single non-isometric particle can be derived.

$$\frac{dm}{dt} = -k\Gamma v^{2/3} S \quad = \quad -k\Gamma \left(\frac{m}{\rho}\right)^{2/3} S$$

$$\frac{dm}{dt} = -kS\left[c_1 + \frac{c_2}{u^* - c_3 t}\right]\left(\frac{m}{\rho}\right)^{2/3}$$

Integrating the above equation between the appropriate limits,

$$\int_{m_0}^{m} \frac{dm}{m^{2/3}} = -\frac{kS}{\rho^{2/3}} \int_{0}^{t} \left[c_1 + \frac{c_2}{\left(u^* - c_3 t\right)}\right] dt$$

Hence,

$$(m_0)^{1/3} - (m)^{1/3} = \frac{kS}{3\rho^{2/3}}\left[c_1 t - \frac{c_2}{c_3}\ln\left(\frac{u^* - c_3 t}{u^*}\right)\right] \qquad \text{VI.2-4}$$

Eq.VI.2-4 can be written in a more concise form;

$$(m_0)^{1/3} - (m)^{1/3} = \left[Bt - D\ln\left(\frac{u^* - c_3 t}{u^*}\right)\right] \qquad \text{VI.2-5}$$

where

$$B = \frac{c_1 kS}{3\rho^{2/3}} \qquad \text{VI.2-6}$$

$$D = \frac{c_2 \rho^{1/3} h_0}{6} \qquad \text{VI.2-7}$$

Eq. VI.2-5 is the general case of the Hixson-Crowell cube root law. For an isometric particle such as a cube or a sphere the shape factor is independent of the dissolution time, hence c_2 and thereby D is equal to zero. In that case Eq. VI.2-5 reverts to the Hixson-Crowell cube root law for isometric particles, which predicts a linear relationship between the cube root difference and dissolution

time. With a prior knowledge of the constants ρ, k, S and the parameters c_1, c_2, c_3, and u* the cube root difference can be calculated from Eq.VI.2-4. The comparison of the predicted and the experimental values for the cube root difference are shown in Fig.VI.2-7. It can be seen that consideration of non-isometry accounts for the positive deviations from the Hixson-Crowell cube root law. In Eq. VI.2-5, the argument of the logarithmic term is a fractional quantity. This results in a net positive contribution to the linear term in t. For a single isometric particle, the surface volume shape factor would be constant. In short, c_2 and hence the coefficient B in Eq. VI.2-5 would be zero. In that case Eq. VI.2-5 reduces to the normal Hixson-Crowell cube root law, which predicts a linear relationship between the cube root difference and t. The straight line in Fig. VI.2-7 depicts this scenario, where c_2 is equal to zero and c_1 in Eq. VI.2-6 is equal to Γ_0.

From Fig. VI.2-7 it can be seen that the model described in this section explains the upward curvature observed in the cube root law plot. This can be attributed to the non-isometry of the dissolving particle. The positive differences between the observed values of cube root difference and the ones calculated from Eq. VI.2-5 were less than the negative differences between the observed values and the predictions of the cube root law for an isometric particle.

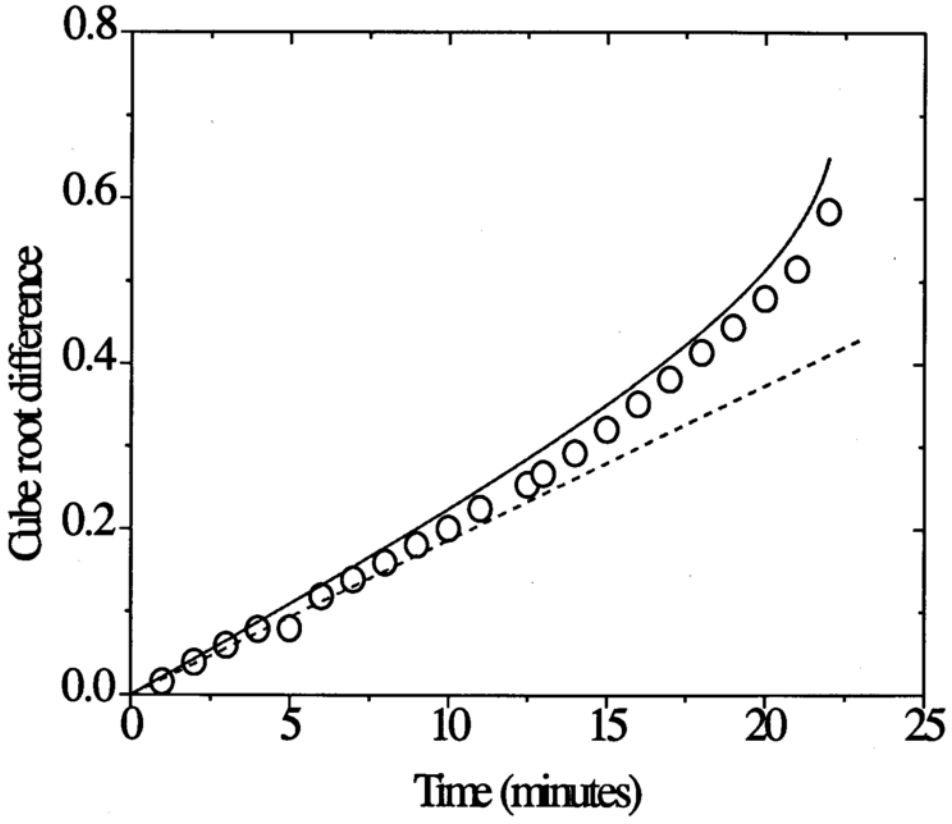

Fig. VI.2-7 Cube root difference plotted against time for crystal A. The circles represent experimental data points, squares represent the values calculated via Eq.VI.2-4, and the dotted line follows from the Hixson-Crowell cube root law for an isometric particle.

This was true for all crystals. There could be several reasons for the observed differences in the experimental values and the predicted values from the model. Firstly, potassium dichromate exhibits a triclinic pinacoidal crystal system. None of the angles between the three defining axes are equal to 90°. Secondly, by visual inspection, it was observed that towards the end of the dissolution event, the dissolving crystal assumed irregular shapes. Thus the geometry on which the model for the single particle was based did not hold towards the end of dissolution.

Thus, studies on single crystals of potassium dichromate have given us a sense for the nature of the change in shape factors of a non-isometric *real* particle. α_v decreases while Γ increases with dissolution time. The upward curvature in the cube root law plot for the dissolution of a non-isometric particle, as also reported by Lai and Carstensen [Lai and Carstensen, 1978], can be explained on the basis of the changing surface-volume shape factor of the dissolving particle. Thus a parallelepiped serves as a good model for particles that can be approximated by this geometry.

VI.2.3 *Change in the volume shape factor as a function of dissolution time*

It has been shown that for real crystals the surface volume shape factor increases as the particle dissolves. Since non-isometry is the issue under consideration, it is

important to have an insight into the nature of change of the volume shape factor for a single crystal. It will serve as the basis for extending this model for a single non-isometric particle to multiparticulate systems.

With the knowledge of ℓ_0, b_0, h_0, and u, one can calculate the instantaneous length, breadth, and height of the dissolving particle.

$$v = \ell bh \qquad \text{VI.2-8}$$

$$v = \alpha_v (b)^3 \qquad \text{VI.2-9}$$

Thus α_v could be calculated at every time point during the dissolution of a single crystal. Fig. VI.2-8 shows the change in α_v for the single crystals of potassium dichromate. α_v decreases with dissolution time and there is a similar tendency for the change to be insignificant in the early stages of dissolution with an eventual increase in rate of decrease of α_v.

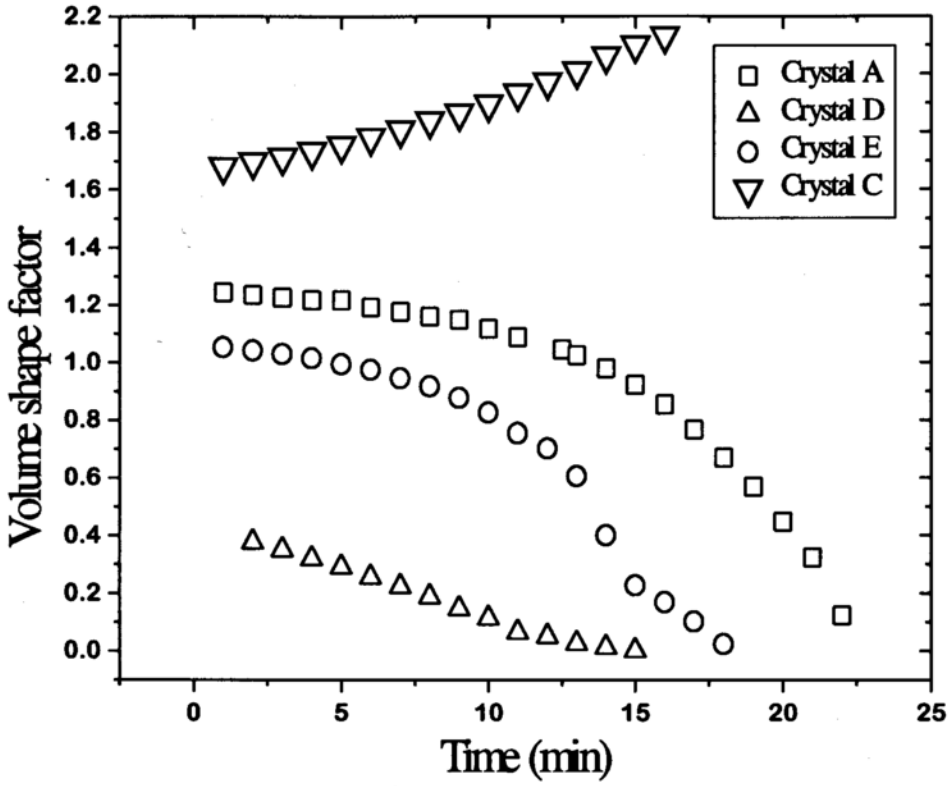

Fig. VI.2-8 Change in the volume shape factor of single crystals of potassium dichromate as a function of dissolution time.

This question now arises: is this observation reasonable? Does α_v always decrease as a function of dissolution time? The derivative of α_v with respect to time should provide the necessary clues to answer this question.

At any time t,

$$\alpha_v = \frac{\ell h}{b^2} \qquad \text{VI.2-10}$$

$$\frac{d\alpha_v}{dt} = \frac{b^2\left(h\frac{d\ell}{dt} + \ell\frac{dh}{dt}\right) - 2\ell bh\frac{db}{dt}}{b^4} \qquad \text{VI.2-11}$$

$$= \frac{-b^2(Kh + K\ell) + 2\ell bhK}{b^4} \quad \text{(assuming isotropic dissolution)}$$

$$= \frac{K}{b^2}\left[\frac{2\ell h}{b} - (h + \ell)\right]$$

For this derivative to be a negative quantity,

$$(h + \ell) > \frac{2\ell h}{b}$$

In terms of the initial dimensions,

$$(h_0 + \ell_0) > \frac{2\ell_0 h_0}{b_0} \qquad \text{VI.2-12}$$

Expressing this in terms of the shape ratios m and n defined earlier, the condition for decrease in α_v as a function of dissolution time is:

$$m + n > 2mn \qquad \text{VI.2-13}$$

where

$$m = \frac{\ell_0}{b_0} \quad \text{and} \quad n = \frac{h_0}{b_0}$$

From Eq. VI.2-13, for certain values of m one can arrive at the restrictions on the value of n such that α_v would be a decreasing function of time. Table VI.2-5 illustrates this point.

For the three crystals shown in Fig. VI.2-8 the values of m and n comply with Eq. VI.2-13. Most crystalline powders will have m values that fall between 5 and 15. For such crystals, if the n value is greater than 0.55, then one would expect the volume shape factor to increase with dissolution time. For crystal C, $m=1.99$ and $n=0.84(>0.67)$. In this case, $2mn>m+n$, α_v would be expected to increase as dissolution proceeds, and so it does. This is true for crystal C as shown in Fig.VI.2-8.

Table VI.2-5 The restrictions on n for various length to breadth ratios such that α_v for a single particle decreases with time.

m	n should be less than
2	0.67
3	0.60
5	0.55
9	0.53
15	0.52

VI.2.4 *Linear decrease in the dimensions of a non-isometric particle*

The theoretical basis for the linear decrease in the dimensions of a parallelepiped was discussed in chapter IV. It must be noted that such zero order kinetics for the disappearance of the respective dimensions of a non-isometric particle is a direct consequence of the sink conditions that prevail during the dissolution process. There is evidence for this in the literature [Edmundson and Lees, 1965, Schoonen, 1979]. In the present work several experiments were conducted to actually measure the length, breadth, and height of the crystal as it underwent dissolution. The crystals were removed from the dissolution medium at regular intervals, the stop clock was stopped, and the dimensions were measured. Subsequently, they were replaced in the medium. The results of this study are shown in Fig. VI.2-9. The change in α_v, α_s, and Γ with respect to dissolution time is shown on one plot in Fig.VI.2-10. The shape factor values have been normalized to the respective largest value to represent them on one plot.

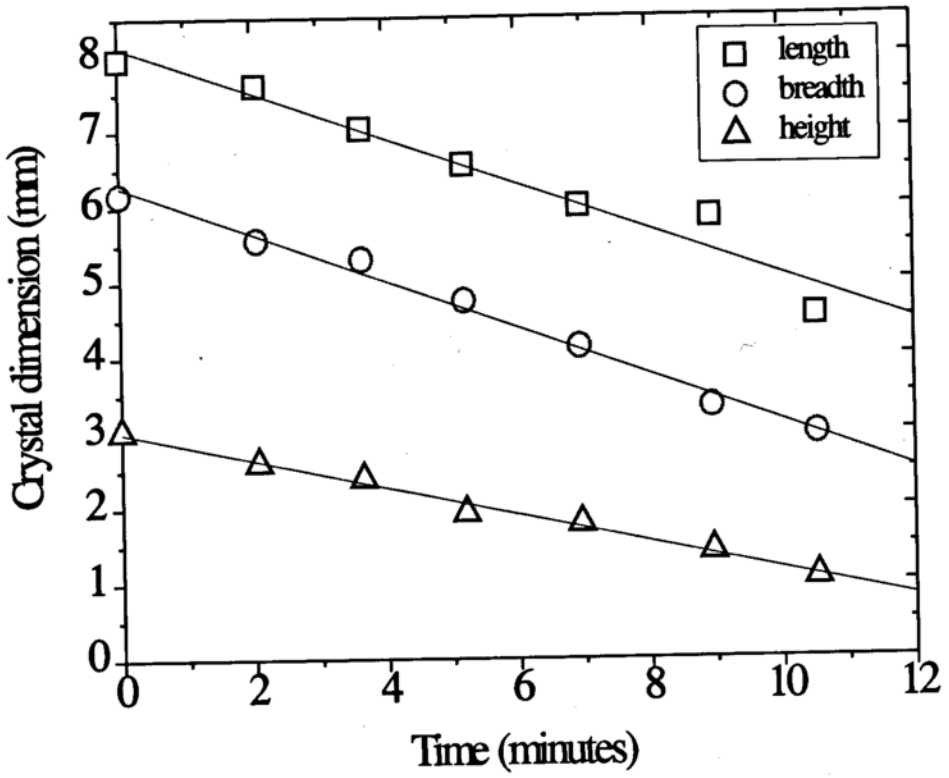

Fig. VI.2-9 Decrease in the length, breadth, and height of a triclinic crystal of potassium dichromate as a result of dissolution in 0.1N H_2SO_4 at 50 rpm and 25°C under sink conditions. The regression on the three dimensions are:

length : $y = 8.12 - 0.304x$, $R^2=0.953$

breadth : $y = 6.28 - 0.314x$, $R^2=0.991$

height : $y = 3.00 - 0.183x$, $R^2=0.992$

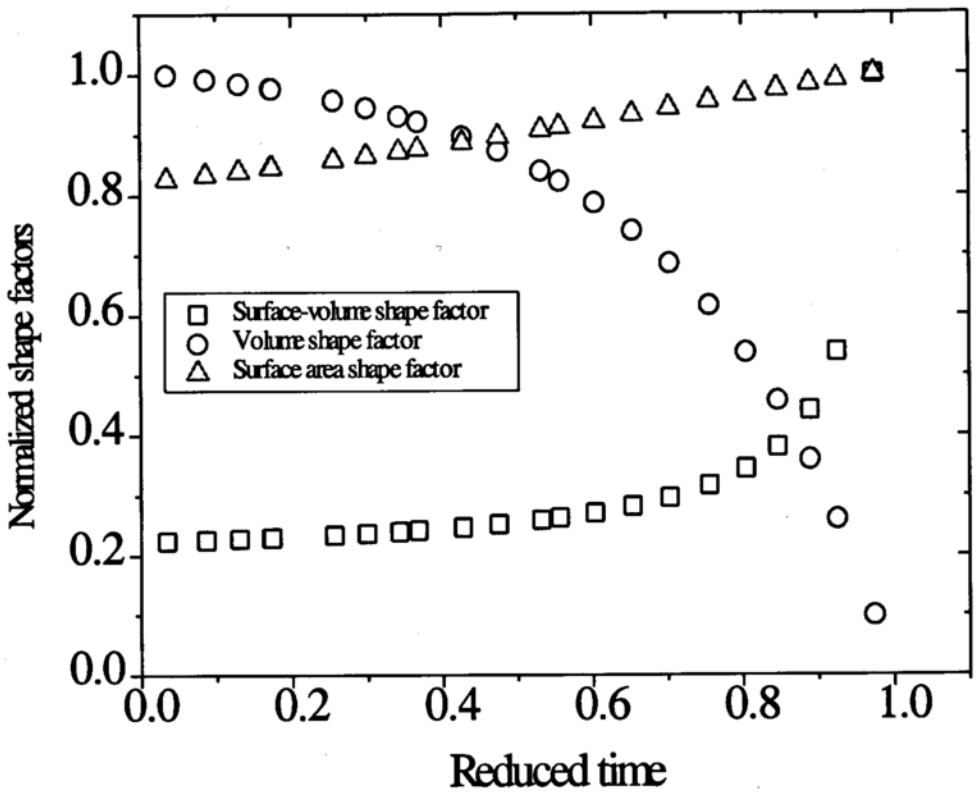

Fig.VI.2-10 Change in α_v, α_s, and Γ with reduced time for crystal A.

VI.3. Particle size distributions from microscopy

As mentioned earlier, four compounds have been selected for powder dissolution studies. The particle size data obtained from microscopy are presented in this section. Two of the three dimensions of the particle can be measured by microscopy. This technique has one major advantage over other methods that are based on electrical resistance and laser diffraction, in that one can see what one actually measures. Hence the experimenter is not committed to making any spherical approximations regarding the particles. This is quite important for well-defined crystal habits like needles, platelets, and prisms, which exhibit high degrees of non-isometry.

The most logical characterization of the distribution for a polydisperse sample is by way of the mean and standard deviation of a representative sample from its population. It is quite common to ascribe a particular type of distribution function to multiparticulate solids; for instance, a Gaussian or a log-normal function. This does not imply that powder technologists have restricted themselves to these two functions only. A completely general approach can be taken by representing the raw data in terms of histograms and obtaining the average, $\overline{X}$ and variance, s^2 of the distribution as follows, where X is any dimension like b_0.

$$\overline{X} = \frac{\sum_{i=1}^{n} N_i X_i}{N_{total}} = \sum_{i=1}^{n} f_i X_i \qquad \text{VI.3-1}$$

$$s^2 = \left[\frac{\sum_{i=1}^{n} N_i X_i^2}{N_{total}} - \overline{X}^2 \right] = \left[\sum_{i=1}^{n} f_i X_i^2 - \overline{X}^2 \right] \qquad \text{VI.3-2}$$

where N_i is the number of particles with the dimension X_i. f_i is the normalized frequency. Typically, a fixed number of intervals are created, which are dictated by the total number of particles counted, N_{total}, and by Sturges rule. The number of intervals, T is given by the following expression:

$$T = 1 + 3.322(\log_{10} N_{total}) \qquad \text{VI.3-3}$$

An account of the number of particles within each interval can be obtained. In this particular case, the midpoint of each interval is denoted by X_i and the number of particles therein is denoted by N_i. It will be shown that this approach can be extended further to obtain the probability density function. It is important to mention that the distributions considered here, are on a *number basis*, rather than weight basis. The fact that the critical time in powder dissolution is approached when the number of particles begin to decrease, justifies this choice.

In the following three methods have been recognized to get the mean and standard deviation of a distribution within a mesh cut. These methods are mutually exclusive, and if they are shown to be self-consistent, then the easiest one would be chosen. Four sieve fractions for oxalic acid dihydrate, three for salicylic acid, two for phthalimide, and unsieved powder of acetaminophen form the lot of powders to be subjected to particle size distribution determinations. The three methods will be demonstrated for a -30/+40 mesh fraction of oxalic acid dihydrate.

VI.3.1 Cumulative percent undersize and probability plots against particle size

The shape of oxalic acid dihydrate crystals from a -30/+40 mesh fraction is shown in Fig.VI.3-1. For the purpose of illustration, the breadth of the particle will be considered, as also, it is the dimension on which the model for multiparticulate dissolution is based. The first step is to obtain the cumulative undersize frequency. The transformation of these values to the standard normal variate (z) can be brought about using statistical tables [Natrella, 1966].

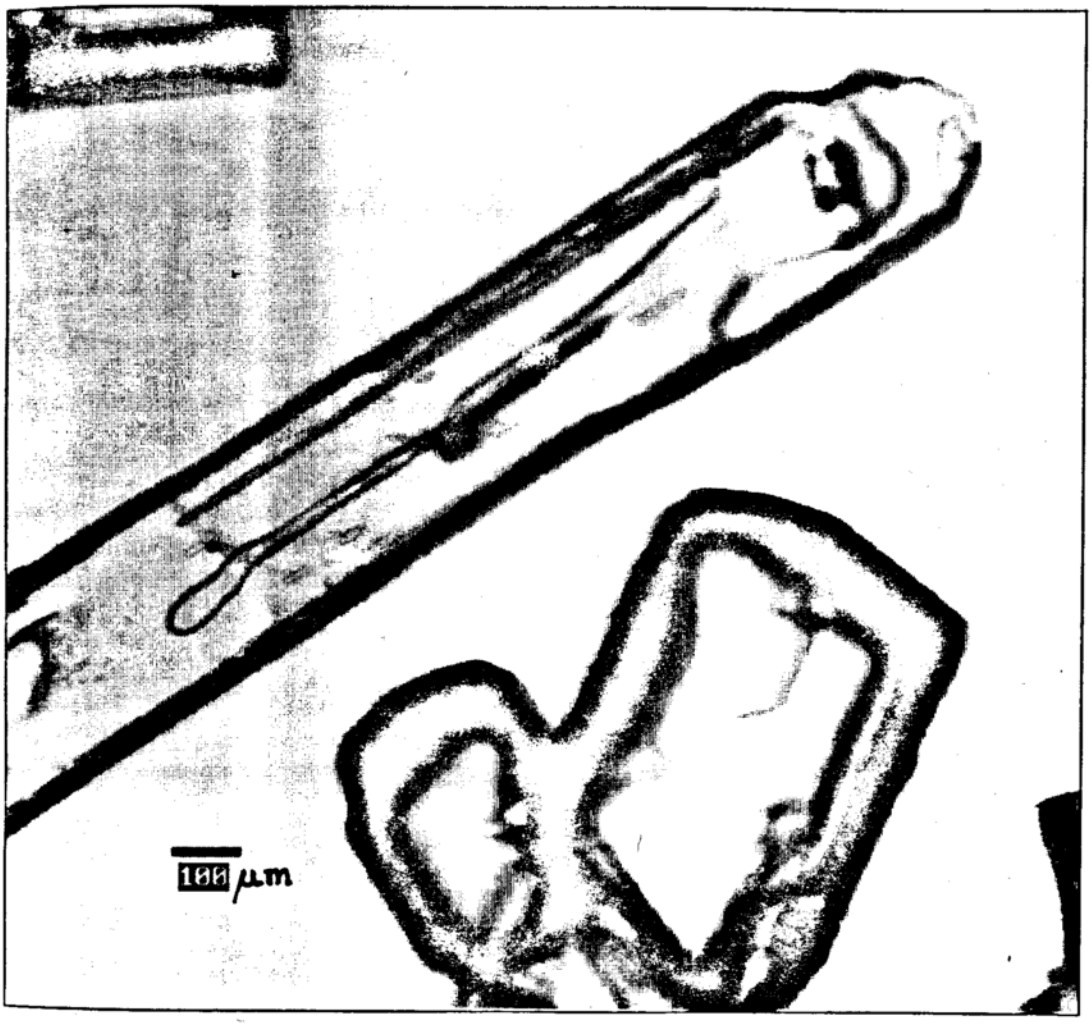

Fig. VI.3-1 Oxalic acid dihydrate crystals from a -30/+40 mesh fraction.

For a sample of -30/+40 mesh fraction of oxalic acid dihydrate,

$N_{total} = 259$, hence $T = 9$

$b_0^{min} = 249$ microns

$b_0^{max} = 622$ microns

Range = 373

Size of interval = $373/9 \approx 41.5$

The data for the number of particles within each interval is given in Table VI.3-1. From the number frequency normalized with respect to N_{total}, the percent cumulative undersize values can be calculated. This plot is shown in Fig. VI.3-2. When the abscissa in this figure is plotted on a probability scale (z values), against mean of the interval, Fig. VI.3-3 results. This plot is useful because, (i) the linearity indicates that the distribution of breadths can be best approximated to a normal distribution (ii) the value of the ordinate at $z=0$ gives the mean of the distribution, which in this case is 394 μm, and (iii) the standard deviation is [ordinate (at $z=1$) - ordinate (at $z=2$)], which is 76 μm.

Table VI.3-1 Results from particle size analysis by microscopy of a -30/+40 mesh fraction of oxalic acid dihydrate.

Interval	Midpoint of interval	Number frequency	Normalized frequency*	%Cumulative undersize	Probability density$
248.5 - 290.5	269.5	11	0.04247	0.00	0.001011
290.5 - 332	311.25	27	0.10425	14.67	0.002512
332 - 373.5	352.75	45	0.17374	32.04	0.004186
373.5 - 415	394.25	51	0.19691	51.74	0.004745
415 - 456.5	435.75	47	0.18147	69.88	0.004323
456.5 - 498	477.25	33	0.12741	82.62	0.003070
498 - 539.5	518.75	32	0.12355	94.98	0.002977
539.5 - 581	560.25	10	0.03861	98.84	0.000930
581 - 622.5	601.75	3	0.01158	100.00	0.000279

* Normalized frequency = Number frequency/N_{total}

$ Probability density function = $f(b_0)$ = Normalized frequency/41.5

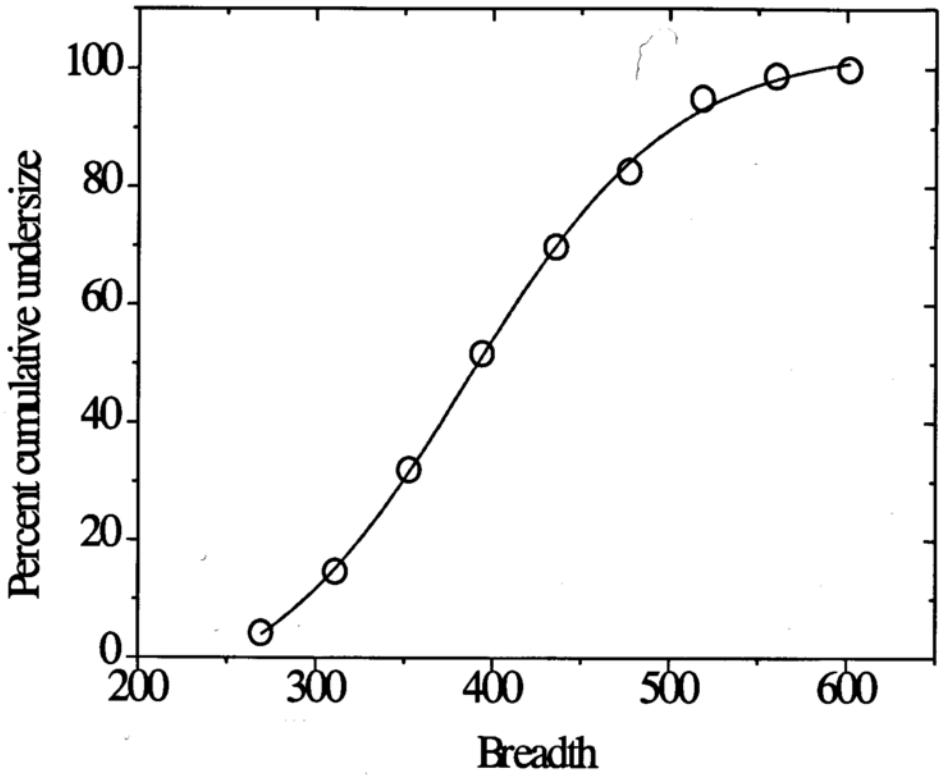

Fig. VI.3-2 Percent cumulative undersize (breadth) versus mean of the interval for a -30/+40 mesh fraction of oxalic acid dihydrate.

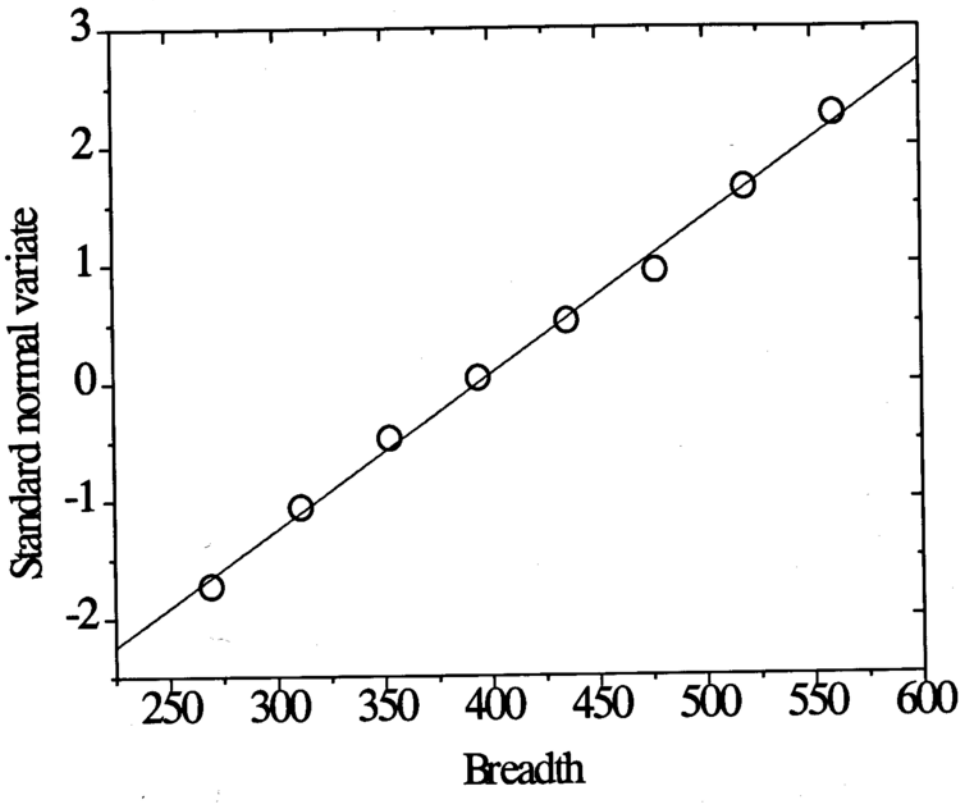

Fig.VI.3-3 Representation of the distribution of the breadths of oxalic acid dihydrate particles (-30/+40 mesh fraction) in terms of the standard normal variate. The regression is $y = -5.213 + 0.0132x$, $R^2=0.996$.

VI.3.2 Model-independent approach to get mean and standard deviation from particle size data

From the normalized frequencies in each class interval given in Table VI.3-1, a histogram can be generated. This is shown in Fig. VI.3-4. Using Eqs. VI.3-1 and VI.3-2 the mean and standard deviation of the distribution can be calculated. The first, second, and third moments (M_1, M_2, and M_3 respectively) of the normalized frequency function are given by the following expressions:

$$M_1 = \sum_{i=1}^{N_{total}} f(b_{0_i}) b_{0_i} \qquad \text{VI.3-4}$$

$$M_2 = \sum_{i=1}^{N_{total}} f(b_{0_i}) \left(b_{0_i}\right)^2 \qquad \text{VI.3-5}$$

$$M_3 = \sum_{i=1}^{N_{total}} f(b_{0_i}) \left(b_{0_i}\right)^3 \qquad \text{VI.3-6}$$

These three moments bear physical significance. M_1 is the mean of the distribution, $(M_2 - M_1^2)$ is the variance, and M_3 is a measure of the total volume of the system of particles. With reference to Table VI.3-1, b_{0i} would be the midpoint of the interval and $f(b_{0i})$ is the normalized frequency.

The following program in Microsoft Basic was written to calculate M_1, M_2, and M_3 for the data presented in Table VI.3-1.

```
100 INPUT "Number of intervals="; Q1
110 INPUT "Total number of particles counted="; Ntotal
120 LPRINT "_____"
130 LPRINT "b0i",   "f(b0i) b0i", "f(b0i)b0i^2","", "f(b0i)b0i^3"
140 LPRINT "_____"
200 READ N1, D1
210 N2 = N2+1
211 N3 = N2/Ntotal
212 N4 = N4+N3
220 X1 = (N3*D1)
230 X2 = X2+X1
240 X3 = (N3*(D1^2))
250 X4 = X4+X3
260 X5 = (N3*(D1^3))
270 X6 = X6+X5
280 LPRINT D1, X1, X3, X5
290 IF N2 = Q1 GOTO 510
300 GOTO 200
400 DATA 11, 269.5
410 DATA 27, 311.25
```

420 DATA 45, 352.75

430 DATA 51, 394.25

440 DATA 47, 435.75

450 DATA 33, 477.25

460 DATA 32, 518.75

470 DATA 10, 560.25

480 DATA 3, 601.75

500 LPRINT D_1, X_1, X_2

510 LPRINT "$\sum f(b_{0i})$ =" ; N_4

520 LPRINT "$\sum f(b_{0i})\ b_{0i}$ = Mean = M_1 =" ; X_2

530 LPRINT "$\sum f(b_{0i})\ b_{0i}^2$ = M_2=" ; X_4

540 LPRINT "$\sum f(b_{0i})\ b_{0i}^3$ = M_3=" ; X_6

550 VAR = X_4 - (X_2)^2

560 SD = (VAR)^(0.5)

570 LPRINT "Standard deviation ="; SD

The data statements in this program refer to the -30/+40 mesh fraction of oxalic acid dihydrate. The output of this program is complied in Table VI.3-2. The mean and standard deviation for this mesh fraction, by this method are found to be 415 μm and 77 μm.

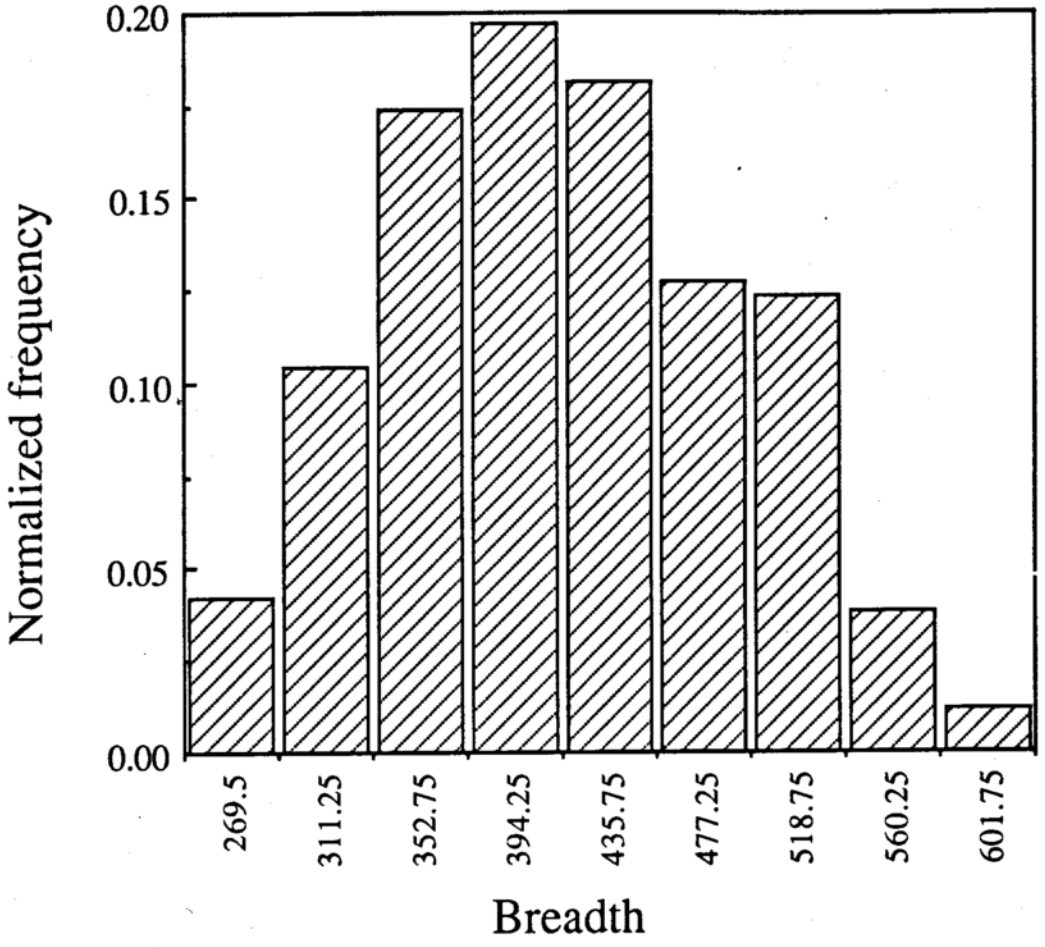

Fig.VI.3-4 Histogram for the distribution of breadths of oxalic dihydrate particles from a -30/+40 mesh fraction.

Table VI.3-2 A discrete approach to determine the mean and standard deviation of a -30/+40 mesh fraction of oxalic acid dihydrate.

Number frequency	b_{0i} /μm	$f(b_{0i})$	$f(b_{0i})b_{0i}$/μm	$f(b_{0i})b_{0i}^2$ /μm^{-2}	$f(b_{0i})b_{0i}^3$ /μm^{-3}
11	269.5	0.042471	11.44	3084.68	831321.08
27	311.25	0.104247	32.45	100099.09	3143342.07
45	352.75	0.173745	61.28	21619.54	7626291.17
51	394.25	0.196911	77.63	30606.48	12066604.65
47	435.75	0.181467	79.07	34456.60	15014464.48
33	477.25	0.127413	60.81	29020.54	13850056.74
32	518.75	0.123552	64.09	33248.03	17247418.80
10	560.25	0.038610	21.63	12118.91	6789618.89
3	601.75	0.011583	6.97	4194.24	2523883.78

The sums of each column are:

259	-	1.0000	415.4	1.7845×10^5	7.9093×10^7

VI.3.3 Continuous functions to characterize particle size distributions

Continuous functions were alluded to at a point when particle size distributions were discussed in the first chapter. It is a convenient means of representing the polydispersity in a multiparticulate system. Just as in the case of discrete distributions, the various moments can be defined. In this case, the summations are replaced by integrals.

$$I_j = \int_{-\infty}^{\infty} (b_0)^j f(b_0)\, db_0 \qquad \text{VI.3-7}$$

where j = 0, 1, 2, and 3.

For real distributions, there is always a smallest and a largest dimension. Hence for such truncated distributions the limits of integration have to be finite real numbers. There is one subtle difference between the discrete and continous functions. The normalised frequency $f(b_{0\,i})$ from discrete distributions is not the same as $f(b_0)$ in Eq.VI.3-7. The latter is the probability density function, which can be obtained from the normalized frequency in the following manner.

$$f(b_0) = \frac{f(b_{0i})}{b_{int}} \qquad \text{VI.3-8}$$

where b_{int} is the size of the interval in the discrete distribution. The calculated values for $f(b_0)$ for a -30/+40 mesh fraction of oxalic acid dihydrate with an interval size of 41.5 μm are shown in Table VI.3-1. These are the abscissa values in the plot shown in Fig.VI.3-5. Each value of $f(b_0)$ corresponds to a midpoint of the interval. The data suggest that a normal distribution could be a good approximation. The data are fitted to the following equation by non-linear regression to get the mean M_{b0}, and standard deviation σ of the distribution.

$$f(b_0) = \frac{1}{\sigma\sqrt{2\pi}} \exp\left\{ -\frac{(b_0 - M_{b_0})^2}{2\sigma^2} \right\} \qquad \text{VI.3-9}$$

From Fig.VI.3-5, M_{b0} = 410 μm and σ = 85 μm. These values are in good agreement with the ones calculated from the first two methods. Hence, from here on, continous distributions would be the representation of choice for the sieve fractions of all compounds. It was observed that the size distribution of powders from all the four sieve fractions of oxalic acid dihydrate could be best described with a normal distribution. The probability plots for these sieve fractions were

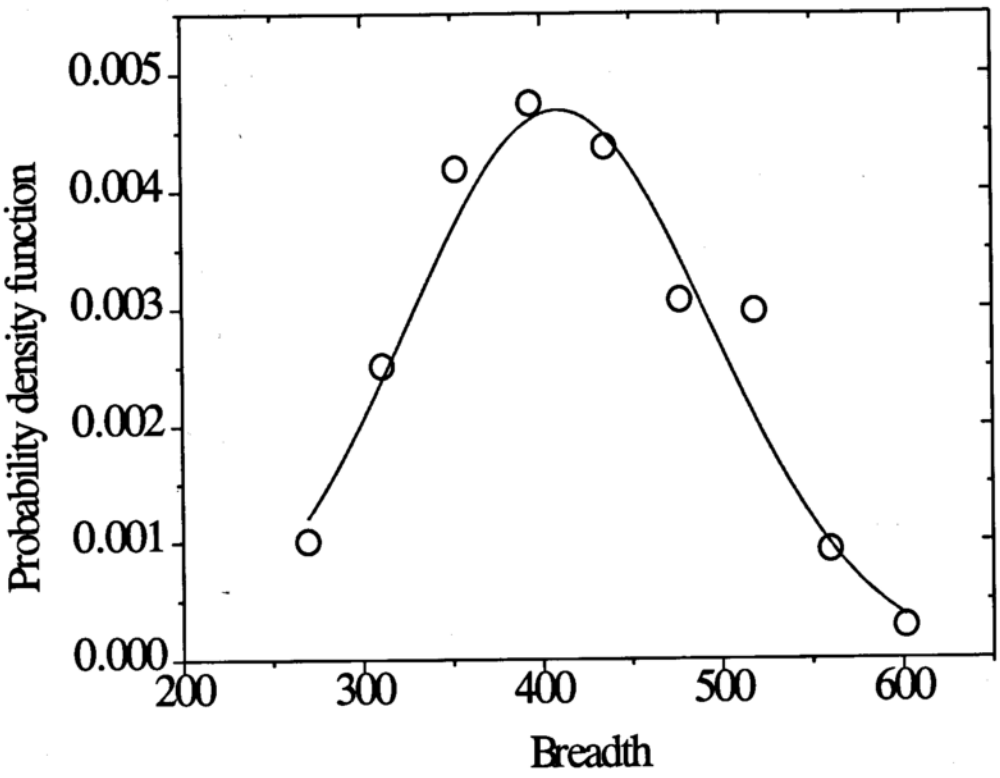

Fig. VI.3-5 Continuous distribution for a -30/+40 mesh fraction of oxalic acid dihydrate. χ^2 for the fit = 1.77×10^{-7}.

Table VI.3-3 The mean and standard deviation of breadths of oxalic acid dihydrate particles from different sieve fractions and unsieved acetaminophen that followed a gaussian distribution.

Sieve Fraction	Sieve opening in μm	M_{b0} in μm	σ in μm	b_0^{min} in μm	b_0^{max} in μm
Oxalic acid dihydrate -					
-30/+40	-600/+425	410	85	249	622
-40/+50	-425/+300	299	55	202	436
-50/+60	-300/+250	240	40	148	323
-60/+80	-250/+177	155	32	92	256
Acetaminophen -					
unsieved	-	167	60	50	382

linear with respect to breadth of the particle. The results of particle size analysis for these fractions are compiled in Table VI.3-3. The first, second, and third moments (I_1, I_2, and I_3) of the probability density function were computed by numerical integration. These values compared very well with the moments, M_1, M_2, and M_3 respectively (obtained from discrete distributions) for the -30/+40 mesh fraction of oxalic acid dihydrate. The utlility of these integrals will be discussed in detail in subsequent sections of this chapter. For the -30/+40 mesh fraction, I_0 = 0.96457, I_1 = 399.6 μm, I_2 = 171270 μm^2, and I_3 = 75759800 μm^3. The value of I_0 is close to unity. If that is normalized to 1, then I_1, I_2, and I_3 assume the following values: 414 μm, 177560 μm^2, and 78542563 μm^3. There is good agreement between these integral sums and the sums given in Table VI.3-2.

VI.3.4. Skewed distributions

The mesh fractions of salicylic acid, and phthalimide were "wider" than those of oxalic acid. Histograms for the breadths of particles of these compounds indicated that they were skewed to the right. In most instances, such distributions have been approximated to a log-normal function. As discussed earlier, in a log-normally distributed sample, the logarithm of the sizes are normally distributed.

As a direct consequence of that, the probability density function for skewed populations have to be computed differently than what was done for sieve fractions of oxalic acid dihydrate. This is shown in Table VI.3-4 for a -60/+100 mesh fraction of salicylic acid. When a logarithmic transformation of the ordinate values is carried out, the width of the intervals for the breadths becomes unequal. This has to be taken into consideration when one calculates the probability density function from the frequency function.

$$f(b_0) = \frac{1}{\ln(\sigma_g)\sqrt{2\pi}} \exp\left\{-\frac{\left[\ln(b_0) - \ln(M_{b_0})\right]^2}{2\ln^2 \sigma_g}\right\} \qquad \text{VI.3-10}$$

In this equation, M_{b0} is the geometric mean of breadth and σ_g is the geometric standard deviation.

For a sample from a -60/+100 mesh fraction of salicylic acid,

$N_{total} = 342$, hence T=9

$b_0^{min} = 23\ \mu$

$b_0^{max} = 197\ \mu$

Range = $174\ \mu$

Size of interval = $174/9 \approx 19.5$ (linear scale)

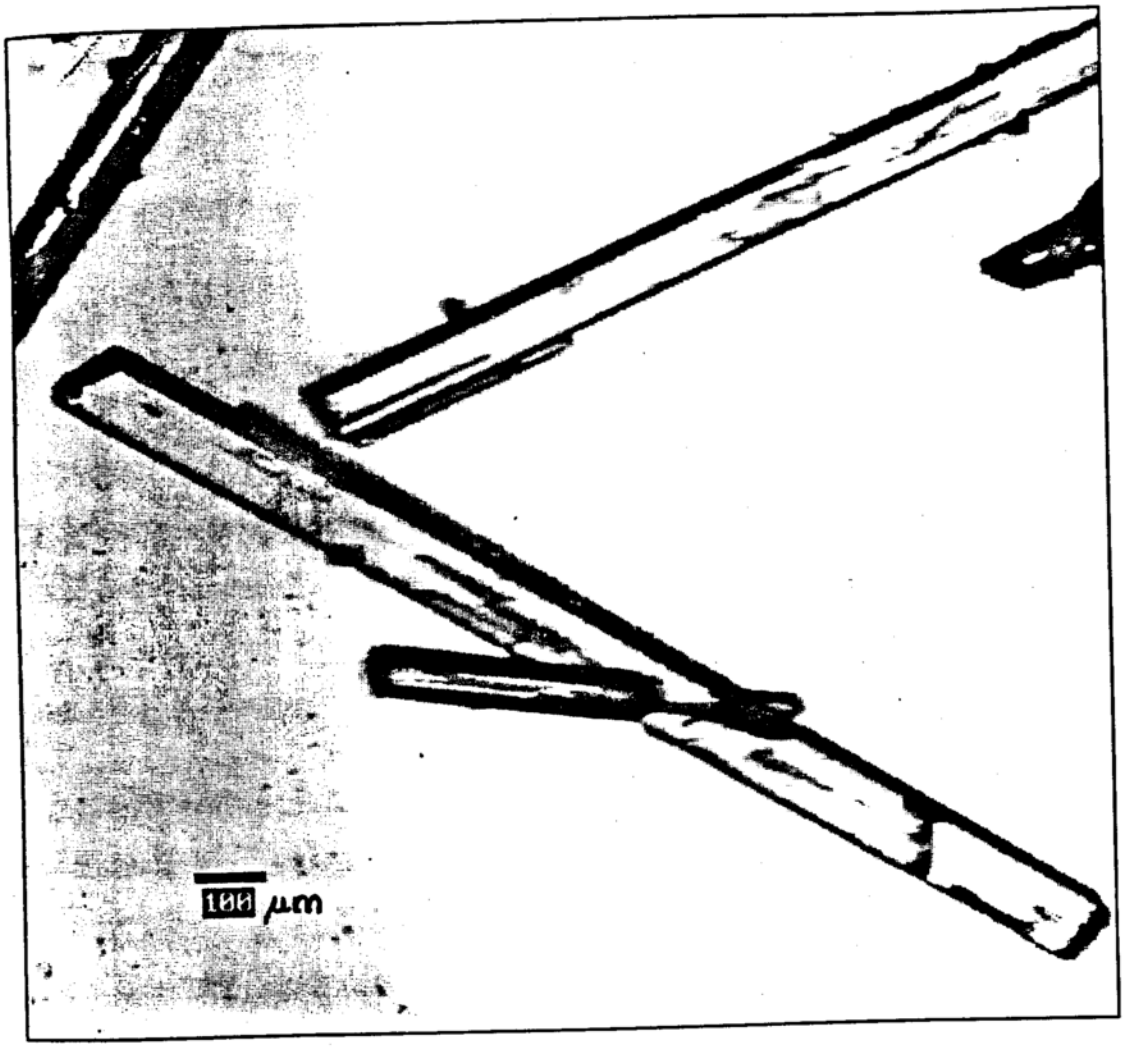

Fig. VI.3-6 Salicylic acid crystals from a -60/+100 mesh fraction.

Table VI.3-4 Particle size analysis data for a -60/+100 mesh fraction salicylic acid and the computation of probability density function.

Lower limit of interval (L) μm	Upper limit of interval (U) μm	Number frequency (N_i)	Fractional frequency (f_i) $= \frac{N_i}{N_{total}}$	Probability density $f(b_0)$ $= \frac{f_i}{\exp(\ln U - \ln L)}$	Mid point of interval $= \exp\left(\frac{\ln U + \ln L}{2}\right)$ in μm
22.5	42	21	0.06140	0.03289	30.7
42	61.5	70	0.20468	0.13978	50.8
61.5	81	86	0.25146	0.19092	70.6
81	100.5	90	0.26316	0.21210	90.2
100.5	120	44	0.12865	0.10775	109.8
120	139.5	17	0.04970	0.04276	129.4
139.5	159	8	0.02339	0.02052	148.9
159	178.5	4	0.01169	0.01042	168.5
178.5	198	2	0.00585	0.00527	188.0

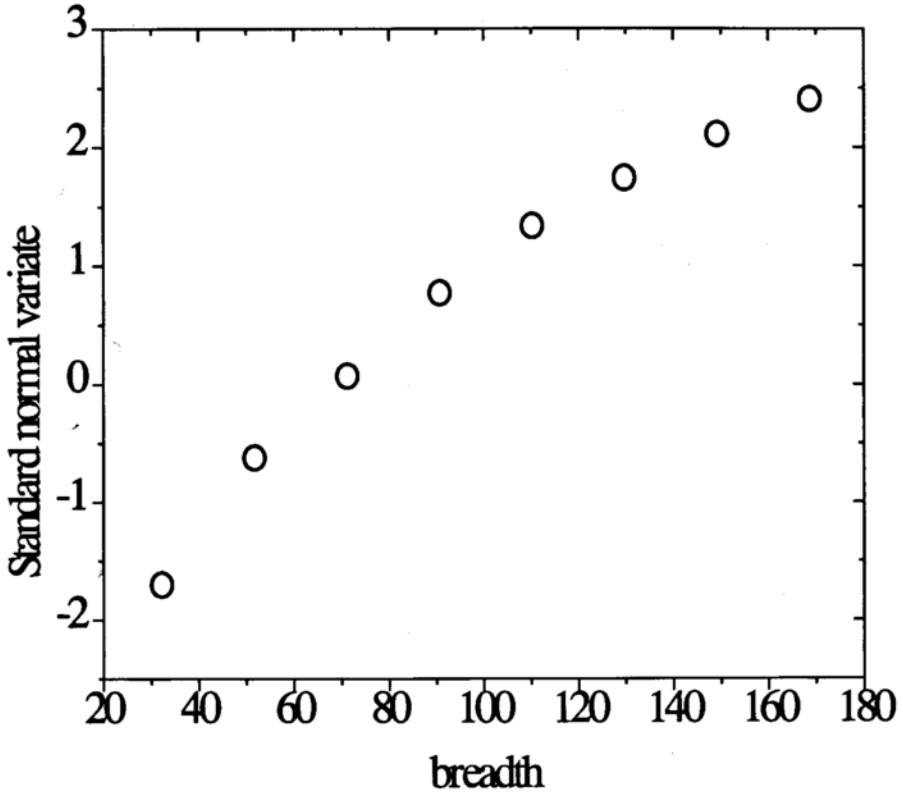

Fig. VI.3-7 Standard normal variate (z) plotted versus interval mean of the breadth for a sample from a -60/+100 mesh fraction of salicylic acid.

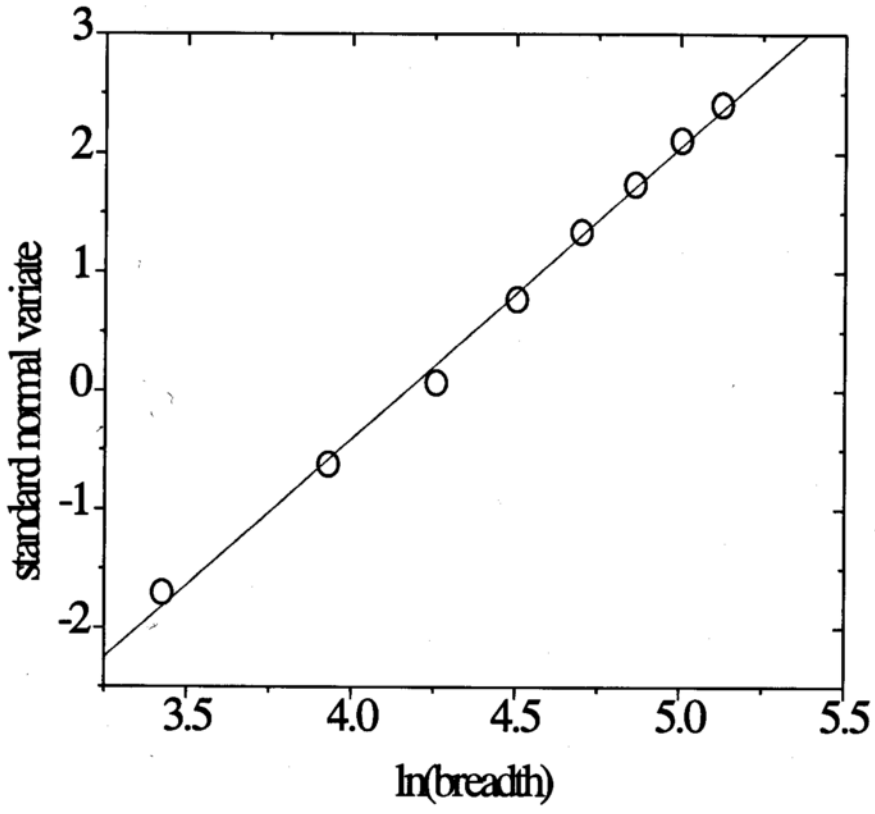

Fig.VI.3-8 Standard normal variate (z) plotted versus logarithm of interval mean of the breadth for a sample from a -60/+100 mesh fraction of salicylic acid.

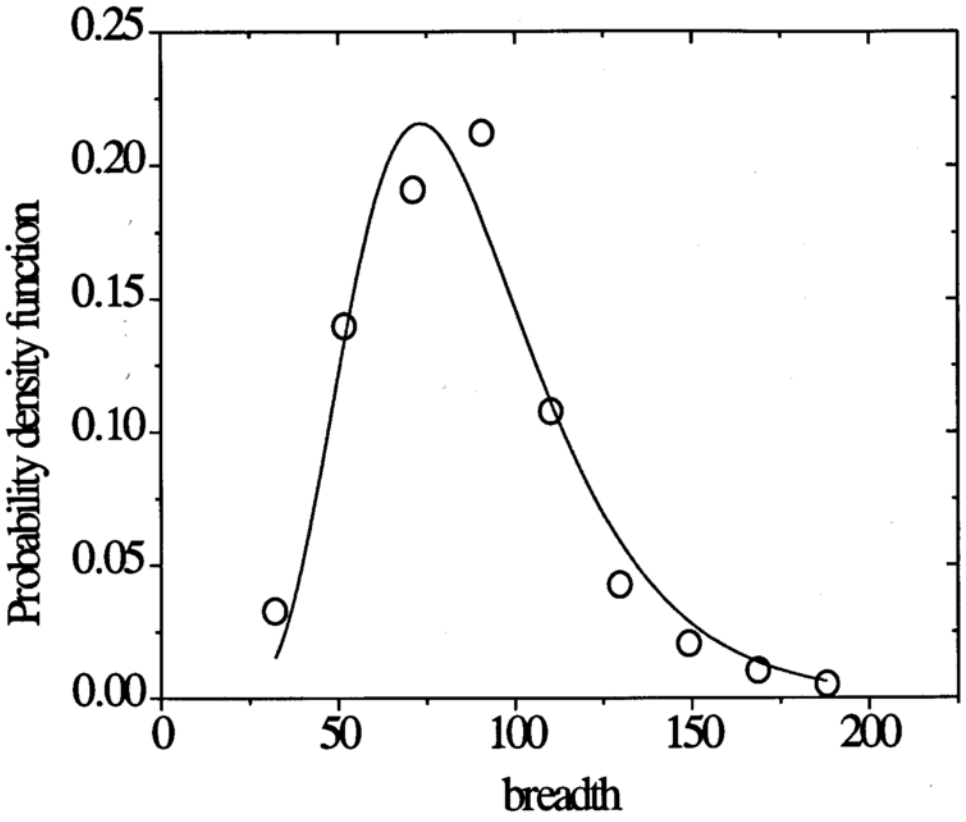

Fig. VI.3-9 Log-normal distribution function for a -60/+100 mesh fraction of salicylic acid. χ^2 for the fit = 0.00041.

As in the case of oxalic acid dihydrate, from the normalized frequency, the cumulative undersize frequency can be calculated. From standard statistical tables, z value for each breadth interval was determined. This is plotted in Fig.VI.3-6 on a linear scale. The curvature in the plot indicates that the breadths of these salicylic acid particles are not normally distributed. In the subsequent graph in Fig.VI.3-7 the ordinates are plotted on a logarithmic scale. The linearity in this plot lends support to the fact that a log-normal function would represent the data more closely. The calculation of probability density function is shown in the fifth column of Table VI.3-4. These values have been plotted in Fig.VI.3-8. The non-linear fit to the data is governed by the following equation:

$$f(b_0) = \frac{\phi}{\ln(\sigma_g)\sqrt{2\pi}} \exp\left\{-\frac{\left[\ln(b_0) - \ln(M_{b0})\right]^2}{2\ln^2 \sigma_g}\right\} \qquad \text{VI.3-11}$$

In the process of carrying out a non-linear regression analysis of the data, a pre-exponential factor had to be introduced in Eq. VI.3-10. Hence there were three parameters to be estimated in the minimization routine; ϕ, M_{b0}, and σ_g. The pre-exponential factor seems to be an outcome of the normalization process for skewed distributions. Its presence in Eq.VI.3-11 has no bearing on the estimated value of the geometric mean and standard deviation. This will become more clear

by if one examines the following calculation. For salicylic acid powder belonging to the -60/+100 mesh fraction,

$\phi = 0.195$, $M_{b0} = 72\ \mu m$, and $\sigma_g = 1.43$ or $\ln(\sigma_g) = 0.36$

Numerical integration yielded the following results:

$$I_0^* = \int_{23}^{197} f(b_0)\, d\ln b_0 = 0.1950$$

$$I_1^* = \int_{23}^{197} \left[f(b_0)\, b_0\right] d\ln b_0 = 14.92$$

$$I_2^* = \int_{23}^{197} \left[f(b_0)\,(b_0)^2\right] d\ln b_0 = 1289.7$$

$$I_3^* = \int_{23}^{197} \left[f(b_0)\,(b_0)^2\right] d\ln b_0 = 125240$$

The value of the first integral is equal to the pre-exponential factor. The integrals are then normalized by dividing each one of them by I_0^* giving,

$I_0 = 1$

$I_1 = 76.5\ \mu m$

$I_2 = 6610.2\ \mu m^2$

$I_3 = 642255.4\ \mu m^3$

The geometric mean obtained by numerical integration is in good agreement with the estimated value from the fit. The breadths of particles from two other seive fractions of salicylic acid, viz., -40/+60 and -100/+200, the -40/+60 and -60/+100 mesh fractions of phthalimide, all followed log-normal distribution. The results from particle size analysis of these compounds are presented in Table VI.3-5.

Powder aggregation problems were encountered with salicylic acid and phthalimide. On a comparative basis phthalimide aggregated to a greater extent than salicylic acid. This is a common problem with many low solubility, hydrophobic drug compounds. Such interparticle cohesion has been attributed, amongst other physical factors, to the presence of static charge on the surface of the particles [Hollenbach, 1983]. A recent report claims that use of silicon dioxide at low concentrations can potentially reduce aggregation by adhering to

Table VI.3-5 The mean and standard deviation of breadths of salicylic acid and phthalimide particles from different sieve fractions that followed a log-normal distribution.

Sieve Fraction	Sieve opening in μm	M_{b0} in μm geometric mean	σ_g	b_0^{min} in μm	b_0^{max} in μm
Salicylic acid -					
-40/+60	-425/+250	91	1.38	32	249
-60/+100	-250/+177	72	1.43	23	197
-100/+200	-177/+150	50	1.43	11	124
Phthalimide -					
-40/+60	-425/+250	50	1.53	20	145
-60/+100	-250/+177	41	1.52	14	121

the surface of such cohesive particles and thereby modifying their surface characteristics [Desai et al., 1996]. The particle size analysis data in Table VI.3-5 and microscopy give a clear indication of aggregation of salicylic acid and phthalimide particles. Sieving does not seem to be desegregate the particles. Therefore the average of the sieve opening of the upper and lower sieve does not match with the geometric mean of the breadth of the particle. However, the purpose of sieving was to classify the crystalline substance into fractions such that, each of these fractions could be characterized with a distinct average aspect ratio. The methodology worked well for oxalic acid dihydrate and to some extent for salicylic acid. The values of the integrals I_j (j=0 to 3) for the four compounds are listed in Table VI.3-6. The knowledge of these integrals will be helpful in sections VI.4 and VI.5.

For individual particles, the length and the breadth of the particles were measured. Up to this point the distribution of the breadths was considered. In order to characterize the shape of the particles in terms of the shape factors that were discussed in chapter IV, the distribution of the lengths of the particles within a sieve fraction also needs to be considered. For all the sieve fractions of oxalic acid dihydrate and unsieved acetaminophen crystals, the lengths were normally distributed.

Table VI.3-6 Values of the integrals I_j obtained by numerical integration for the four compounds which were studied.

Sieve fraction	I_0	I_1 μm	I_2 μm^2	I_3 μm^3
Oxalic acid dihydrate -				
-30/+40	1.0	414	177560	785542237
-40/+50	1.0	303	94586	30199172
-50/+60	1.0	239	58577	14650474
-60/+80	1.0	157	25478	4280250
Salicylic acid -				
-40/+60	1.0	97	10333	1216790
-60/+100	1.0	76	6614	642256
-100/+200	1.0	53	3142	208506
Phthalimide -				
-40/+60	1.0	53	3253	225425
-60/+100	1.0	44	2290	137096
Acetaminophen -				
Unsieved	1.0	170	32255	6618166

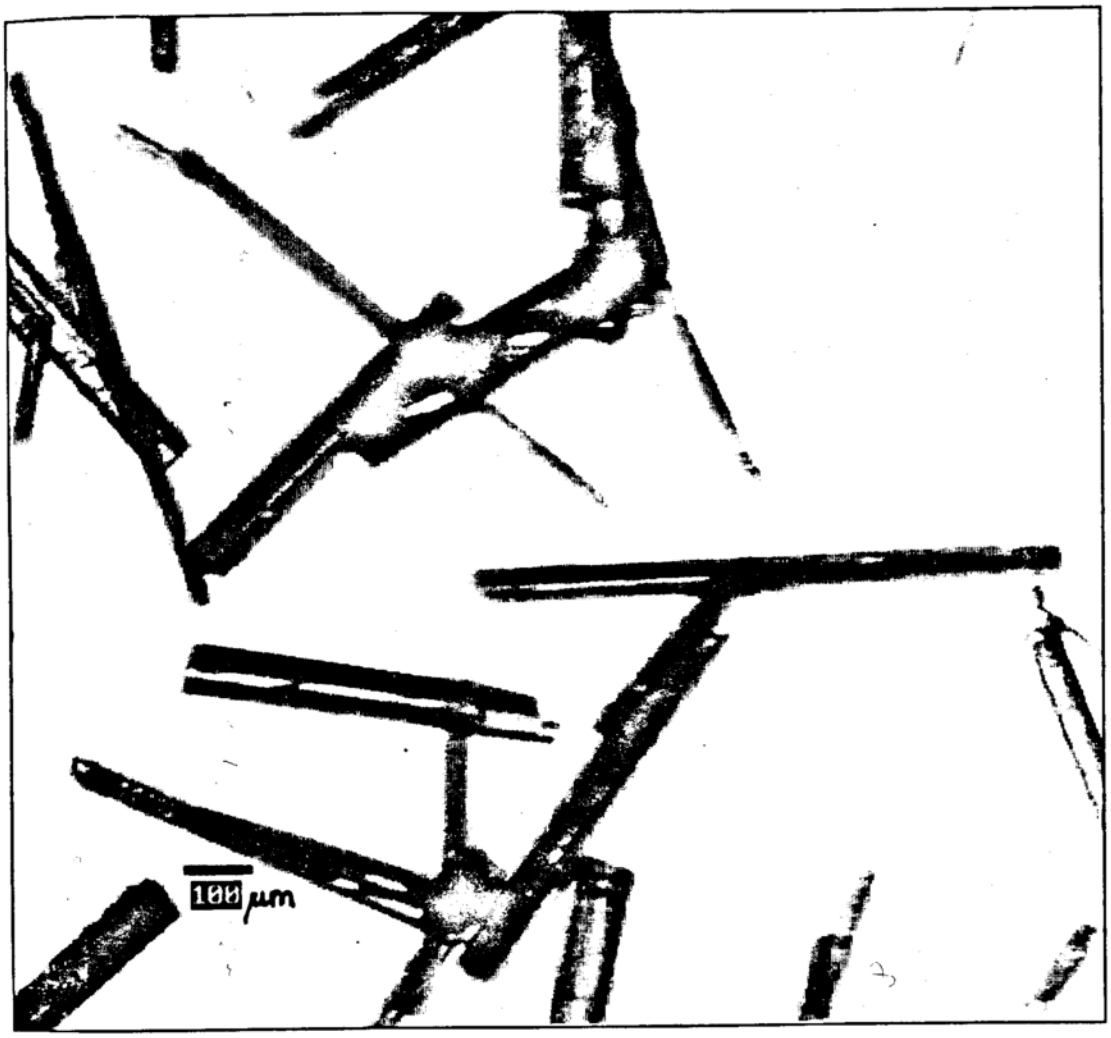

Fig. VI.3-10 Phthalimide crystals from a -40/+60 mesh fraction.

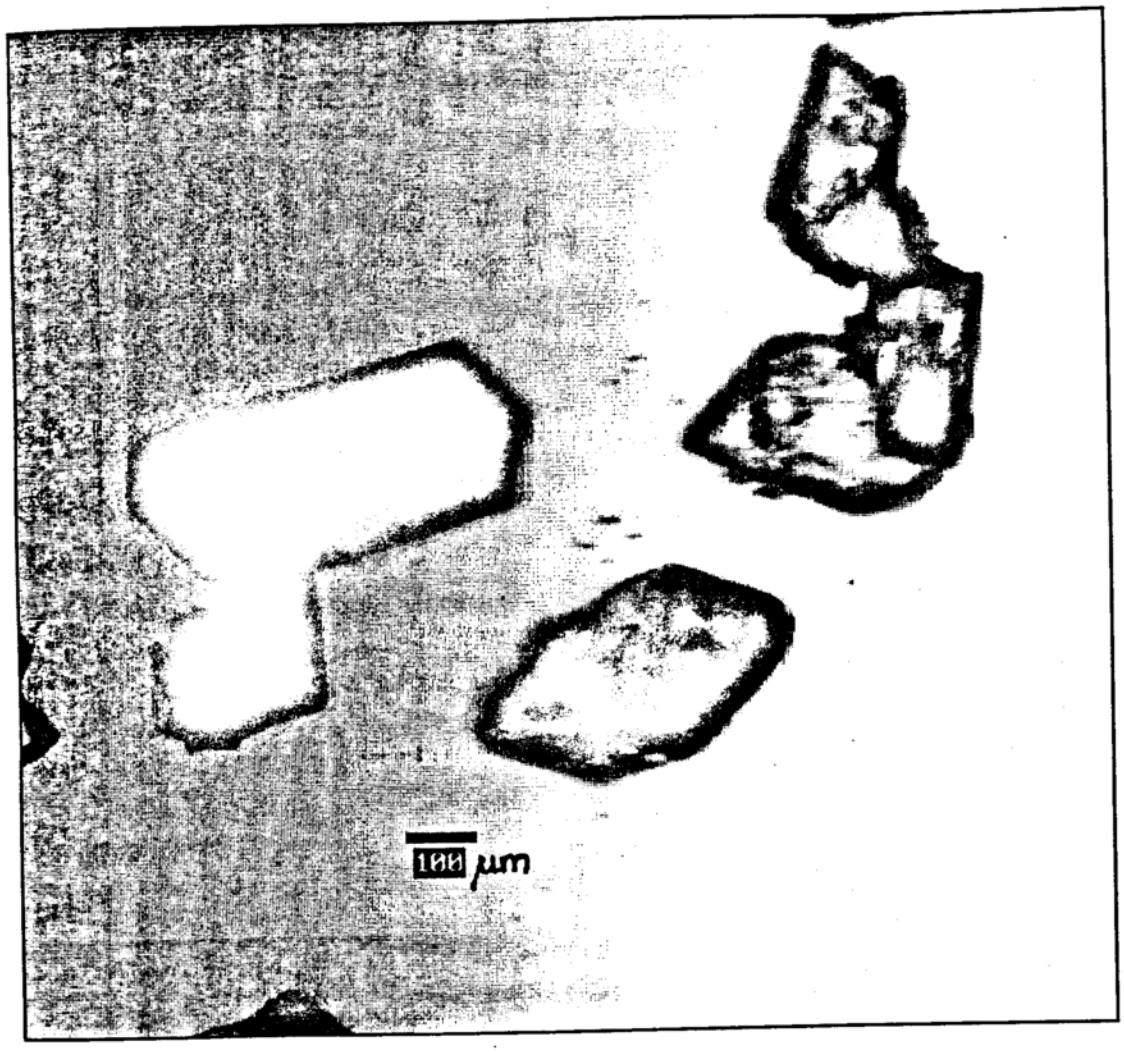

Fig. VI.3-11 A recrystallized sample of acetaminophen (unsieved).

On the other hand, for salicylic acid and phthalimide, the lengths were found to follow a log-normal distribution. From the length and breadth of individual crystals, the distribution of the ratio could be obtained. Thus the probability density functions were computed. Two such curves are shown in Figs. VI.3-11 and VI.3-12. From these the mean and the standard deviation of the distribution were determined. In a subsequent section it will be shown that the mean of the length to breadth ratio is one form of the volume shape factor. This value can be compared with the one that can be obtained from powder dissolution data. A list of these ratios for all the compounds is given in Table VI.3-7.

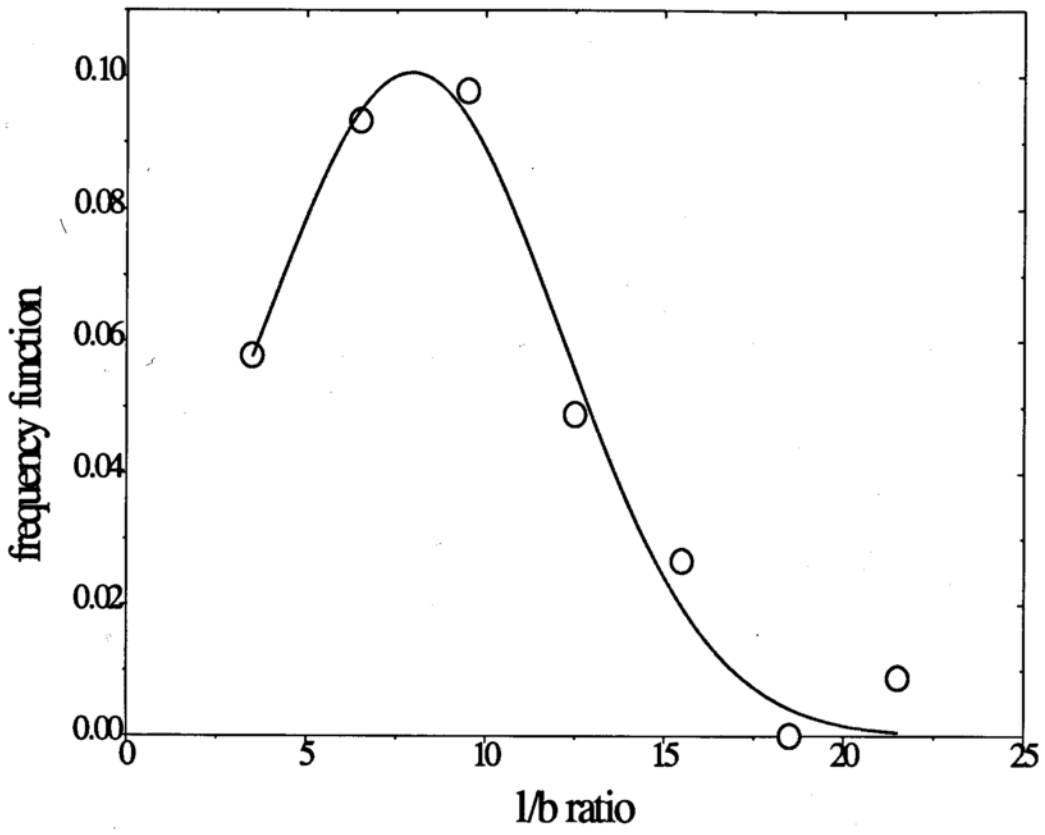

Fig. VI.3-12 Normal distribution of the length to breadth ratio of oxalic acid dihydrate crystals from a -40/+50 sieve fraction. The mean and standard deviation are 7.9 and 4.2 respectively. χ^2 for the fit is 4.96×10^{-5}.

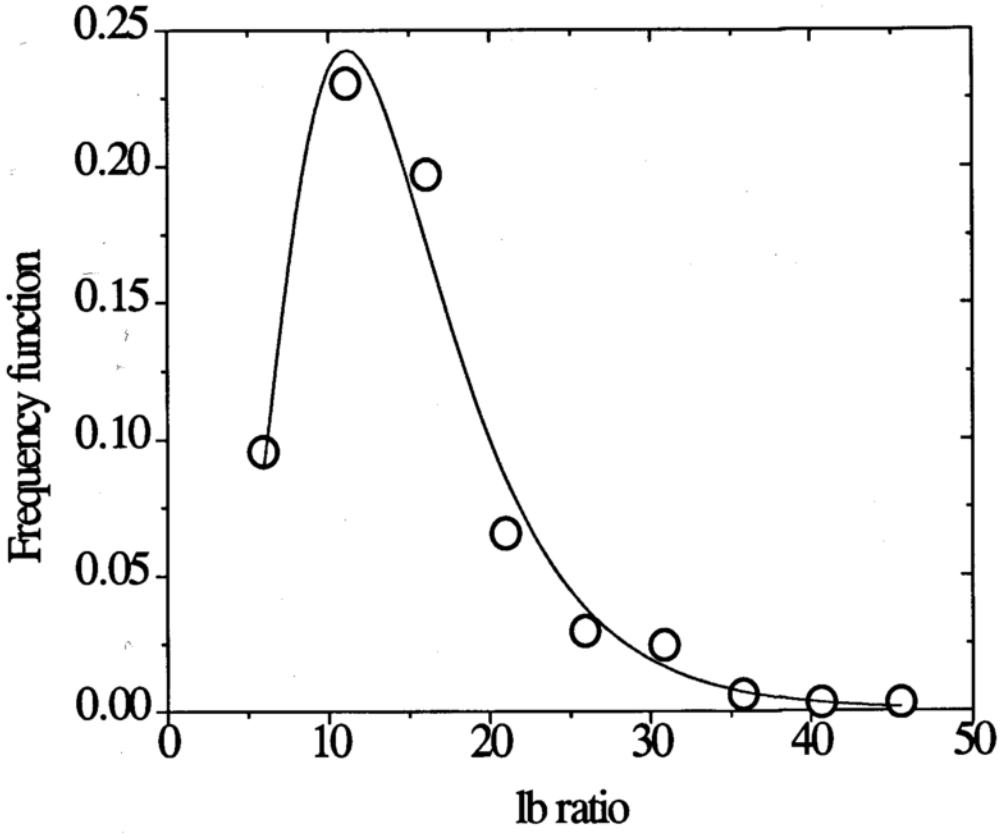

Fig. VI.3-13 Log-normal distribution of the length to breadth ratio of phthalimide crystals from a -40/+60 sieve fraction. The geometric mean and geometric standard deviation are 11.1 and 1.55 respectively. χ^2 for the fit is 0.00023.

Table VI.3-7 Descriptive statistics on the length to breadth ratios for particles of all the four compounds.

Sieve fraction	Mean $\left(\frac{\ell_0}{b_0}\right)$	Standard dev of $\left(\frac{\ell_0}{b_0}\right)$
Oxalic acid dihydrate (normally distributed)		
-30/+40	4.8	2.61
-40/+50	8.0	4.19
-50/+60	8.8	3.96
-60/+80	12.5	4.88
Acetaminophen (normally distributed)		
unsieved	1.7	0.54
Salicylic acid (log-normally distributed)		
-40/+60	11.1 *	0.52 $
-60/+100	14.6 *	0.49 $
-100/+200	15.7 *	0.59 $
Phthalimide (log-normally distributed)		
-40/+60	11.0*	0.44 $
-60/+100	13.1*	0.47 $

* = geometric mean, $ = ln(geometric standard deviation)

VI.4. Determination of intrinsic dissolution rate constants from powder dissolution data

In this section, the method for calculating the intrinsic dissolution rate constant of a powder substance from pre-critical time dissolution data is described. As discussed in chapter IV (Eq.IV.2-4), the K value can be obtained from the fraction undissolved and the values of integrals given in Table VI.3-6. From the density and saturation solubility of the substance in the dissolution medium, the intrinsic dissolution rate constant under the specified hydrodynamic conditions can be calculated.

The methodology described above is exemplified for the dissolution of the -40/+60 mesh fraction of phthalimide. From the biphasic nature of the cube root plot shown in Fig.VI.4-1 an estimate of the critical time can be obtained. For the -40/+60 mesh fraction this was found to be 39 minutes. The fraction undissolved prior to this time period can be plotted as a function of dissolution time. This is shown in Fig. VI.4-2. It follows from Eq.IV.2-4 that these data can be fitted to a third degree polynomial. From the coefficient of the term in t and the value of the integrals I_2 and I_3, K can be evaluated.

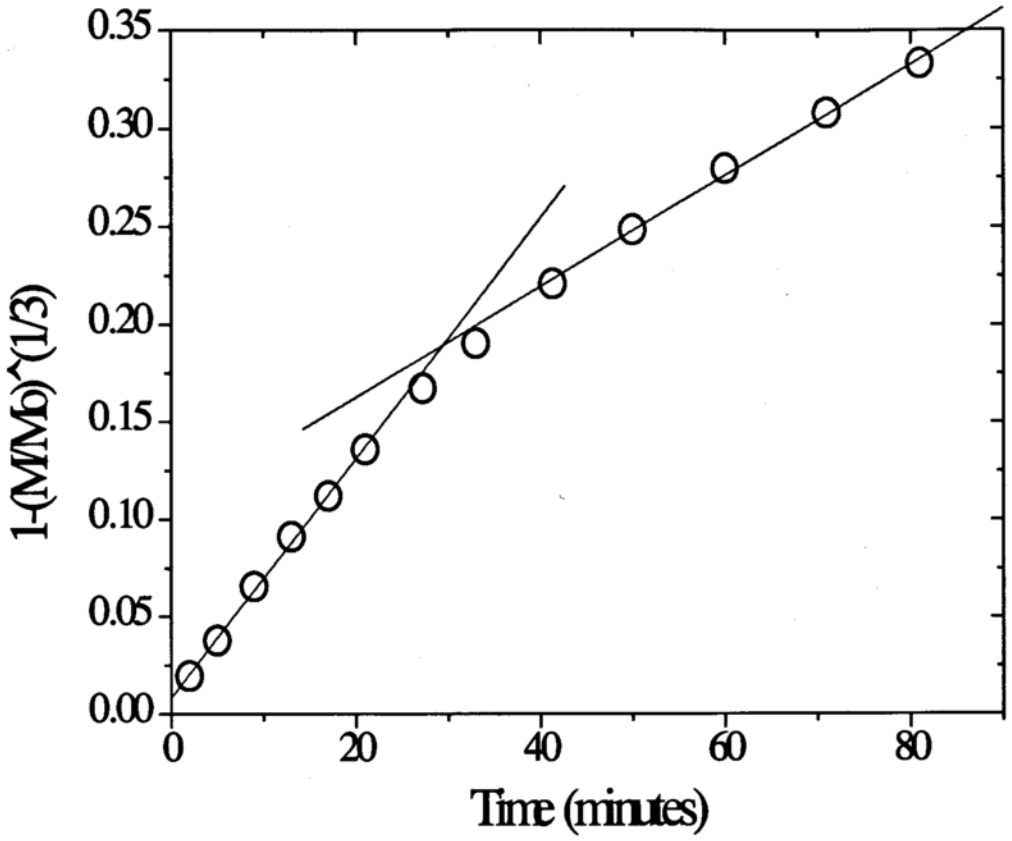

Fig. VI.4-1 Cube root law plot for the dissolution of a -40/+60 mesh fraction of phthalimide in 0.1N HCl containing 0.0005% Tween 80 at 50 rpm and 25°C. Linear regression for the pre-critical time dissolution is $y=0.0084+0.00615x$, $R^2=0.998$, and linear regression for post-critical time is $y=0.1061+0.00284x$, $R^2=0.997$.

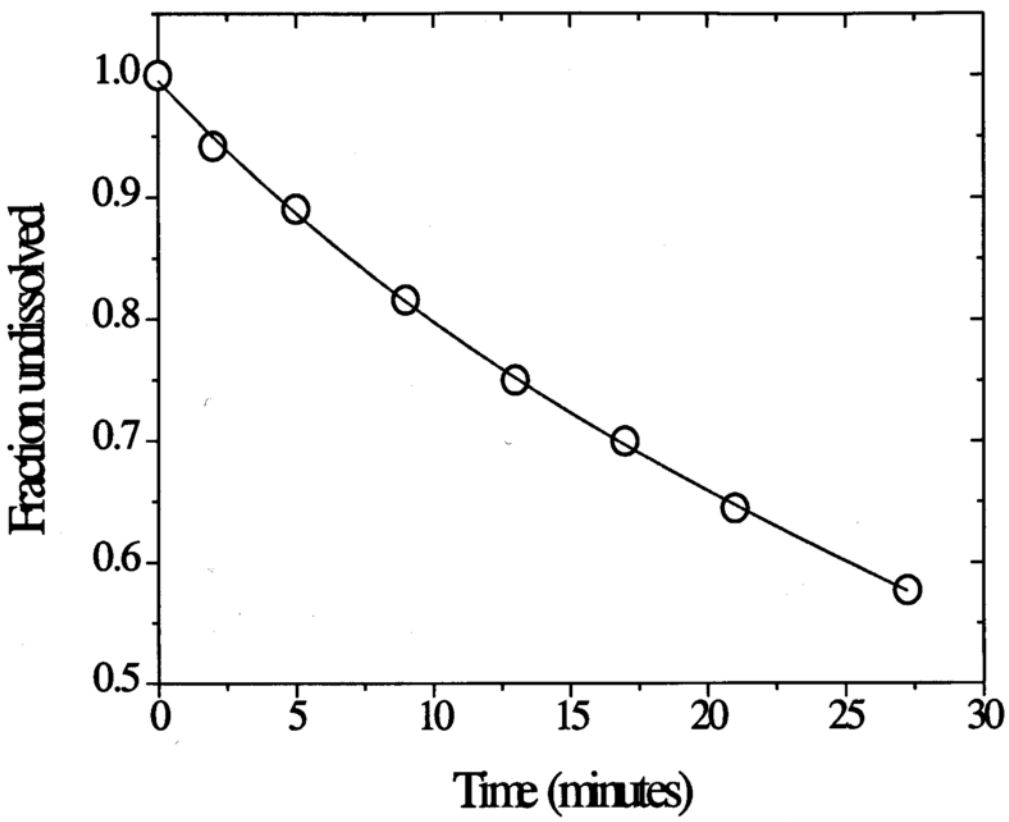

Fig. VI.4-2 Fraction undissolved for the dissolution of a -40/+60 mesh fraction of phthalimide in 0.1N HCl containing 0.0005% Tween 80 at 50 rpm and 25°C. Multiple regression on the data gave the following result:

$y=0.99582 - (0.02384)x + (4.63E\text{-}4)x^2 - (5.61E\text{-}6)x^3$, $R^2=0.999$.

It may be recalled that the fraction undissolved is given by the following expression:

$$\frac{M}{M_0} = 1 - \left\{ \frac{\int_{b_0^{min}}^{b_0^{max}} \left[3(b_0)^2 f(b_0)db_0\right]Kt - \int_{b_0^{min}}^{b_0^{max}} \left[3b_0 f(b_0)db_0\right]K^2t^2 - \int_{b_0^{min}}^{b_0^{max}} \left[f(b_0)db_0\right]K^3t^3}{\int_{b_0^{min}}^{b_0^{max}} \left[(b_0)^3 f(b_0)db_0\right]} \right\}$$

In terms of the integrals I_j defined earlier, the second term in the above equation (the term in t), is given by

$$3K\left(\frac{I_2}{I_3}\right)t$$

With the knowledge of I_2 and I_3 for a -40/+60 mesh fraction of phthalimide (Table VI.3-6), and by equating this to 0.02384 t, the value of K emerges to be 0.47 μm/min. This corresponds to 7.8×10^{-7} cm/s.

Since $K = \frac{2kS}{\rho}$,

the intrinsic dissolution rate constant for phthalimide under the hydrodynamic conditions of study was found to be 1.3×10^{-3} cm/s.

Validation of K-values

If a substance is recrystallized from an aqueous medium and then redissolved in the same, two aspects appear to hold. First, is a linear decrease of the smallest dimension of a particle with respect to time and second, the Hixson-Crowell cube root law before the critical time.

From the single crystal studies on potassium dichromate [Dali and Carstensen, 1996] and other reports from the literature [Schoonen, et al., 1979], the following is shown to be true.

$$b^{min} = b_0^{min} - Kt \qquad \text{VI.4-1}$$

where b_0^{min} is the smallest breadth at t=0 and b^{min} is breadth of that same particle at any time t. At the critical time, t^*, b^{min} diminishes to zero and hence the following expression holds.

$$K = \frac{b_0^{min}}{t^*} \qquad \text{VI.4-2}$$

For the dissolution of a -40/+60 mesh fraction of pthalimide, the value of t^* was found to be 39 minutes. With a b_0^{min} equal to 20 μm, the value of K obtained via

Eq.VI.4-2 is 8.5 x 10^{-7} cm/s. This value is in excellent agreement with the K value calculated from the pre-critical dissolution curve.

Brooke proposed an equation that describes the dissolution of polydisperse spherical particles that follow a log-normal distribution. In Brooke's model, the geometric mean, μ, and the geometric standard deviation, σ_g, of the diameter of spherical particles is taken into account.

$$1-\left(\frac{M}{M_0}\right)^{1/3} = \left[\frac{\exp\left(-2.54 \ln^2 \sigma'_g\right)}{\mu}\right]\left[\frac{2kS}{\rho}\right]t \qquad \text{VI.4-3}$$

This equation was an outcome of simulated dissolution profiles prior to the critical time. One can obtain an estimate of the K value using Brooke's model, by arriving at a distribution of spherical equivalent diameters for these phthalimide particles, provided the distribution can be approximated to a log-normal distribution. To accomplish this, one needs to know the distribution of volumes of these particles. What is not known is the height of each particle. Under the microscope, phthalimide crystals appeared close to cylindrical in shape. It would, therefore, be reasonable to set the height of each particle equal to its breadth. In the next section, through the evaluation of shape factors from dissolution data, a means of obtaining the mean height to breadth ratio for such particles will be pre-

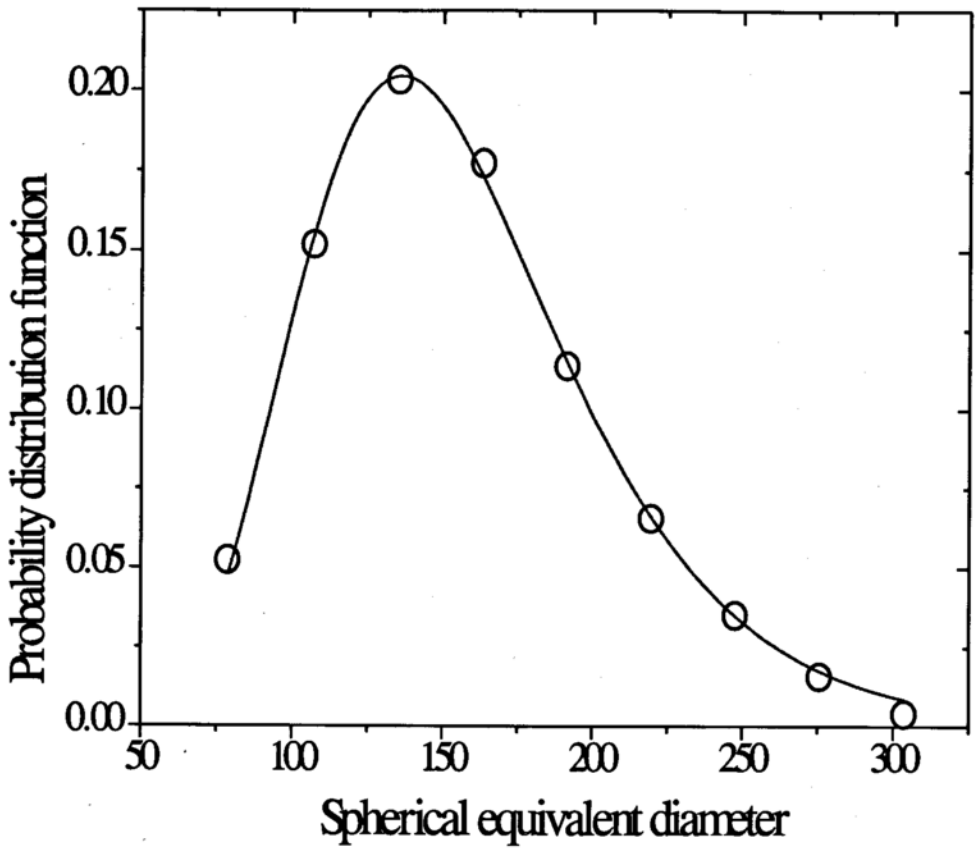

Fig.VI.4-3 Distribution of the hypothetical spherical equivalent diameters for the particles from a -40/+60 mesh fraction of phthalimide by assuming the height to be equal to the breadth. The distribution has a geometric mean of 136 μm and $\ln\sigma = 0.319$, χ^2 for the fit = 1.27E-5.

sented. It will be shown that for the phthalimide particles within this mesh fraction, the mean height of the particle is equal to the mean breadth of the particle. It is noted that some of the results that are presented in the next section will be used in this section, a priori, to get an estimate of the geometric mean and geometric standard deviation of the spherical equivalent diameter.

From the volume distribution for a -40/+60 mesh fraction of phthalimide, a distribution of diameters of hypothetical spheres with the same respective volumes can be obtained. This is shown in Fig.VI.4-3 and confirms that such a distribution follows a log-normal function. With the knowledge of the value of μ and $\ln\sigma$ and of the value of the slope of the cube root law plot before the critical time (Fig.VI.4-1), one can now use Eq.VI.4-3 to calculate the K value. Thus using Brooke's model and a hypothetical distribution of spherical equivalent diameters for the phthalimide particles, the K value was found to be 25.4×10^{-7} cm/s. This is a rather higher estimate in comparison with the K values obtained earlier. This treatment could only be adopted for sieve fractions of phthalimide and salicylic acid because their distributions were log-normal.

In this manner the K values and the intrinsic dissolution rate constants for the four compounds studied were calculated from powder dissolution data before the critical time. Also from the smallest particle in a particular sieve fraction and

the critical time from the cube root law plot, an estimate K could be obtained. In subsequent figures the cube root law plots and the pre-critical time fraction undissolved plots for a sieve fraction of oxalic acid dihydrate and salicylic acid and an unsieved sample of acetaminophen are given. Finally all these results with the comparisons between Brooke's model and parallelepiped model for two of the four compounds are presented in Table VI.4-1.

In all the cases biphasic behavior was evident from the cube root law plots. There was good agreement between the K values obtained from fraction undissolved and those obtained from the smallest breadth and critical time, in all cases except for acetaminophen.

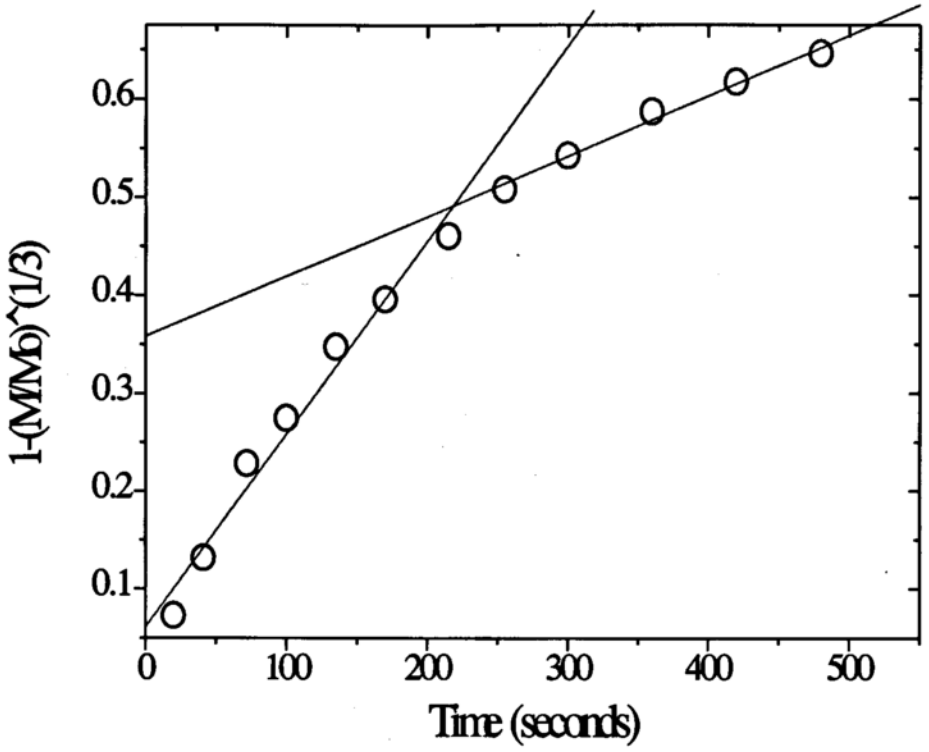

Fig. VI.4-4 Cube root law plot for the dissolution of a -30/+40 mesh fraction of oxalic acid dihydrate in 0.1N HCl at 50 rpm and 25°C. Linear regression for the pre-critical time dissolution is $y=0.0613+0.00197x$, $R^2=0.976$, and linear regression for post-critical time is $y=0.3586+0.00061x$, $R^2=0.988$.

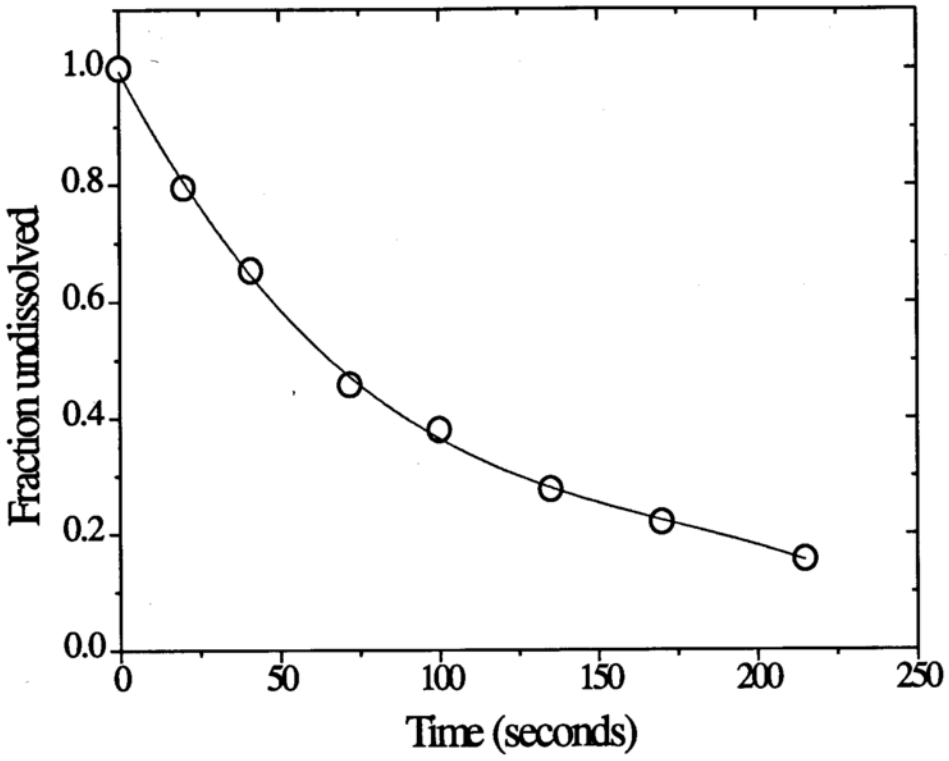

Fig. VI.4-5 Fraction undissolved for the dissolution of a -30/+40mesh fraction of oxalic acid dihydrate in 0.1N HCl at 50 rpm and 25°C. Multiple regression on the data gave the following result:

$y=0.9955 - (0.01048)x + (5.155E\text{-}4)x^2 - (9.767E\text{-}6)x^3$, $R^2=0.999$.

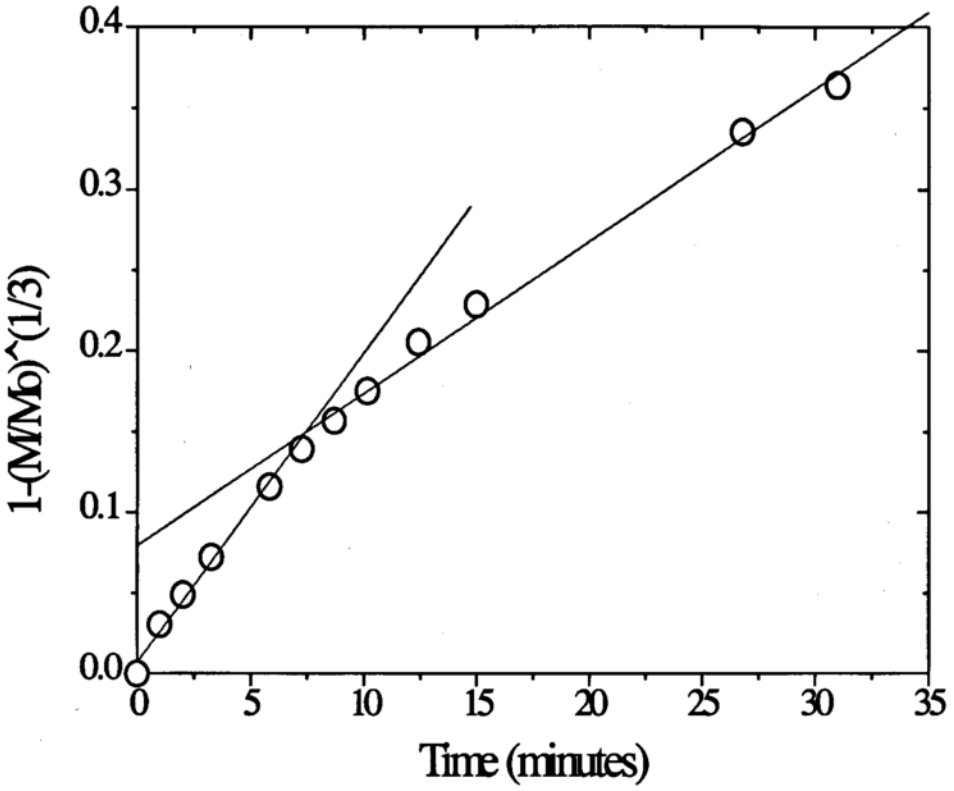

Fig. VI.4-6 Cube root law plot for the dissolution of a -60/+100 mesh fraction of salicylic acid in 0.1N HCl containing 0.0005% Tween 80 at 50 rpm and 25°C. Linear regression for the pre-critical time dissolution is $y=0.0070+0.01919x$, $R^2=0.987$, and linear regression for post-critical time is $y=0.0797+0.00941x$, $R^2=0.993$.

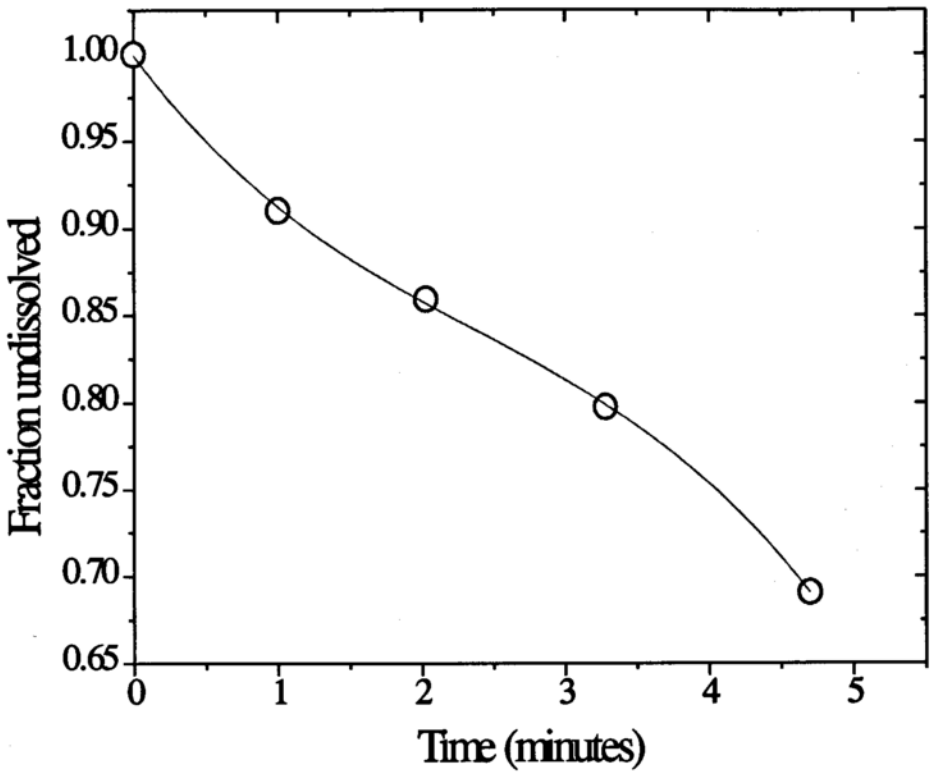

Fig. VI.4-7 Fraction undissolved for the dissolution of a -60/+100 mesh fraction of salicylic acid in 0.1N HCl containing 0.0005% Tween 80 at 50 rpm and 25°C. Multiple regression on the data gave the following result:

$y=0.9994 - (0.11098)x + (2.805E\text{-}2)x^2 - (3.919E\text{-}3)x^3$, $R^2=0.999$.

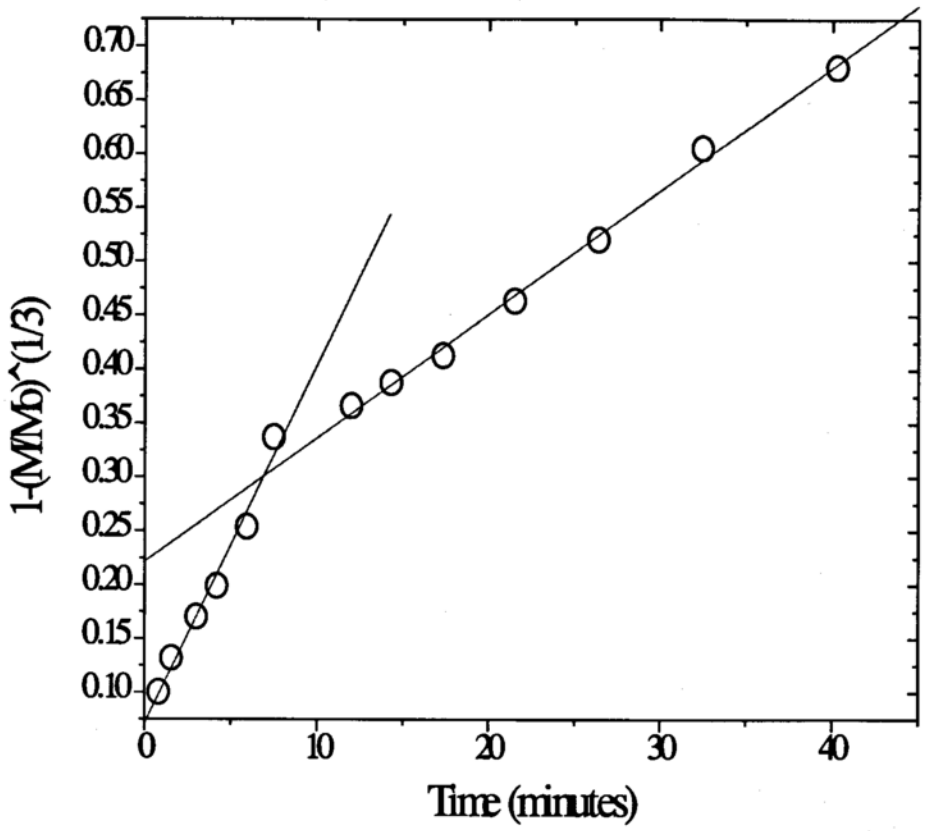

Fig. VI.4-8 Cube root law plot for the dissolution of an unsieved sample of acetaminophen in 0.1N HCl containing 0.0005% Tween 80 at 50 rpm and 25°C. Linear regression for the pre-critical time dissolution is $y=0.0711+0.0333x$, $R^2=0.981$, and linear regression for post-critical time is $y=0.2218+0.01147x$, $R^2=0.996$.

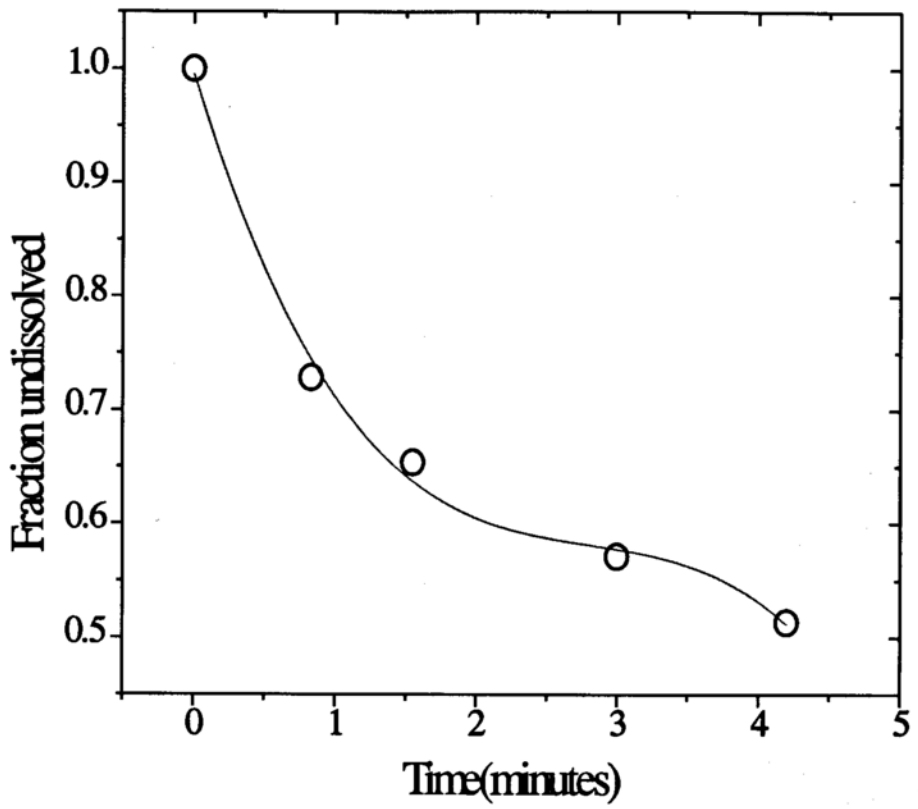

Fig. VI.4-9 Fraction undissolved for the dissolution of an unsieved sample of acetaminophen in 0.1N HCl containing 0.0005% Tween 80 at 50 rpm and 25°C. Multiple regression on the data gave the following result:

$y=0.9956 - (0.4049)x + (0.1373)x^2 - (0.01625)x^3$, $R^2=0.996$.

Table VI.4-1 Intrinsic dissolution rate constants of the four compounds calculated from the fraction undissolved. The K values are reported as the mean and standard deviation of three dissolution runs. The intrinsic dissolution rate constants are calculated from the mean value of K.

Compound	Sieve fraction	K cm/s	k cm/s
Oxalic acid	-30/+40	$(1.47 \pm 0.06)\times10^{-4}$	0.83×10^{-3}
dihydrate	-40/+50	$(1.40 \pm 0.15)\times10^{-4}$	0.79×10^{-3}
	-50/+60	$(1.40 \pm 0.43)\times10^{-4}$	0.79×10^{-3}
	-60/+80	$(1.43 \pm 0.11)\times10^{-4}$	0.81×10^{-3}
Salicylic acid	-40/+60	$(0.48 \pm 0.05)\times10^{-5}$	2.0×10^{-3}
	-60/+100	$(0.59 \pm 0.02)\times10^{-5}$	2.5×10^{-3}
	-100/+200	$(0.56 \pm 0.06)\times10^{-5}$	2.4×10^{-3}
Phthalimide	-40/+60	$(7.8 \pm 1.39)\times10^{-7}$	1.3×10^{-3}
	-60/+100	$(8.5 \pm 0.8)\times10^{-7}$	1.4×10^{-3}
Acetaminophen	unsieved	$(0.33 \pm 0.11)\times10^{-4}$	1.4×10^{-3}

Table VI.4-2 Intrinsic dissolution rate constants for the four compounds calculated from critical times and smallest breadth in the distribution.

Compound	Sieve fraction	b_0^{min} (μm)	Critical time t^* (s)	K cm/s from t^*	k cm/s from t^*
Oxalic acid dihydrate	-30/+40	249	220	1.1×10^{-4}	0.62×10^{-3}
	-40/+50	202	200	1.0×10^{-4}	0.56×10^{-3}
	-50/+60	148	150	0.99×10^{-4}	0.56×10^{-3}
	-60/+80	92	110	0.84×10^{-4}	0.47×10^{-3}
Salicylic acid	-40/+60	32	540	0.59×10^{-5}	2.5×10^{-3}
	-60/+100	23	450	0.51×10^{-5}	2.1×10^{-3}
	-100/+200	11	300	0.37×10^{-5}	1.6×10^{-3}
Phthalimide	-40/+60	20	2340	8.5×10^{-7}	1.4×10^{-3}
	-60/+100	14	1800	7.8×10^{-7}	1.3×10^{-3}
Acetaminophen	unsieved	50	420	0.12×10^{-4}	0.49×10^{-3}

Table VI.4-3 Comparison between K values obtained from the fraction undissolved and those estimated by making a spherical approximation and thereby using Brooke's model.

Compound	Sieve fraction	K from fraction undissolved cm/s	K from Brooke's model cm/s
Salicylic acid	-40/+60	$(0.48 \pm 0.05)\times10^{-5}$	$(0.56 \pm 0.09)\times10^{-5}$
	-60/+100	$(0.59 \pm 0.02)\times10^{-5}$	$(0.60 \pm 0.07)\times10^{-5}$
	-100/+200	$(0.56 \pm 0.06)\times10^{-5}$	$(0.62 \pm 0.05)\times10^{-5}$
Phthalimide	-40/+60	$(7.8 \pm 1.39)\times10^{-7}$	$(19.5 \pm 5.3)\times10^{-7}$
	-60/+100	$(8.5 \pm 0.8)\times10^{-7}$	$(14.2 \pm 4.4)\times10^{-7}$

The following values for the mean height to breadth ratios have been used to estimate the geometric mean and standard deviation for the spherical equivalent diameters (see next section for details):

For salicylic acid: -40/+60 sieve fraction: 0.86; -60/+100 sieve fraction: 0.92; -100/+200 sieve fraction: 0.99.

For phthalimide: -40/+60 sieve fraction: 0.94; -60/+100 sieve fraction: 0.98;

VI.5. Determination of volumetric shape factors from powder dissolution data

The volume shape factor α_v, which was introduced in the theoretical section is the parameter that will be sought in this section. In the following, the mass undissolved as a function of time will be utilized to calculate the average initial volume shape factor for a particular distribution. Just as in the determination of K from fraction undissolved, the term in t from the expression for mass undissolved will be used to estimate the average α_{v0} for a sieve fraction. For clarity of the argument this term is given below (from Eq. IV.2-3).

$$\left[3N\rho\alpha_{v0} \int_{b_0^{min}}^{b_0^{max}} (b_0)^2 f(b_0)\, db_0 \right] K t$$

The value of the coefficient of t in this expression can be obtained by multiple regression of the data for amount undissolved. The integral is indeed I_2, the second moment of the frequency function. With the knowledge of K and ρ and by determining the total number of particles (N) in a given sample, the value of α_{v0} can be obtained.

It is important to recall the assumptions made in chapter IV in this regard. An average initial volume shape factor is assigned to a sieve fraction. Also it is assumed that this value does not change significantly until the critical time.

By definition,

$$\alpha_{v0} = \left(\frac{\ell_0}{b_0}\right)\left(\frac{h_0}{b_0}\right) \qquad \text{VI.5.1}$$

As mentioned before, it is difficult to measure the third dimension (height) of a particle when it is placed in its most stable position. So from microscopy, at best, one can get an estimate of the mean length to breadth ratio, the first term in the parenthesis in Eq.VI.5.1. The second term, the ratio of height to breadth should be a fractional quantity. Since all the three dimensions of the particle have complete access to the dissolution medium, the average initial volume shape factor ($\alpha_{v0}^{\text{dissolution}}$), so obtained from powder dissolution data must be smaller in magnitude than the length to breadth ratio obtained from microscopy ($\alpha_{v0}^{\text{microscopy}}$). The comparison of these two values gives us a sense of the consistency in the determination of volume shape factor from powder dissolution data. In short,

$$\alpha_{v0}^{\text{microscopy}} = m \qquad \text{VI.5-2}$$

and

$$\alpha_{v0}^{\text{dissolution}} = mn \qquad \text{VI.5-3}$$

where

$$m = \frac{\ell_0}{b_0} \quad \text{and} \quad n = \frac{h_0}{b_0}$$

the condition being, $\alpha_{v0}^{\text{microscopy}} \geq \alpha_{v0}^{\text{dissolution}}$

The utility of a non-isometric model geometry is very obvious now. Such a treatment can potentially allow characterization of shape of several non-isometric particles. Trends and comparisons between the particles belonging to different mesh fractions can then be made.

The amount undissolved versus dissolution time for a -60/+100 sieve fraction of salicylic acid is shown is Fig.VI.5-1. As envisaged, the data follow a third degree polynomial. The estimated value for N for a initial weight of the powder equal to 0.15004 g is 12,200. This was obtained by microscopy by recording the weight of a smaller sample of 300 particles, and then scaling it up to the required weight.

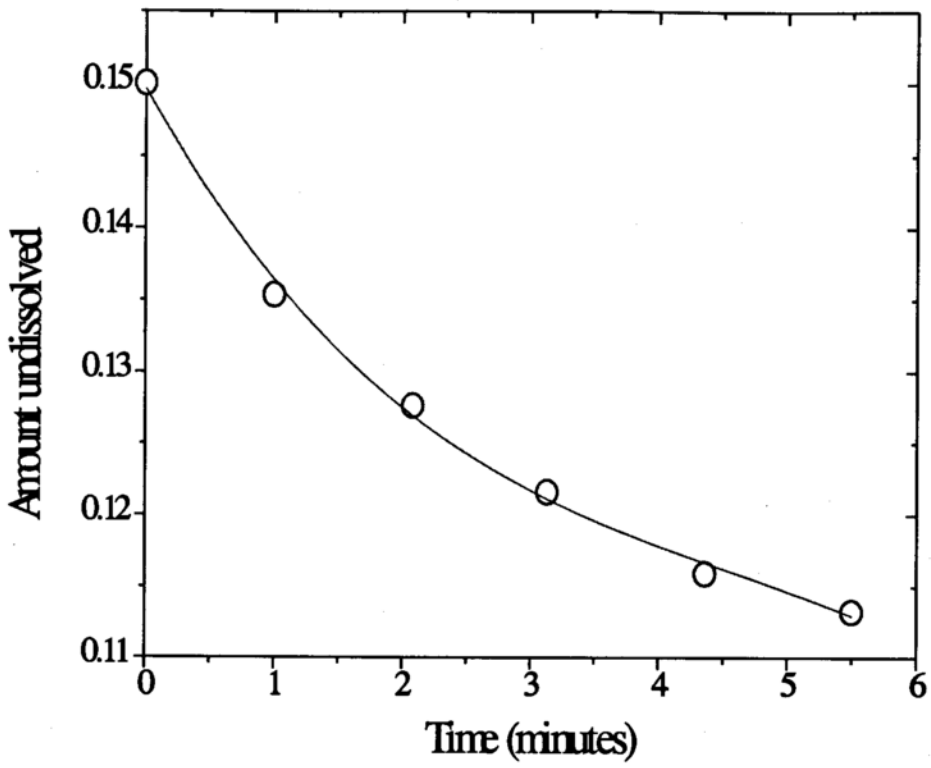

Fig. VI.5-1 Amount undissolved for the dissolution of a -60/+100 mesh fraction of salicylic acid in 0.1N HCl containing 0.0005% w/w Tween 80 at 50 rpm and 25°C. Multiple regression on the data gave the following result:

$y=0.14967-(0.01587)x+(0.0028)x^2-(0.00021)x^3$, $R^2=0.997$.

Thus, $3N\rho\alpha_{v0} I_2K = 0.01587$

Substituting for N(12,200), K($0.34x10^{-3}$ cm/min), I_2(6614 μm^2), and ρ(1.44 g/mL), the mean initial volume shape factor for a -60/+100 sieve fraction of salicylic acid was found to be 13.4. Likewise α_{v0} values for all the other sieve fractions of salicylic acid, phthalimide, and oxalic acid dihydrate, and unsieved acetaminophen were calculated. These values can be compared with the mean ℓ_0/b_0 ratios from Table VI.3-7. These results have been compiled in Table VI.5-1. For the same sieve fraction the mean length to breadth ratio is 14.59 (Table VI.3-7). The ratio 13.4/14.59 = 0.92 gives an estimate of the mean height to breadth ratio for this sieve fraction.

The effect of shape of a particle on such processing variables as flow rates, syringeability, mixing, and also dissolution has always been of concern in pharmaceutics, but relatively few articles have been published dealing with the experimental quantitative evidence of this. Ridgway and Rupp are the sole investigators to show, by direct experiment, the effect of shape factors on flow rates, apparent densities, and repose angles [Ridgway and Rupp, 1969]. In the present work, a method has been proposed for the determination of three-dimensional volume shape factors.

Table VI.5-1 Initial volume shape factors obtained from dissolution data and microscopy.

Compound	Sieve fraction	α_{v0} from amount undissolved	α_{v0} from microscopy	Mean h_0/b_0
Oxalic acid	-30/+40	2.7	4.8	0.56
dihydrate	-40/+50	3.8	8.0	0.47
	-50/+60	4.2	8.8	0.47
	-60/+80	7.6	12.5	0.61
Salicylic acid	-40/+60	9.5	11.1	0.86
	-60/+100	13.4	14.6	0.92
	-100/+200	15.5	15.7	0.99
Phthalimide	-40/+60	10.3	11.0	0.94
	-60/+100	12.9	13.1	0.98
Acetaminophen	unsieved	1.0	1.7	0.59

Table VI.5-2 Total initial number of particles within a certain weight for the four compounds.

Compound	Sieve fraction	Weight (g)	Number of particles
Oxalic acid	-30/+40	3.0	8,980
dihydrate	-40/+50	3.0	18,450
	-50/+60	3.0	31,040
	-60/+80	3.0	58,850
Salicylic acid	-40/+60	0.150	9,380
	-60/+100	0.150	12,200
	-100/+200	0.150	32,400
Phthalimide	-40/+60	0.035	12,380
	-60/+100	0.035	16,000
Acetaminophen	unsieved	1.0	114,850

The three-dimensional shape factors obtained from short term dissolution data were found to be less than or almost equal to the mean length to breadth ratio obtained from microscopy. Oxalic acid dihydrate particles have an acicular crystal shape. On the other hand, salicylic acid and phthalimide crystals can be well described as thin needles. On the contrary, acetaminophen crystals were prismatic, but they exhibited a significantly lower length to breadth ratio than any of the other compounds. These attributes of the crystal shape have been captured to some extent by the volume shape factors listed in Table VI.5-1. It appears that both α_{v0} from microscopy and α_{v0} from dissolution follow the same trend in going from a coarser to a finer sieve fraction. Hence consistency prevails in the estimated values of these parameters. The mean volume shape factor increases in going from a coarser to a finer sieve fraction. This may in part, be due to the effective decrease in the breadth of the particle. The acicular nature of oxalic acid dihydrate crystals is reflected in a lower height to breadth ratios ($n \sim 0.5$-0.6) than the ones for salicylic acid and phthalimide particles. In the latter two cases, the particles being very thin needles, one would expect the mean height of the crystal to be very close to the mean breadth ($n > 0.9$). Acetaminophen crystals possessed the least degree of non-isometry, in that the mean length to breadth ratio was less than 2.

VI.6. Determination of particle size distribution parameters from powder dissolution data

Particle size distribution of a certain batch of a bulk drug substance can be important information because this may influence properties such as content uniformity and dissolution of their solid dosage forms. To manufacture solid dosage forms with acceptable content uniformity and reproducible dissolution, drug particle size specifications are routinely established. Sieve analysis is not a direct measurement because the mean opening of the upper and lower sieve constitutes the mean particle size of the powder which is retained on the lower sieve. Bulk drug particles that tend to aggregate will cause problems during the sieving process. Instruments based on electrical zone sensing techniques, like the Coulter counter are not devoid of problems. Dissolution of solid in the vehicle, and concomitant passing of more than one particle through the pinhole (coincidence) are some of the problems. Methods based on laser light scattering and also microscopy use a small sample size. Effective sampling is very crucial in getting reliable and representative results.

In section VI.4 it was seen how one can obtain the intrinsic dissolution rate constant from powder dissolution and particle size analysis. A pragmatic, valuable application of the present work is the potential of obtaining the particle

size distribution parameters from dissolution data. The basic idea underlying this thought is that, if the value of K for any substance under study is known, then it is possible to work our way backwards to get the mean and standard deviation from the fraction undissolved. For the sake of argument the equation for fraction undissolved is recalled here.

$$\frac{M}{M_0} = 1 - 3K\left(\frac{I_2}{I_3}\right)t + 3K^2\left(\frac{I_1}{I_3}\right)t^2 - K^3\left(\frac{I_0}{I_3}\right)t^3 \qquad \text{VI.6-1}$$

All the assumptions that were invoked in this model will still continue to hold in the following approach. The treatment will be until the critical time and dissolution is assumed to occur under sink conditions. The scenario calls for the determination of the integrals I_j. Let the powder for which the size distribution parameters are sought be subjected to dissolution. If the cube root law is applicable to its dissolution, then Eq.VI.6-1 would be valid, and one can fit the data to a third degree polynomial in time. From the coefficients of t and the value of K (known *a priori*), the integrals I_j can be evaluated. Imposing the restrictions of a normalized frequency function, I_0 can be set to unity. As a result I_3 can be calculated which leads to the determination of I_1 and I_2. The mean is equal to I_1 and the variance is given by I_2-I_1^2.

An important feature about this approach is that a large sample size can be afforded. Furthermore, the dissolution itself can serve as a specification test or criterion for quality control of the raw material. To test this proposal, dissolution of three sieve fractions of oxalic acid dihydrate was carried out. An average K value (1.4 μm/s) was used. From the fraction undissolved the mean and standard deviation of the distribution could be calculated.

These results are given in Table VI.6-1. The means obtained by working backwards are significantly lower than the mean of the breadth that was determined by microscopy. From the average value of n for each of these sieve fractions, the mean height for the particles from any sieve fraction can be estimated. This has been shown in Table VI.6-1. It is noted that the mean obtained from dissolution data is comparable to the predicted mean of height. Thus it appears as though this method gives the distribution parameters for the smallest of the three dimensions of the particle, viz., height. The standard deviations on the breadth and the ones obtained by this method are comparable too. Thus the mean and standard deviation of the distribution obtained from dissolution could be validated with the ones obtained from microscopy. Sieve fractions of oxalic acid dihydrate followed normal distributions. The same methodology was applied to dissolution of salicylic acid particles. However, in

this case the derived statistical parameters were significantly lower than predicted geometric mean height and its geometric standard deviation. The method did not work as expected for log-normal distributions.

VI.7. Computer simulations for the *anisotropic* dissolution profiles of log-normally distributed parallelepipeds

For the model discussed in section IV.3 six parameters have been defined. The parameter design has been simplified so that for one interaction, e.g. μ_b' and P, there can be 25 experiments (5 levels for each parameter) at a particular level of the other four parameters namely σ_b, Q, K_b, and R . This same interaction needs to be considered at the remaining four levels of these parameters. Thus for a μ_b' X P interaction there would be 25X5=125 dissolution experiments. Six parameters considered on a two-way interaction basis calls for ${}^6C_2=15$ different combinations. These two-way interactions are given below with each box enclosing 125 experiments. That makes a total of 1,875 experiments which will be realised by computer simulations.

Table VI.6-1 Distribution parameters determined indirectly from dissolution data and comparison with those obtained from microscopy.

Sieve fraction	M_{b0} from microscopy (microns)	σ_b from microscopy (microns)	Mean from dissolution (microns)	Std dev from dissolution (microns)	n	Predicted M_{h0} (microns)
-30/+40	410	85	**222**	84	0.56	**230**
-40/+50	299	55	**167**	70	0.47	**140**
-50/+60	240	32	**120**	33	0.47	**113**

μ_b' X P				
μ_b' X σ_b	P X σ_b			
μ_b' X Q	P X Q	σ_b X Q		
μ_b' X K_b	P X K_b	σ_b X K_b	Q X K_b	
μ_b' X R	P X R	σ_b X R	Q X R	K_b X R

Dissolution profiles were generated using Eq.IV.3-14 by considering a range of values for the six parameters mentioned earlier. A program was written in STUDENT MATLAB in order to generate these profiles. The individual functional dependencies of the six parameters were deduced from the slope of the plot of $\{1-(M/M_0)^{1/3}\}$ versus t. The goal of these simulations is to arrive at a global equation which describes the dissolution of parallelepiped-like particles. The following table gives the design of the parameters considered in the simulations, each at five different levels. Dissolution curves were obtained from these 1,875 simulations with the values of the parameters as mentioned in section IV.3. The cube root law plots until the critical time were linear in t.

$$1-\left(\frac{M}{M_0}\right)^{1/3} = K t \qquad \text{VI.7-1}$$

The slope κ of the cube root law plots is a function of all the six parameters. It is reasonable to expect these functions to be products. So a logarithmic transformation of κ would separate the dependencies into sums. However at this stage there is no precedence to assume complete independence of the parameters. From the 1,875 simulations, the following relationships between κ and the respective parameters were obtained.

$$\ln(\kappa) = A_1 - \ln(\mu_b') \qquad \text{VI.7-2}$$

$$\ln(\kappa) = A_2 + B_2\,(1/P) \qquad \text{VI.7-3}$$

$$\ln(\kappa) = A_3 - B_3\,(\sigma_b^2) \qquad \text{VI.7-4}$$

$$\ln(\kappa) = A_4 - B_4\,(Q^2) \qquad \text{VI.7-5}$$

$$\ln(\kappa) = A_5 + \ln(K_b) \qquad \text{VI.7-6}$$

$$\ln(\kappa) = A_6 + B_6\,(R) \qquad \text{VI.7-7}$$

The corresponding plots are shown in Figs. VI.7-1, VI.7-3, and VI.7-3. The coefficient B_4 is negligibly small. It is quite possible that the parameter Q may not have a strong bearing on the slope of the cube root law plot. In other words, assuming the geometric standard deviations of the two dimensions to be comparable might not alter the specificity of the model.

Table VI.7-1 Values of the six parameters used in the simulation of anisotropic dissolution profiles.

Level	μ_b'	P	σ_b	Q	K_b	R
	microns				μ/unit time	
1	32	4	0.2	0.64	1	2
2	64	7	0.3	0.88	2.5	3
3	128	11	0.4	1.12	5	4
4	256	14	0.6	1.36	7.5	5
5	512	18	0.8	1.6	10	6

The relationships in Eqs.VI.7-2, VI.7-4, and VI.7-6 are as envisaged. It is noted that P, Q, σ_b, and R bear an exponential dependence, κ is linear in K_b and is an inverse function of μ_b'. κ decreases as μ_b', P, σ_b, and Q increase, while it increases as K_b and R increase. With this information it would be desirable to convolute these relationships into one equation that would hold for a polydisperse system of parallelepiped-like particles. Also it is interesting to note that Brooke found a similar relationship between $\ln(\kappa)$ and σ^2 for spherical particles, but in that case the coefficient B_3 was 2.54 as against 0.5 in the case of parallelepipeds. Brooke proposed the following equation for the dissolution of spherical particles before the critical time.

$$1-\left(\frac{M}{M_0}\right)^{1/3} = \left[\frac{\exp\left(-2.54\ln^2\sigma'_g\right)}{\mu'}\right]\left[\frac{2kS}{\rho}\right]t$$

Thus the slope of the cube root law plot according to this equation would be

$$\text{Slope} = \left[\frac{\exp\left(-2.54\ln^2\sigma'_g\right)}{\mu'}\right]\left[\frac{2kS}{\rho}\right] \qquad \text{VI.7-8}$$

$$\ln(\text{Slope}) = \ln\left(\frac{2kS}{\rho}\right) - \ln(\mu') - 2.54\sigma_g^2 \qquad \text{VI.7-9}$$

Eq.VI.7-2 and VI.7-6 are in agreement with Eq. VI.7-9 as far the dependencies of K and μ are concerned. As mentioned before Eq.VI.7-4 has the same functional dependency for the geometric standard deviation, except that the coefficient is different.

The simulations which led to these relationships between the slope of the cube root law plot before the critical time and the six respective parameters, were carried out by changing two parameters at a time and keeping the rest of the four unchanged. In actuality it is difficult to test Eqs.VI.7-2 to VI.7-7 on an individual basis because it is not possible to achieve this level of control over the parameters, through bench experiments, as was done with the simulations.

Preliminary attempts to convolute these dependencies for the six parameters into one simple solution form did not yield satisfactory results. It is important to know whether or not these parameters are mutually exclusive and independent. At this juncture that question could not be addressed. However, this part of the thesis is an adjunct to the earlier sections and it certainly does not comprise the main core.

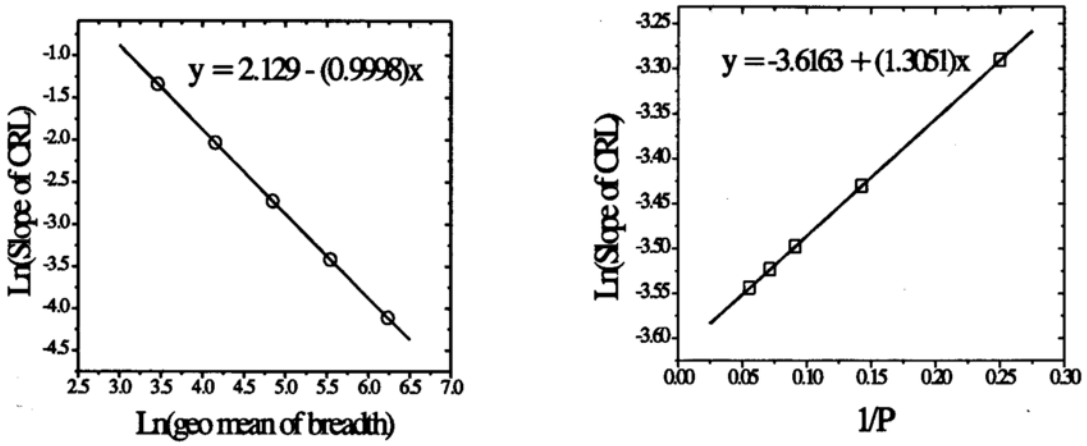

(a) (b)

Fig.VI.7-1 Relationships between the slope of the cube root law plot (κ) and (a)the geometric mean of the breadth and (b)the non-isometry ratio P

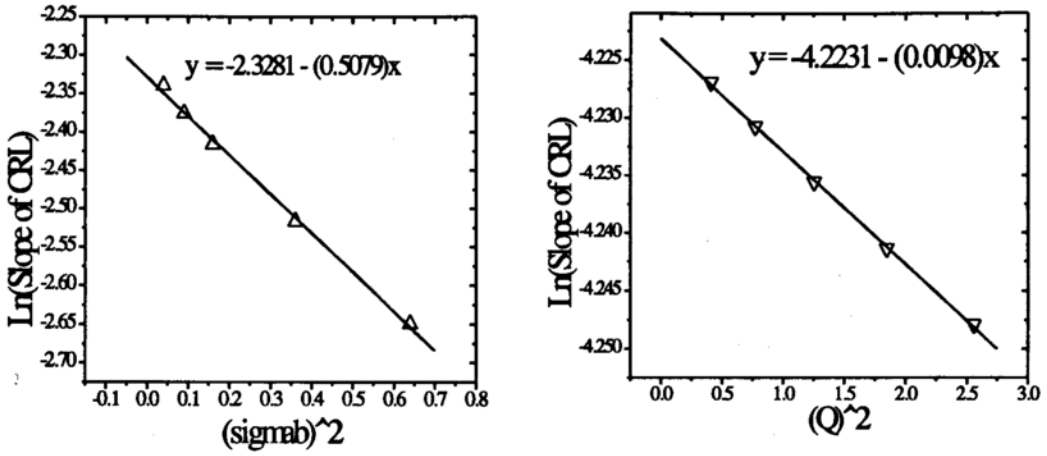

(a) (b)

Fig.VI.7-2 Relationships between the slope of the cube root law plot (κ) and (a)the geometric standard deviation of the breadth and (b)the ratio of the standard deviations of length and breadth (Q)

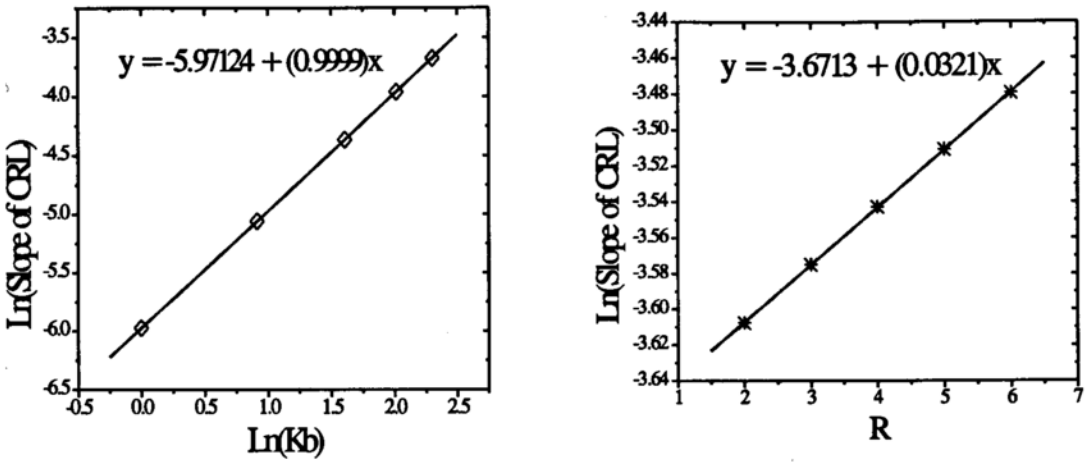

Fig.VI.7-3 Relationships between the slope of the cube root law plot (κ) and **(a)**the dissolution rate constant K_b and **(b)**the ratio (R) of the dissolution rate constants for the two faces of the tetragonal prism.

CHAPTER VII. SUMMARY

Single crystal dissolution kinetics -

A parallelepiped geometry has been suggested to mimic the shape of commonly encountered crystal shapes like needles, platelets, and prisms. The non-isometry in such particles has been accounted for, by taking into consideration the change in the surface-volume shape factor of the single particle as a function of dissolution time. A phenomenological approach led to the derivation of a modified form of the Hixson-Crowell cube root law for a non-isometric particle. It was observed that both the surface-volume shape factor and the volume shape factor are fairly constant in the early stages of dissolution of the single particle. Only after about 60% of the crystal height had dissolved did these shape factors show significant change from their initial value. The modified form of the Hixson-Crowell cube root law explains the upward curvature in the cube root law plot for the dissolution of a single crystal of potassium dichromate.

Multiparticulate dissolution kinetics -

(i) *Intrinsic dissolution rate constants*

Isotropic, intrinsic dissolution rate constants could be obtained from powder dissolution data. These values were in good agreement with those calculated from

critical times and the smallest breadth in the distribution. For the log-normally distributed sieve fractions, the predictions from Brooke's model for spherical particles compared well with the values obtained from dissolution data. Fair degree of precision was observed between the intrinsic dissolution rate constants for all the sieve fractions of the same compound. The method was valid under sink conditions and only until the critical time.

(ii) *Volumetric shape factors*

In the present work, the shape of a non-isometric particle has been quantitatively characterized by α_v, the volume shape factor. A polydisperse powder was segregated into sieve fractions and a mean volume shape factor for the distribution of particles within that sieve fraction was obtained. This could be calculated from the amount undissolved versus time by knowing the initial total number of particles, their density and the dissolution rate constant. One important feature about the mean volume shape factors obtained from dissolution data is that all the three dimensions of the particle are taken into account and a relatively large sample size can be afforded. By microscopy, size information of only two of the three dimensions of the particle could be obtained. The shape factors obtained from microscopy were higher in magnitude than those obtained from dissolution.

Since it was not possible to measure the third dimension of particles, comparison of the shape factors obtained by the two methods was one way of ascertaining the order of magnitude of α_v. It was observed that α_v increased in going from a coarser sieve fraction to a finer sieve fraction. Salicylic acid and phthalimide crystallized as thin needles while oxalic acid dihydrate crystals were more acicular. These differences in the shape were manifested in the volume shape factors. Similar sieve fractions of salicylic acid and phthalimide were found to have higher volume shape factors than oxalic acid dihydrate. On the other extreme, acetaminophen crystals exhibited a platy habit with a comparatively low length to breadth ratio.

Particle size distributions from powder dissolution data -

It was demonstrated that it is possible to get the mean and standard deviation of a polydisperse powder that follows a normal distribution. This is an important practical application of the present work, because particle size distributions form an important raw material specification in the quality control of pharmaceutically important solids. Also much larger sample sizes can be afforded and the method is less tedious than microscopy. The validation of the methodology by which this was realized was demonstrated for the normally distributed sieve fractions of

oxalic acid dihydrate. It was found that the particle size distribution parameters obtained from dissolution data pertained to the smallest dimension of the crystals, viz., the height. This inference was drawn from the shape factor analysis on these crystals.

Dissolution anisotropy -

For all of the above isotropic dissolution was assumed. Although dissolution anisotropy is a fundamental property of all non-isometric crystals, this aspect of dissolution has received very little attention. If different crystallographic faces of a crystal can grow at different rates, then it is quite reasonable to expect them to dissolve at different rates as well. A model comprising a log-normally distributed ensemble of parallelepipeds was set up with a group of six parameters that accounted for the distribution and anisotropy in the system. Equations were developed to describe the dissolution of the particles until the critical time. With the aid of a fractional factorial design, at two levels (changing two parameters at a time), dissolution profiles were generated by computer simulations. On those grounds, relationships between the slope of the cube root law plot and the various parameters in the model were discerned.

CHAPTER VIII. CONCLUSIONS

Solid dosage forms continue to be the preferred choice of drug delivery. Whenever a new drug candidate is recognized as a lead compound by the drug discovery and preformulation group in a research and development setting, several physico-chemical properties of that drug compound need to be evaluated to determine whether or not it is a suitable candidate for the oral route of administration. Amongst these properties, the intrinsic dissolution rate constant is one, and a goal of this thesis was to determine this parameter for a compound under relevant hydrodynamic conditions. By this it is implied that the dissolution carried out in a USP paddle apparatus at about 50 rpm (which is the official method for dissolution testing for most solid dosage forms) would give meaningful estimates of this fundamental property of a drug substance. As opposed to this the Wood's apparatus (constant surface area rotating disc) does not render itself to the same hydrodynamic conditions that would exist when a solid dosage form disintegrates into primary particles prior to the process of dissolution. It is also very common for the chemists from the drug discovery group to modify the crystallization process/solvent for a drug candidate. Whether or not this has any bearing on its physical appearance and the dissolution rate is important from the preformulator's point of view.

Estimation of shape factors and particle size distributions is an important outcome of this work. The proposal for a non-isometric geometry, namely a parallelepiped, is much more realistic than the traditional spherical approximation, which lacks the physical picture of a *real* particle. The idea of a spherical average diameter relinquishes any possibility for the characterization of the shape of the particle. As a routine, in-process quality control specification on raw materials, these two aspects can potentially serve as useful tools. Quite often batches of solid dosage forms are known to fail dissolution tests. This may be directly related to the shape of the particle but also to a certain extent these failures may be attributed to the failing of content uniformity requirements. There is a good possibility that improper flow of the powder through the hopper, or segregation of particles during the tablet manufacturing process may emerge as the culprit as a direct upshot of trouble shooting. This is precisely where a specification on particle size and shape can play an important role in the processing of solids and manufacture of solid oral dosage forms.

CHAPTER IX. SUGGESTIONS FOR FUTURE WORK

The following aspects of the thesis form a good basis for future work:

1. *Study of flow properties of powders from different mesh fractions and with differing shape factors* - Up till now, only particle size has been employed to quantitate the rheological properties of powders. Having a three-dimensional shape factor will greatly help in the interpretation of flow rates, compression pressures, shear loci, and bulk properties like apparent density.

2. *Determination of intrinsic dissolution rate constant under different hydrodynamic conditions* - Dissolution studies can be carried out at different speeds of stirring in the USP paddle apparatus and the validity of Levich equation can be checked.

3. *Study powder dissolution beyond the critical time.*

4. *Determination of particle size distribution parameters for broad distributions.*

LIST OF SYMBOLS

m = mass undissolved for a single crystal at any time t

m_0 = initial mass of a single crystal

M = mass undissolved for a polydisperse powder at any time t

M_0 = initial mass of a polydisperse powder

N = total number of particles in a polydisperse powder

F = fraction undissolved

u = reduced time in terms of the smallest dimension of a single crystal

k = intrinsic dissolution rate constant of any substance

A = surface area of the dissolving powder

a = surface area of a single particle

V = total volume of the powder sample

v = volume of a single particle

S = saturation solubility of a substance

C = concentration at any time t during dissolution

ρ = true density of the substance

Γ = surface-volume shape factor at any time t

α_s = surface shape factor at any time t

α_v = volume shape factor at any time t

ℓ = length of a crystal at any time t

b = breadth of a crystal at any time t

h = height of a crystal at any time t

(these symbols with a subscript "0" implies the respective initial dimensions)

a = any dimension of the particle in general

a_0^{min} = smallest initial dimension

a_0^{max} = largest initial dimension

M_{a0} = arithmetic mean of distribution of a_0.

σ_a = standard deviation of the distribution of a_0.

μ' = geometric mean of a dimension of a crystal from a log-normal population

σ' = geometric standard deviation of a dimension of a crystal from a log-normal population (a subscript on these two symbols indicates the dimension; length, breadth)

m,n = shape ratios for a crystal

k_ℓ, k_b, k_h = anisotropic intrinsic dissolution rate constants

P = parameter signifying the degree of non-isometry

Q = ratio of geometric standard deviation of length to that of the breadth in a log-normal powder population

R = anisotropy parameter

κ = slope of the cube root law plot for dissolution of polydisperse powders

$$K = \frac{2kS}{\rho}$$

$f(b_0)$ = initial probability density function for the distribution of breadths of the particles.

REFERENCES

Allen, T., "Particle size measurement." Chapman and Hall, London, 1968.

Barnett, M. I. and Nystrom, C., "Coulter counter and microscopes for the measurement of particles in the sieve range." *Pharm. Technol.* (1982)49-50.

Bennett, C. A. and Franklin, N. L., "Statistical analysis in chemsitry and the chemical industry." Wiley & Sons Inc., New York, 1961.

Brooke, D., "Dissolution profile of log-normal powders: exact expression." *J. Pharm. Sci.* **62**(1973)795-798.

Brooke, D., "Dissolution profiles of log-normal powders II: Dissolution before critical time." *J. Pharm Sci.* **63**(1974)344-346.

Budavari, S., (ed.), "The Merck Index: An encyclopedia of chemicals, drugs, and biologicals." Merck Research Labs, NJ, 1996.

Burt, H. M. and Mitchell, A. G., "Crystal defects and dissolution." *Int. J. Pharm.* **9**(1981)137-152.

Burt, H. M. and Mitchell, A. G., "Dissolution anisotropy in nickel sulfate α-hexahydrate crystals." *Int. J. Pharm.* **3**(1979)261-274.

Burt, H. M. and Mitchell, A. G., "Effect of habit modification on dissolution rate." *Int. J. Pharm.* **5**(1980)239-251.

Cabana, B. E. and O'Neil, R., "FDA's report on dissolution." *Pharm. Forum* **6**(1980)71-75.

Carstensen, J. T., "Modeling and data treatment in the pharmaceutical sciences." Technomic Publ., Lancaster, PA, 1996.

Carstensen, J. T., "Pharmaceutics of solids and solid dosage forms." Wiley-Interscience, New York, 1977.

Carstensen, J. T., "Theory of pharmaceutical systems." Academic Press, New York, 1973.

Carstensen, J. T. and Chan, P. C., "Flow rates and repose angles of wet-processed Granulations." *J. Pharm. Sci.* **66**(1977)1235-1238.

Carstensen, J. T., Dali, M. V. and Pudipeddi, M., "Blending validation of low drug content dosage forms." *Pharm. Dev. Technol.* **1**(1996)113-114.

Carstensen, J. T. ,Ertell, C. and Geoffroy, J. M., "Physicochemical properties of particulate matter." *Drug Dev. Ind. Pharm.* **19**(1993)195-219.

Carstensen, J. T. and Laughlin, S. M., "Dynamic flow rates of granular particles." *Powder Technol.* **23**(1979)79-84.

Carstensen, J. T. and Musa, M. N., "Dissolution rate patterns of log-normally distributed powders." *J. Pharm.Sci.* **61**(1972)223-227.

Carstensen, J. T. and Patel, M., "Dissolution patterns of polydisperse powders: oxalic acid dihydrate." *J. Pharm. Sci.* **64**(1975)1770-1776.

Carstensen, J. T. and Rodriguez-Hornedo, N., "Expected particle size distributions of crystals produced from non-isothermal crystallization." *J. Pharm. Sci.* **74**(1985)1322-1326.

Chakrabarti, S., van Severen, R. and Braeckman, P., "Studies on the crystalline form of phenytoin." *Pharmazie* **33**(1978)338-339.

Choulis, N. H. and Loh, L. H., "Critical micelle concentration determination of some nonionic surfactants using interference refractometry." *Can. J. Pharm. Sci.* **6**(1971)93-94.

Chow, A. H. and Grant, D. J. W., "Physical factors influencing the aqueous dissolution rate of acetaminophen crystals doped with p-acetoxyacetanilide: Evaluation by multiple linear regression." *Int. J. Pharm.* **51**(1989)129-135.

Chow, A. H. L., Gordon, J. D., Szeitz, A. and Young, J. W. M., "Modification of phenytoin crystals III. Influence of 3-butanoyloxymethyl-5,5-diphenylhydantoin on solution phase crystallization and related crystal properties." *Int. J. Pharm.* **126**(1995)11-19.

Cleave, J. P., "Some geometrical considerations concerning the design of tablets." *J. Pharm. Pharmacol.* **17**(1965)698-702.

Cobby, J. ,Mayersohn, M. and Walker, G. C., "Influence of shape factors on kinetics of release from matrix tablets I: Theoretical." *J. Pharm. Sci.* **63**(1974a)725-732.

Cobby, J. ,Mayersohn, M. and Walker, G. C., "Influence of shape factors on kinetics of release from matrix tablets II: Experimental." *J. Pharm. Sci.* **63**(1974b)732-737.

Dali, M. V. and Carstensen, J. T., "Effect of change in shape factor of a single crystal on its dissolution behavior." *Pharm. Research* **13**(1996)155-162.

Dallavalle, J. M., "Micromeretics." Pitman Publ. Co., New York, NY, 1948.

Desai, D. S., Randive,S. A., Lang,B. A., Mueller,R. L., and Varia,S. A., "Particle-size determination of aggregating drug substances." *Pharm. Technol.* 1996)56-64.

Edmundson, I. C. and Lees, K. A., "A method for determining the solution rate of fine particles." *J. Pharm. Pharmacol.* **17**(1965)193-201.

El-Arini, S. K. and Leuenberger, H., "Dissolution properties of Praziquantel-β-cyclodextrin systems." *Pharm. Dev. Technol.* **1**(1996)307-315.

Fick, *Phil. Mag.* **10**(1885)3.

Fini, A., Fernandez-Hervas, M. J., Holgado, M. A., Rabasco, A. M., "Influence of crystallization solvent and dissolution behavior for a diclofenac salt." *Int. J. Pharm.* **21**(1995)19-26.

Frank, F. C., "The influence of dislocations on crystal growth." *Discuss. Farad. Soc.* **5**(1949)48-54.

Heywood, H., "Numerical definitions of particle size and shape." *Chemistry and Industry* (1937)149-154.

Higuchi, W. I. and Hiestand, E. N., "Dissolution Rates of Finely Divided Powders I. Effect of Distribution of Particle Size in a Diffusion-controlled process." *J. Pharm. Sci.* **52**(1963)67-71.

Higuchi, W. I.,Rowe, E. L. and Hiestand, E. N., "Dissolution rates of finely divided drug powders II." *J. Pharm. Sci.* **52**(1963)162-164.

Hintz, R. J. and Johnson, K. C., "The effect of particle size distribution on dissolution rate and oral absorption." *Int. J. Pharm.* **51**(1989)9-17.

Hixson, A. W. and Crowell, J. H., "Dependence of reaction velocity upon surface and agitation I - Theoerical considerations." *Ind. Eng. Chem* **23**(1931)923-931.

Hollenbach, M., Peleg,M., and Rufner,R., "Interparticle surface affinity and bulk properties of conditioned powders." *Powder Technol.* **35**(1983)51-62.

Hostomsky, J., Halasz, Z., and Nyvlt, J., "Size analysis of non-spherical particles A correlation between the results of photosedimantation technique and microscopy." *Powder Technol.* **49**(1986)45-51.

Irani, R. R. and Callis, C. F., "Particle Size: Measurement, interpretation, and application," p. 34-57. John Wiley Publ., New York, 1963.

Johanson, J. R., "Predicting segregation of bimodal particle mixtures using the flow properties of bulk solids." *Pharm. Technol.*(1996)48-57.

Kitamori, N. and Iga, K., "Dissolution of non-spherical powders." *J. Pharm. Sci.* **67**(1978)1674-1676.

Lai, T. Y. and Carstensen, J. T., "Effect of shape factor on cube root dissolution behavior." *Int. J. Pharm.* **1**(1978)33-40.

LeBlanc, H. S. and Fogler, S. E., "Population balance modeling of the dissolution polydisperse solids: rate limiting regimes." *A.I.Ch.E. J.* **33**(1987)54-63.

Levy, G., "Comparison of Dissolution and Absorbtion Rates of Different Commercial Aspirin Tablets." *J. Pharm. Sci.* **50**(1961)388-392.

Lu, A. T. K. ,Frisella, M. E. and Johnson, K. C., "Dissolution modelling: Factors affecting the dissolution rates of polydisperse powders." *Pharm. Research* **10**(1993)1308-1314.

Martin, A. ,Swarbrick, J. and Cammarata, A., "Physical Pharmacy - physical chemical priciples in the paharmaceutical sciences." p. 302. Varghese Publ., Bombay, 1983.

Mitchell, A. G. ,Milaire, B. L. ,Saville, D. J. and Griffiths, R. V., "Aspirin dissolution: Polymorphism, crystal habit or crystal defects." *J. Pharm. Pharmacol.* **23**(1971)534-535.

Mullin, J. W., "Crystallization." CRC Press, Ohio, 1972.

Natrella, M. G., "Experimental Statistics: Handbook 91." National Bureau of Standards, Washington, D.C., 1966.

Nelson, E., "Influence of Dissolution Rate and Surface on Tetracycline Absorption." *J. Am. Pharm. Assoc. Sci. Ed.* **48**(1959)96-103.

Nernst, *Z. Physik. Chem.* **47**(1904)52.

Noyes, A. S. and Whitney, W. R., "The rate of solutions of solid substances in their own solutions." *J. Am. Chem. Soc.* **19**(1897)930-934.

Nyvlt, J. and Zacek, S., "Size distribution analysis of needle-shaped crystals." *Cryst. Res. Technol.* **27**(1992)1073-1077.

Pedersen, P. G. and Brown, K. F., "Experimental evaluation of three single particle - dissolution models." *J. Pharm. Sci.* **65**(1976b)1442-1447.

Pedersen, P. V. and Brown, K. F., "Size distribution effects in multiparticulate dissolution." *J. Pharm. Sci.* **64**(1975)1981-1986.

Pedersen, P. V. and Brown, K. F., "Theoretical isotropic dissolution of non-spherical particles." *J. Pharm. Sci.* **65**(1976a)1437-1442.

Pitkin, C. and Carstensen, J. T., "Effect of particle shape on some bulk solid properties." *Drug Dev. Ind. Pharm.* **16**(1990)1-12.

Podczeck, F. and Newton, J. M., "The evaluation of a three-dimensional shape factor for the quantitative assessment of the sphericity and surface roughness of pellets." *Int. J. Pharm.* **124**(1995)253-259.

Pothisiri, P. and Carstensen, J. T., "Nonsink dissolution rate equation." *J. Pharm. Sci.* **62**(1973)1468-1470.

Ramadan, M. A. and Tawashi, R., "Effect of surface geometry and morphic features on the flow characteristics of microsphere suspensions." *J. Pharm. Sci.* **79**(1990)929-933.

Ridgway, K. and Rupp, R., "The effect of particle shape on powder properties." *J. Pharm. Pharmac.* **21**(1969)

Rodley, G. A., Chan, H.-K. and Gonda, I., "Dissolution studies of hexamethylmelamine." *Int. J. Pharm.* **95**(1993)143-151.

Rupp, R., "Flow and other properties of granulates." *Boll. Chim. Farm.* **116**(1977)251-266.

Schoonen, A. J. M. ,de Vries-Nijboer, G. W. and Huizinga, T., "Solution rate of crytstals at the fluid-fluid interface." *J. Pharm. Sci.* **68**(1979)163-168.

Steiner, G., Patel, M. and Carstensen, J. T., "Effects of milling on granulation particle size distribution." *J. Pharm. Sci.* **63**(1974)1395-1398.

Swarbrick, J. and Ma, D., "In-vitro dissolution of dapsone." *J. Pharm. Pharmacol.* **31**(1981)787-789.

Ullah, I. and Cadwallader, D. E., "Dissolution of slightly soluble powders under sink conditions I: Development of an apparatus and dissolution studies of salicylic acid powders." *J. Pharm. Sci.* **59**(1970)979-984.

Underwood, F. L. and Cadwallader, D. E., "Effects of various hydrodynamic conditions on dissolution rate determinations." *J. Pharm. Sci.* **65**(1976)697-700.

Vasil'Chenko, M. A., Shakhtshneider, T. P., Naumov, D. Y. and Boldyrev, V. V., "Topochemistry of the initial stages of the dissolution of single crystals of acetaminophen." *J. Pharm. Sci.* **85**(1996)929-934.

Weintraub, H. and Gibaldi, M., "Physiologic surface -active agents and drug absorption IV: Effect of pre-micellar concentrations of surfactant on dissolution rate." *J. Pharm. Sci.* **58**(1969)1368-1372.

Yonezawa, Y., Shinohara, I., Sasaki, M., Otsuka, A. and Sunada, H., "Dissolution of solid dosage form IV. Equation for non-sink dissolution of a monodisperse system." *Chem. Pharm. Bull.* **42**(1994)349-353.